PHYSICS
ფიზიკა

35

PHYSICS

ფიზიკა

35

БEK 22.3
УДК 53
ჳ 505

EQUATIONS OF LONGITUDINAL SOUND PROPAGATION IN SUPERFLUID HELIUM FILLED POROUS MEDIA AND VELOCITIES OF PROPAGATING WAVES AT LOW FREQUENCIES

Sh. Kekutia, N. Chkhaidze, O. Tkeshelashvili

ABSTRACT. A theory is developed for the propagation of longitudinal waves in a system porous media-superfluid He^4. The obtained equations are applied for determination of velocities of wave propagation at low frequencies for any value of porosity and tortuosity. There are two ways of solution, the first of which is combination of the first and fourth sounds. Temperature oscillation is possible in the second sound.

1. INTRODUCTION

Flow phenomena in porous media are important to a wide variety of problems and have been studied theoretically and experimentally for a long time. Actuality of study of the processes, which occur in the porous media, is enhanced because of special properties of superfluid helium that fills porous media. Two types of motion are known to exist in superfluid helium, corresponding to the normal and superfluid components. The existence of these two motions (superfluid and normal) produces distinctive wave processes in liquid He II. The propagation of two undamped sound waves is possible in an unbounded volume filled with liquid He II. The first wave, which is called the first sound with velocity, $C_{10}^2 = \partial P / \partial \rho$, is characterized by the fact that normal and superfluid components oscillate in phase. In the propagation of the second wave, or second sound $U_{20}^2 = \sigma^2 (\sigma^s / \sigma^n)(\partial \sigma / \partial T)$, the superfluid and normal fluid components oscillate oppositely to one another. Moreover, transverse waves exist in connection with the motion of only the normal component and are called viscous waves. They occur at the walls of a vessel filled with He II and are of the same nature as viscous waves in

an ordinary fluid. However, because of the special properties of superfluid helium, wave processes can take place not only in large vessels, but also in very narrow channels, whose width Λ is much smaller than the viscous-wave penetration depth $\lambda_\upsilon = (2\eta/\omega\rho'')^{1/2}$ $\gg \Lambda$. Here η is the viscosity of the normal component, and ω is the frequency of the oscillations. In this case the sound propagates through the superfluid component and is called fourth sound. So the fourth sound involves the motion of the superfluid component only, with the normal fluid clamped by its viscosity inside a porous medium, and it can be used to determine the superfluid fraction or for understanding the effects of pore structure [1].

On the other hand, in a series of papers [2,3], Biot proposed a simple phenomenological theory of elastic and viscous behavior in porous, macroscopically homogeneous and isotropic, elastic media saturated with a compressible viscous fluid. Because the motion of the solid and fluid parts is followed separately and on equal footing, this theory represents the most general theory possible for two-component porous solid – fluid system. The theory takes into account the motion of the fluid in the interconnected voids of a porous solid and predicts the existence of two types of bulk compressional waves and a single shear wave. These waves satisfy a pair of coupled differential equations that describe the coupled motion of the fluid and solid phases. These equations contain a mass coupling coefficient, which arises from the fact that in a fluid-saturated porous solid the microscopic motion of the porous solid-fluid is not uniform and in general is not in the direction of the macroscopic pressure gradient. This leads to an apparent density, which differs from the actual bulk density. One bulk compressional wave is a standard compressional wave whose phase velocity is almost independent of frequency at low frequencies. At propagation of this wave there is no relative motion between fluid and solid. The other bulk compressional wave is slow and it propagates in the manner of a diffusion wave at low frequency. The phase velocity of latter wave approaches zero at the zero-frequency limit, and it is highly dispersive and attenuated at low frequencies. As the frequency increases, the slow compressional wave takes on the character of a propagating wave. So, it is possible for the fluid part and the solid matrix to move in opposite directions, resulting
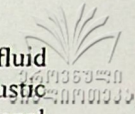
in the second kind mode. Confirmation of Biot's theory that fluid saturated porous media support two distinct longitudinal acoustic modes was reported by Plona [4]. Plona observed these compressional waves in a water-saturated porous structure of sintered glass beads. The fast compressional wave had speed comparable to the compressional wave speed of the constituent glass beads and the slow compressional wave propagated with speed less than the speed of sound in water.

Our aim is to generalize Biot's theory in case the porous media is saturated with liquid He II. In our article we study the theory for three-component pore solid-superfluid systems. Superfluid He^4 is interesting acoustically because it can support more than one mode of sound propagation in contrast to ordinary liquid. Therefore it makes sense to use the superfluid Helium as a probe of the transport properties of porous media as a great number of different types of waves can propagate in the superfluid Helium. This approach is justified, as rich and valuable information on the properties of superfluid helium-saturation porous media can be obtained from the analysis of oscillations propagating in it.

According to the above mentioned the purpose and objective of the article include: the development of the theory of propagation of longitudinal waves in a porous elastic solid containing superfluid Helium and estimation velocities of propagating waves in conditions of low frequencies.

2. EQUATIONS OF LONGITUDINAL SOUND PROPAGATION IN SUPERFLUID HELIUM-FILLED POROUS MEDIA

Let's introduce a rectangular system of coordinates and examine the unit cube containing a great number of pores. Under mechanical equilibrium of this picked out in the internal part of the system, resultant forces acting on this volume from the other parts are equal to zero. Under deformation the system is getting out from equilibrium state in which it had been initially. In this case there appear forces seeking to return the system to the equilibrium state. Also all points of the unit element displace under deformation and by U_x, U_y, U_z we denote the components of the displacement vector of the solid part.

This vector is defined here as the displacement of the skeletal frame considered to be uniform and averaged over the element. In a similar way we define displacement vector $\bar{U}_l$ determining a flow of liquid part of the cube. Due to two possible types of motion in He II, $\bar{U}_l$ breaks down into the sum of two parts

$$\bar{U}_l = \frac{\rho^s}{\rho}\bar{U}^s + \frac{\rho^n}{\rho}\bar{U}^n \tag{1}$$

corresponding to displacement of superfluid and normal components.

To establish relation between forces and accelerations we'll use generally acknowledged Lagrange formalism and concept of generalized coordinates. We assume that pores have less dimensions as compared with dimensions of the unit cube of the system, which we consider as an element. In turn, we assume that dimensions of the element of the system are less than the wavelength of the wave. We choose nine average displacement components of the system. As a result kinetic energy of the system per unit volume takes the following form:

$$2T = \rho_{11}(V_x^2 + V_y^2 + V_z^2) + 2\rho_{12}^s(V_x V_x^s + V_y V_y^s + V_z V_z^s) +$$
$$+ 2\rho_{12}^n(V_x V_x^n + V_y V_y^n + V_z V_z^n) + \rho_{22}^s\left[(V_x^s)^2 + (V_y^s)^2 + (V_z^s)^2\right] +$$
$$+ \rho_{22}^n\left[(V_x^n)^2 + (V_y^n)^2 + (V_z^n)^2\right]. \tag{2}$$

Expression (2) suggests statistic isotropy of the system, which implies that the directions x, y, z are equivalent and uncoupled dynamically.

Let's inquire into the nature of mass coefficients in expression (2). As kinetic energy is a positive definite quadratic form, mass coefficients satisfy the following inequalities:

$$\rho_{11} \gg 0; \quad \rho_{22}^s > 0; \quad \rho_{22}^n > 0;$$

6

$$\begin{vmatrix} \rho_{11} & \rho_{12}^{s} \\ \rho_{11}^{s} & \rho_{12}^{s} \end{vmatrix} > 0; \qquad \begin{vmatrix} \rho_{11} & \rho_{12}^{n} \\ \rho_{12}^{n} & \rho_{22}^{n} \end{vmatrix} > 0; \qquad \begin{vmatrix} \rho_{11} & \rho_{12}^{s} & \rho_{12}^{n} \\ \rho_{12}^{s} & \rho_{22}^{s} & 0 \\ \rho_{12}^{n} & 0 & \rho_{22}^{n} \end{vmatrix} > 0 . \qquad (3)$$

Let's assume there is no relative motion between solid and liquid as well as between components of liquid $V_x = V_x^{s} = V_x^{n}$. We examine motion in x-direction without loss of generality.

Then from (2) we have:

$$\rho_{sys} = \rho_{11} + \rho_{22}^{s} + \rho_{22}^{n} + 2(\rho_{12}^{s} + \rho_{12}^{n})$$

where ρ_{sys} represents the total mass of the superfluid helium-solid system per unit volume. If we denote density of a solid with ρ_{sol}, we have:

$$\rho_{sys} = \rho_{sol}(1 - \Phi) + (\rho^{s} + \rho^{n})\Phi = \rho_{sol} + \Phi(\rho^{s} + \rho^{n} - \rho_{sol}), \qquad (4)$$

where Φ is porosity. With q_x denoting total force acting on a solid part of unit volume and by Q_x^{s} and Q_x^{n} correspondingly total forces acting on superfluid and normal components of superfluid liquid per unit volume, then Lagrange's equations have the following form:

$$\frac{\partial}{\partial t}\left(\frac{\partial T}{\partial V_x}\right) = \frac{\partial}{\partial t}(\rho_{11}V_x + \rho_{12}^{s}V_x^{s} + \rho_{12}^{n}V_x^{n}) = q_x ,$$

$$\frac{\partial}{\partial t}\left(\frac{\partial T}{\partial V_x^{s}}\right) = \frac{\partial}{\partial t}(\rho_{12}^{s}V_x + \rho_{22}^{s}V_x^{s}) = Q_x^{s} , \qquad (5)$$

$$\frac{\partial}{\partial t}\left(\frac{\partial T}{\partial V_x^{n}}\right) = \frac{\partial}{\partial t}(\rho_{12}^{n}V_x + \rho_{22}^{n}V_x^{n}) = Q_x^{n} .$$

7

Let's lead Newton's equation for superfluid and normal components:

$$\Phi \rho^s \frac{\partial V_x^s}{\partial t} = Q_x^s ,$$

$$\Phi \rho^n \frac{\partial V_x^n}{\partial t} = Q_x^n .$$

(6)

Comparison of Eq. (6) with Eq. (3) and (5), when there is no relative motion between superfluid liquid and solid skeleton

$$V_x = V_x^s = V_x^n$$

yields

$$\Phi \rho^s = \rho_{22}^s + \rho_{12}^s; \qquad \Phi \rho^n = \rho_{22}^n + \rho_{12}^n;$$

$$(1-\Phi)\rho_{sol} = \rho_{11} + \rho_{12}^s + \rho_{12}^n \qquad \qquad .(7)$$

Coefficients ρ_{12}^s and ρ_{12}^n are mass parameters of coupling between a solid and correspondingly, superfluid and normal components of superfluid liquid or the term $\rho_{12}^{s(n)}$ describes the inertial (as opposed to viscous) drag that the fluid exerts on the solid as the latter is accelerated relative to the former and vice-versa. It is vividly seen if we examine the case when averaged displacement of both components of superfluid liquid are zero: $U_x^s = U_x^n = 0$. Then Eq. (5) takes the following form:

$$\frac{\partial \rho_{11} V_x}{\partial t} = q_x; \qquad \frac{\partial \rho_{12}^s V_x}{\partial t} = Q_x^s; \qquad \frac{\partial \rho_{12}^n V_x}{\partial t} = Q_x^n. \qquad (8)$$

Equations (8) show that when a solid is accelerated, the force $Q_x^s (Q_x^n)$ acting on superfluid (normal) component of liquid retards it,

8

which is characterized by coefficients ρ_{12}^s, ρ_{12}^n. As Q_x^s and Q_x^n act against acceleration of a solid, then
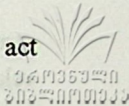
$$\rho_{12}^s < 0; \quad \rho_{12}^n < 0. \tag{9}$$

The first Eq. (8) shows that ρ_{11} is a total effective density of the solid moving in the He II. It consists of the solid own density $(1-\Phi)\rho_{sol}$ and additional mass ρ_a due to the fluid, so

$$\rho_{11} = (1-\Phi)\rho_{sol} + \rho_a. \tag{10}$$

The third relation from Eq. (7) gives

$$\rho_a = -\rho_{12}^s - \rho_{12}^n = \rho_a^s + \rho_a^n. \tag{11}$$

Finally we have:

$$\rho_{11} = (1-\Phi)\rho_{sol} + \rho_a^s + \rho_a^n,$$
$$\rho_{22}^s = \Phi\rho^s + \rho_a^s,$$
$$\rho_{22}^n = \Phi\rho^n + \rho_a^n, \tag{12}$$
$$\rho_a^s = -\rho_{12}^s > 0,$$
$$\rho_a^n = -\rho_{12}^n > 0.$$

Coefficients ρ_{11}, ρ_{22}^s, ρ_{22}^n, ρ_{12}^s, ρ_{12}^n that have been determined according to relations (9-12) ensure positive definite quadratic form of kinetic energy (2).

In the equations of motion (5) $\bar{q}$ is the force acting on the porous frame per unit volume, which is equivalent to the sum acting forces from surrounding liquid and skeleton. First of them equals to $-(1-\Phi)\nabla P$, taking into account that the porous frame occupies the fraction $(1-\Phi)$ of volume, where P is the fluid pressure. The second force during propagation of longitudinal waves (when we have only

9

stress-dilation deformation) may be written as $-\nabla P_{sc}$, where P_{sc} is related to the speed of longitudinal sound in the skeleton with formula

$$C_{sc}^2 = \frac{\partial P_{sc}}{\partial \rho_{sc}}.$$ (13)

Here ρ_{sc} is a mass density of porous frame and $\rho_{sc} = (1-\Phi)\rho_{sol}$. In Eq. (5) $\bar{Q}^n$ and $\bar{Q}^s$ correspondingly are forces acting on the normal and superfluid components per unit volume. Taking into consideration that fluid occupies fraction of volume Φ and the expression of forces acting on superfluid and normal component per unit volume [5], we have

$$\bar{Q}^n = -\Phi\left(\frac{\rho^n}{\rho}\nabla P + \rho^s\sigma\nabla T\right),$$

$$\bar{Q}^s = -\Phi\left(\frac{\rho^s}{\rho}\nabla P - \rho^s\sigma\nabla T\right),$$ (14)

where σ is entropy of unit fluid mass, and T is temperature. As there are three thermodynamic variables alongside with three velocities in equation of motion we lack three equations for completeness of the equation system. These equations are usually accepted to be the conservation laws of mass for skeleton and fluid as well as the conservation law of entropy superfluid liquid. They have the following form

$$\frac{\partial \rho_{sc}}{\partial t} + \nabla(\rho_{sc}\bar{V}) = 0,$$

$$\frac{\partial \rho}{\partial t} + \nabla(\rho^n\bar{V}^n + \rho^s\bar{V}^s) = 0,$$ (15)

$$\frac{\partial \rho\sigma}{\partial t} + \nabla(\rho\sigma\bar{V}) = 0.$$

10

In Eq. (5) we ignored dissipative processes. In our case the slipping of normal component of superfluid liquid with respect to pore walls is the main mechanism of dissipation. In most cases velocities of macroscopic motion are so low that dissipation is marginal. Such almost reversible processes might be described with the help of dissipative function. It means that the so - called dissipative forces or frictional forces being linear functions of velocities are to be added to the non-dissipative equations of motion where only forces acting on the system have been taken into account. Their forces might be represented in the form of derivatives by generalized velocities from some quadratic function of velocities or from the dissipative function. Then by analogy with Biot [3] about dissipative terms the equations of solid and normal component we have

$$\rho_{11}\dot{\vec{V}} + \rho_{12}^{s}\dot{\vec{V}}^{s} + \rho_{12}^{n}\dot{\vec{V}}^{n} + bF(\omega)(\vec{V} - \vec{V}^{n}) + \nabla P_{sc} + (1-\Phi)\nabla P = 0,$$

$$\rho_{22}^{n}\dot{\vec{V}}^{n} + \rho_{12}^{n}\dot{\vec{V}}^{n} - bF(\omega)(\vec{V} - \vec{V}^{n}) + \Phi\frac{\rho^{n}}{\rho}\nabla P + \Phi\rho^{s}\sigma\nabla T = 0. \quad (16)$$

The Poisseuille flow coefficient b is the ratio of total friction force to the average normal fluid velocity. Complex quantity $F(\omega)$ represents the deviation from Poisseuille friction as the frequency increases.

3. THE LONGITUDINAL WAVES IN LOW-FREQUENCY RANGE

In the low frequency limit normal component of superfluid liquid is completely locked to the matrix due to the viscosity and the pore frame and the normal fluid move together with a velocity $\vec{V}^{n} \neq 0$. In order to consider this situation we must exclude the friction force, the two equations content, and substitute these two equations by a non-equivalent one. Then we have $\vec{V}^{n} = \vec{V}$ in five equations that do not contain the viscosity force. So we derive five equations for five variables. We choose the following independent variables: $\vec{V}^{n} = \vec{V}$,

$\vec{V}^s$, P, P_{sc} and T. In the linear approximation we have the systems of equations:

$$\frac{1}{C_{10}^2}\dot{P} + \rho^n \operatorname{div}\vec{V}^n + \rho^s \operatorname{div}\vec{V}^s = 0$$

$$\frac{\sigma}{C_{10}^2}\dot{P} + \frac{\sigma^2 \rho^s \rho}{\rho^n C_{20}^2}\dot{T} + \rho\sigma \operatorname{div}\vec{V}^n = 0$$

$$\rho_{22}^s \dot{\vec{V}}^s + \rho_{12}^s \dot{\vec{V}}^n + \Phi\frac{\rho^s}{\rho}\nabla P - \Phi\rho^s\sigma\nabla T = 0 \tag{17}$$

$$\left(\rho_{11} + 2\rho_{12}^n + \rho_{22}^n\right)\dot{\vec{V}}^n + \rho_{12}^s\dot{\vec{V}}^s + \nabla P_{sc} + \left(1 - \frac{\rho^s}{\rho}\Phi\right)\nabla P + \Phi\rho^s\sigma\nabla T = 0$$

$$\frac{\partial\rho_{sc}}{\partial t} + \rho_{sc}\operatorname{div}\vec{V}^n = 0$$

We assume that along with any X-axis in propagating longitudinal waves all dynamical quantities vary according to the law $exp[i(\omega t - kx)]$, corresponding to a travelling wave, with wave number k and cyclic frequency ω. Then from the compatibility conditions for the system of equation (17) we deduce the dispersion relation:

$$\left(C^2 - \frac{C_{10}^2}{\Phi}\right)\left(C^2 - \frac{\rho^n}{\alpha_\infty\rho - \rho^s}C_{20}^2\right) +$$

$$+ \frac{\alpha_\infty\rho^{sc}}{\Phi(\alpha_\infty\rho - \rho^s)}(C^2 - C_{sc}^2)\left(C^2 - \frac{C_{40}^2}{\alpha_\infty}\right) = 0, \tag{18}$$

where $\alpha_\infty \geq 1$ is a purely geometrical quantity independent of solid or fluid densities and it can vary from unity (for straight pores parallel to the motion) to infinity for isolated pores or pores perpendicular to the motion. For the induced mass tensor per unit volume we took

$\rho_{12} = -(\alpha_\infty - 1)\Phi\rho_f$ [6].

$$C_{40}^2 = \frac{\rho^s}{\rho}C_{10}^2 + \frac{\rho^n}{\rho}C_{20}^2$$

is the fourth sound speed without taking into account the tortousity or the fourth sound speed in straight capillaries filled with He II, $C = \omega / k$ is unknown velocity of longitudinal waves.

Two longitudinal sounds are the solutions of dispersion equation (18), when inequalities are valid

$$C_{20}^2 << C_{sc}^2 << C_{10}^2. \qquad (19)$$

The first of these sounds has higher propagation speed and is similar to the first sound in the bulk fluid. The normal and superfluid components of the helium oscillate in phase with one another in this sound though not at the same velocity. This longitudinal wave is called fast mode and it is intermediate one between the first and the fourth sound

$$C_{14}^2 = \frac{(\alpha_\infty\rho - \rho^s) C_{10}^2 + \rho^{sc}C_{40}^2}{\Phi(\alpha_\infty\rho - \rho^s) + \alpha_\infty\rho^{sc}}. \qquad (20)$$

The second solution is an oscillation of a deformation of the porous frame together with the normal fluid combined with a simultaneous out of phase motion of the superfluid component. This slower mode is similar to the second sound

$$C_{2sc}^2 = \frac{C_{20}^2 + \dfrac{\rho^{sc}}{\rho^n}\dfrac{\rho^s}{\rho}C_{sc}^2}{\dfrac{\alpha_\infty \rho - \rho^s}{\rho^n} + \dfrac{\rho^{sc}}{\rho^n}\dfrac{\rho^s}{\rho}} \qquad (21)$$

The dispersion equation (18) transfers into expressions of work [7], where waves propagating in the system superfluid-aerogel have been studied. It should be noted that an intermediate mode between the first and the fourth sound and a mode similar to the second sound propagate in this system. Our results are more general and give a possibility to study dependence of velocities on porosity and tortuosity.

CONCLUSIONS

The equations for the propagation of longitudinal waves in a system porous media –He II, for any significance of frequencies are deduced. The obtained equations are utilized in particular case – for low frequency range. The velocities of propagating sounds for any value of porosity and tortuosity are found. Two solutions the first of which is a combination of the first and fourth sounds are derived. Temperature oscillations are possible in the second sound.

REFERENCES

1. D. L. Johnson. Sen. Phys. Rev B. **24**, 5, 1981, 2486.
2. M. A. Biot. Journal of the Acoust. Soc. of America. **28**, 2, 1956, 168.
3. M. A. Biot. Journal of the Acoust. Soc. of America. **28**, 2, 1956, 179.
4. Thomas J. Plona. Appl. Phys. Lett. **36**, 4, 1980, 259.
5. D. R. Tilley, J. Tilley. Superfluidity and Superconductivity. 1974. Wiley.
6. J. G. Berryman. Appl. Phys. Lett. **37**, 1980, 382.

7. M. J. Mckenna, T. Slawecki, J. D. Maynard. Phys. Rev. Lett. 66, 14, 1991, 1878.

Georgian Academy of Sciences
Institute of Cybernetics

შ. კეკუტია, ნ. ჩხაიძე, ო. ტყეშელაშვილი

გრძივი ბგერების გავრცელების განტოლებები სისტემაში ზეღენადი კელიუმი-ფოროვანი გარემო და გავრცელებადი ბგერების სიჩქარეები დაბალი სიხშირეების ზღვარში

დასკვნა

მიღებულია გრძივი ბგერების გავრცელების განტოლებები სისტემაში ფოროვანი გარემო-ზეღენადი He^4 სიხშირის ნებისმიერი მნიშვნელობებისათვის. მიღებული განტოლებები გამოყენებულია კერძო შემთხვევისათვის, რომელიც შეესაბამება დაბალ სიხშირეებს. ნაპოვნია გავრცელებადი ბგერების სიჩქარეები ნებისმიერი ფოროვნობისა და დაკლაკნილობისათვის. მიღებულია ორი ამოხსნა, რომელთაგან პირველი წარმოადგენს პირველი და მეოთხე ბგერის კომბინაციას, მეორე ამოხსნაში კი ნაჩვენებია, რომ შესაძლებელია ტემპერატურის რხევა.

PROPAGATION OF WAVES IN SUPERFLUID-SATURATED POROUS MEDIA
(High and low frequency ranges)

T. Karchava, Sh. Kekutia, N. Chkhaidze

ABSTRACT. The linearized motion equation system of ideal liquid filled with porous media is constructed, when solid component with ρ_{sl} density motions with $\bar{\upsilon}_{sl}$ velocity and liquid with ρ_f density motions with $\bar{\upsilon}_f$ velocity. Expression of porous medium tortuosity is obtained on the basis of imposition of additional mass. Influence of tortuosity on sound velocity of propagating waves has been determined. The results obtained in work are generally true when the condition $\rho_f \angle \rho_{sl}$ is fulfilled.

Analogously hydrodynamic equation system of motion for He II saturated porous media in high and low frequency limits has been obtained. The solution of these equations is as follows: the first, the second and the fourth sound speeds decrease n-times due to porous media, where n^2 coincides with the tortuosity, when $\rho_f \angle \rho_{sl}$. It is shown that the same conclusion may be done for viscosity wave.

1. INTRODUCTION

It is important to study acoustic nature of He^4 to establish its other properties. He II is described by two-velocity hydrodynamic equation system [1,2], which appropriates to the model, according to which He II is performed with two motions: one normal - with $\bar{\upsilon}_n$ velocity and ρ_s density and the second - superfluid with $\bar{\upsilon}_s$ velocity and ρ_s density. The total density is $\rho = \rho_s + \rho_s$. In case of unlimited geometry this system of equations gives three wave solutions: the first sound, where $\bar{\upsilon}_n = \bar{\upsilon}_s$, i.e. liquid oscillates as entire and generally follows with oscillating of pressure and density. In the process of the

second sound propagation superfluid and normal components of He II are oscillating in the opposite phase. In this case condition $\bar{j} = \rho_s \bar{v}_n + \rho_s \bar{v}_s = 0$ is fulfilled and temperature and entropy oscillate. The third solution is viscous wave, which is provoked by the existence of perpendicular gradient of normal velocity direction. The first and viscous waves also exist in usual liquid, when the second sound is characteristic only for superfluid liquid.

2. WAVE PROCESSES IN POROUS MEDIA

The character of sounds propagating in superfluid helium is changing in conditions of limited geometry and is connected with partial or complete dragging of normal component [3-8]. Complete dragging of normal component of superfluid liquid is noted when the fourth weakly damped sound propagates [3,4,7]. This is characteristic only for superfluid liquid. Waves propagation in He II has been properly studied when parallel plane walls or cylindrical capillaries were filled with superfluid He^4. The obtained results describe qualitatively data of many experiments, when He II is in such geometrical conditions that differ from the above mentioned regular geometry. But in case of regular geometry influence of walls in high frequency range is too little. Sound velocities are significantly decreased in porous medium filled with He II [9,10], i.e. influence of porous particles remain. Hydrodynamic linerized equation of He II must be solved and boundary conditions are to be specified for this aim. Besides, solid component motion must be taken into account, velocity of which differs from liquid velocity. This is reflected in boundary conditions as follows:

$$[\bar{v}_n, \bar{n}] = [\bar{v}_{sl}, \bar{n}] , \qquad (1)$$
$$(\bar{v}_n, \bar{n}) = (\bar{v}_{sl}, \bar{n}) , \qquad (2)$$
$$(\bar{v}_s, \bar{n}) = (\bar{v}_{sl}, \bar{n}) . \qquad (3)$$

$\bar{n}$ is normal of touching solid body's surface and He II.

It should be noted that surfaces of solid components and liquid are occasional, this problem is unsolvable. But we have to find the way

out. In particular, if we analyze results of numerous theoretical studies of propagation of the sound in superfluid liquid, the first (1) condition in regular tasks plays the main role, when conditions (2) and (3) play a passive role. In porous media (2) and (3) boundary conditions play a particular role. That's why we shall consider a case when condition (1) might be neglected. In this case both superfluid and normal components might be considered ideal liquids. Besides, we shall not consider dissipative processes that do not contribute to attenuation of sounds and do not influence velocity of the first and the second sounds. These conditions are being fulfilled in high frequency limit $\omega \gg \omega_c$, where $\omega_c = (2\eta / \rho_n \Lambda^2)$. Here η is viscosity and Λ - hydraulic radius [11].

In order to take into account conditions (2-3) we present the system: porous media - liquid as a single hydrodynamic system, namely, as a mixture of solid particles and liquid with ρ_m density and $\bar{\upsilon}_m$ velocity. Then the continuity equation for this system is as follows [1]

$$\frac{\partial \rho_m}{\partial t} + \mathrm{div}(\rho_m \bar{\upsilon}_m) = 0, \tag{4}$$

where $\rho_m \bar{\upsilon}_m$ is the density of the mixture impulse. If we consider volume of mixture V_o, then ϕV_o is the liquid volume, $(1 - \Phi)V_0$ is a share of volume V_o of a solid component, then we have

$$\rho_m = \phi \rho_f + (1 - \phi)\rho_{sl}. \tag{5}$$

During the sound propagation ideal liquid acquires velocity $\bar{\upsilon}$ and solid component acquires $\bar{u}$ velocity, so

$$\rho_m \bar{\upsilon}_m = \phi \rho_f \bar{\upsilon} + (1 - \phi)\rho_{sl}\bar{u}. \tag{6}$$

Despite the fact we take into account motion of a solid component, we neglect change of ϕ below. It is justified by the fact that

18

dimensions of a solid component are larger than its displacement. If $\rho_m c$ is a mass of a solid component per unit of the mixture volume, then we have the equation

$$\frac{\partial(\rho_m c)}{\partial t} + \text{div}(\rho_m c \vec{u}) = 0, \tag{7}$$

where c is concentration of mass of solid component and $\rho_m c =$
$= (1 - \phi) \rho_{sl}$.
    Then, if it is foreseen (3-4) we'll obtain:

$$\frac{\partial \rho_f}{\partial t} + \text{div}(\rho_f \vec{\upsilon}_m) = 0, \tag{8}$$

$$\frac{\partial \rho_{sl}}{\partial t} + \text{div}(\rho_{sl} \vec{\upsilon}_m) = 0. \tag{9}$$

Consequently the continuity equation of ideal liquid, which fills the porous media, remains unchangeable in the above-cited model. The continuity equation of entropy is not subjected to changes either due to the fact that heat transference between liquid and solid particles is neglected. Thus it follows from equation (6) that equation of motion of unit mixture volume has the following form:

$$\phi \frac{\partial(\rho_f \vec{\upsilon})}{\partial t} + (1 - \phi) \frac{\partial(\rho_{sl} \vec{u})}{\partial t} = \vec{f} \tag{10}$$

where $\vec{f} = -\nabla P = -(1 - \phi)\nabla P - \phi\nabla P$ is a force acting per unit of mixture volume both from the liquid side and from the solid side. The force caused by the solid deformation, which is neglected due to a proposed model, is not taken into account. This force is necessary when infinite claster of a solid is observed which is achieved for a certain porosity value. Comparing experimental data with the results of work we receive $\phi_m = 0.35$.
    Thus results of this study are justified for $0.35 < \phi < 1$.

19

If a solid is not oscillated with the liquid in a process of sound propagation, the equation of a solid mass M and volume V_{sl} has the following form (see [1]):

$$\frac{\partial(Mu_i)}{\partial t} = \rho_f V_{sl} \frac{\partial v_i}{\partial t} - m_{ik} \frac{\partial(u_k - v_k)}{\partial t} . \tag{11}$$

Here boundary conditions (2,3) are taken into account, besides m_{ik} tensor of the added mass is introduced. Its form depends on a concrete form of a solid and it is proportional to the liquid density [1]. We think that equation (11) is justified for all solid particles in volume V_0, the total amount of their masses equals M. If we take $m_{ik} = m\delta_{ik}$, then we obtain:

$$\frac{\partial \bar{u}}{\partial t} = \frac{\rho_f + \Delta\rho}{\rho_{sl} + \Delta\rho} \frac{\partial \bar{v}}{\partial t} \tag{12}$$

where $\Delta\rho$ is induced mass density per unit volume of the solid component and $\Delta\rho = \dfrac{m}{(1-\phi)V_O}$, if we bear in mind (12), equation (10) obtains the following form:

$$n^2 \rho_f \frac{\partial \bar{v}}{\partial t} = \bar{f} \tag{13}$$

where

$$n^2 = \phi + (1-\phi)\frac{1 + \Delta\rho/\rho_f}{1 + \Delta\rho/\rho_{sl}} . \tag{14}$$

Expression (13) is the motion equation of ideal liquid filling the porous media and $\Delta\rho$ depends on the form of a solid body surface. For example, when solid sphere oscillates in the ideal liquid $\Delta\rho = \rho_f/2$ and when the infinite cylinder oscillates with the axis perpendicular to the direction of the sound propagation, the density of induced mass has the form $\Delta\rho = \rho_f$, etc. In our case it is impossible

20

to calculate $\Delta\rho$ due to understandable reasons. But we can always consider $\Delta\rho = K\rho_f$, where K is a constant value for the solid surface of this form. Its estimated value might be established with the help of expression (14) if n is measured experimentally. Quantity n is a coefficient of the sound refraction for the porous media-ideal liquid system. As we can see in equation (14) n simultaneously depends on density of liquid and a solid body. Formally, when $\rho_f > \rho_{sl}$ proceeding from (14), then $n < 1$. It means, that velocity of the sound propagation increases, but in this case velocity of a solid body is larger than liquid velocity [1], which does not correspond to the present model. When $\rho = \rho_{sl}$, $n = 1$. If $\rho_f < \rho_{sl}$, then $n > 1$ and velocity of the solid component is less than liquid velocity. In this case change of ϕ is ignored. Also when $\rho_f < \rho_{sl}$, n^2 is no more dependent on the system of solid component density and we have

$$\alpha = \lim_{\rho_{sl} \to \infty} n^2 = 1 + (1 - \phi)\frac{\Delta\rho}{\rho} = 1 + (1 - \phi)K . \qquad (15)$$

Value α depends on properties of a solid body and that's why it is real tortuosity of porous media. Proceeding from (15) α is always larger than 1. Dependence between α and n is as follows:

$$\alpha = \frac{(1 - \phi)n^2 - (n^2 - \phi)\rho_f / \rho_{sl}}{(1 - \phi)^2 - (n^2 - \phi)\rho_f / \rho_{sl}} . \qquad (16)$$

Let's study porous media filled with superfluid He^4. Then we shall have the following two equations instead of equation (14):

$$\frac{d(Mu_i)}{dt} = V_{sl}\frac{dj_i}{dt} + \frac{m_{ik}}{\rho}\frac{dj_k}{dt} - m_{ik}\frac{du_k}{dt} , \qquad (17)$$

$$\frac{d(Mu_i)}{dt} = \rho V_{sl}\frac{dv_{si}}{dt} + m_{ik}\frac{dv_{sk}}{dt} - m_{ik}\frac{du_k}{dt} . \qquad (18)$$

21

Finally, for superfluid liquid filling the porous media we shall have the following equations taking into account equations (17) and (18)

$$\frac{\partial \rho}{\partial t} + \operatorname{div}\vec{j} = 0,$$ (19)

$$n^2 \frac{\partial \vec{j}}{\partial t} + \nabla p = 0,$$ (20)

$$n^2 \frac{\partial \vec{\upsilon}}{\partial t} + \nabla \mu = 0,$$ (21)

$$\frac{\partial(\sigma\rho)}{\partial t} + \operatorname{div}(\rho\sigma\vec{\upsilon}_n) = 0,$$ (22)

here μ is a chemical potential of the system and due to the fact that we neglect change of ϕ we have: $d\mu = \frac{1}{\rho}dp - \sigma dT$, where T is temperature, σ-entropy of the unit of liquid volume. A system of equations (19-22) is truthful for frequencies $\omega > \omega_c$. A system of equations (19-22) has two solutions. The first propagates with speed:

$$U_{1p} = \frac{1}{n}\sqrt{\left(\frac{\partial p}{\partial \rho}\right)_\sigma}$$ (23)

during its propagation density and pressure oscillate. We have the following relations for oscillating values:

$$\frac{\upsilon_n}{\upsilon_s} = 1; \quad \frac{T'}{\upsilon_s} = 0; \quad \frac{p'}{\upsilon_s} = \rho n^2 U_{1p}; \quad \frac{\rho'}{\upsilon_s} = \frac{\rho}{U_{1p}}.$$ (24)

The second solution has the following form:

$$U_{2p} = \frac{1}{n}\sqrt{\sigma^2 \rho_n / \rho_s \left(\frac{\partial \sigma}{\partial T}\right)_\rho}$$ (25)

22

In this wave the ratio of oscillating quantities equals to:

$$\frac{\upsilon_n}{\upsilon_s} = -\frac{\rho_n}{\rho_s}; \quad \frac{T'}{\upsilon_s} = -n^2 \frac{U_{2p}}{\sigma}; \quad \frac{\sigma'}{\upsilon_s} = -\frac{\rho_n}{\rho_s}\frac{\sigma}{U_{2p}}; \quad \frac{p'}{\upsilon_s} = 0 . \quad (26)$$

It should be noted that low frequencies solution might be obtained from equations (24-26). Due to the fact that we do not take into account dissipation, then $\vec{\upsilon}_n = \vec{u}$ and within $\omega << \omega_c$ equations of hydrodynamics have the following form:

$$\frac{\partial \rho}{\partial t} + \rho_s \text{div}\vec{\upsilon}_s = 0 ,$$

$$n^2 \frac{\partial \vec{\upsilon}_s}{\partial t} + \nabla\mu = 0 , \quad (27)$$

$$\frac{\partial(\rho\sigma)}{\partial t} = 0$$

Proceeding from this

$$U_{4p}^2 = \frac{\rho_s}{\rho}U^2_{1p} + \frac{\rho_n}{\rho}U^2_{2p} . \quad (28)$$

This wave solution is called the fourth sound and U_{1p}, U_{2p} is presented by formula (23,25). Consequently, speeds of sounds decrease by n times in the superfluid liquid filling the porous media. According to [12], experimental data are well described if $n = (2-\phi)^{1/2}$. This relation is obtained from (15), if $\nabla\rho/\rho = 1$ and $\rho << \rho_{sl}$. These conditions are found in the above experiments.

Now we shall consider peculiarity of viscous waves propagation in the liquid-porous media system. Therefore, now we study infinite flat surface oscillating in the porous media filled with liquid according to the law $u = u_o e^{-iwt}$. This surface is in flat yz and a viscous wave

propagates in $x > 0$ direction. We shall use the approach, developed in [1, 24], where the equation

$$\frac{\partial \upsilon_y}{\partial t} = \frac{\eta}{\rho_f} \frac{\partial^2 \upsilon_y}{\partial x^2} \tag{29}$$

is obtained for the common liquid not in the porous media and liquid velocity meets the following boundary conditions:

$$\upsilon_z = 0, \ \upsilon_x = 0, \ \upsilon_y = u, \text{ when } x = 0. \tag{30}$$

As multiplier n^2 appears before the velocity derivative in the porous media, equation (29) changes into the following equation

$$n^2 \frac{\partial \upsilon_y}{\partial t} = \frac{\eta}{\rho_f} \frac{\partial^2 \upsilon_y}{\partial x^2} \tag{31}$$

and a wave vector of a viscous wave will equal

$$k_3 = n\sqrt{\frac{iw\rho_f}{\eta}} = k_{30}.n, \tag{32}$$

where n is presented by the (15) relation. Consequently, a viscous wave velocity decreases by n-times in the porous media like the first, second and the fourth sounds. In case with He II ρ_f is changed by ρ_n in (32).

CONCLUSIONS

Thus, the linerized motion equation system of the ideal liquid and superfluid helium filled porous media is constructed. For this system there is obtained an expression of tortuosity, which depends on porosity and ratio of induced mass to density of liquid. The speeds of

24

the first, fourth and second sounds decrease n-times due to porous media.

REFERENCES

1. L. D. Landau, I.M. Lipchits. Hidrodinamika. Moscow, 1998, (Russian).
2. I. M. Khalatnikov. Teoria Sverkhtekuchesti. Moscow, 1988, (Russian).
3. S. J. Putterman. Superfluid Hydrodynamics. Amsterdam-London-New York. 1974.
4. I. N. Adamenko, M.I. Kaganov. JETP. 53, 1965, 615.
5. K. R. Atkins. Phys. Rev. 133, 1965, 962.
6. B.N. Esselson, N.E. Diumin. JETP. 51, 1966, 1064.
7. D.G. Sanikidze, I. N. Adamenko, M.I. Kaganov. JETP. 52, 1967, 584.
8. T. A. Karchava, D.G. Sanikidze. JETP. 55, 1968, 1809.
9. D.L. Johnson, T.J. Plona, H. Kojima. Physics and chemical porous media. 1987,233, New-York.
10. D.L. Johnson, T.J. Plona, R. Dashen. J.Fluid Mech.,176, 1987, 376.
11. J. Happel, H. Brenner. Low Reynolds number hydrodynamics. 1965.
12. K. Shapiro and I. Rudnick. Phys.Rev., 137, No. 5A,1965, 1383.

Georgian Academy of Sciences
Institute of Cybernetics

თ. ქარჩავა, შ. კეკუტია, ნ. ჩხაიძე

ბგერების გავრცელება ზედენადი სითხით შეჭვჭებულ
ფოროვან გარემოში

დასკვნა

აგებულია ფოროვან გარემოში მყოფი ჩვეულებრივი
სითხის და ზედენადი სითხის გაწრფივებულ განტო-
ლებათა სისტემა მაღალსიხშირულ ზღვარში, რის გამოც
ეს სითხეები შეიძლება ჩაითვალოს იდეალურ სითხეებად.
ამის გარდა შრომის შედეგები სამართლიანია, როცა
სითხის სიმკვრივე p_f ნაკლებია მყარი კომპონენტის p_{se}
სიმკვრივეუბზე. მიღებულია ფოროვანი გარემოს დაკლა-
ნილობის α გამოსახულება, რომელიც დამოკიდებულია
ფოროვნების კოეფიციენტზე და მყარი კომპონენტის
მოცულობის ერთეულზე მოსული მიერთებული მასისა და
სითხის სიმკვრივეის ფარდობაზე. ნაჩვენებია, რომ ამ
პირობებში ფოროვანი გარემოს გავლენით ზედენად
სითხეში და ჩვეულებრივ სითხეში გავრცელებადი
ბგერების (პირველი და მეორე ბგერები, ბლანტი ტალღა)
სიჩქარეები მცირდება n-ჯერ. n დაკავშირებულია ფორო-
ვანი გარემოს დაკლაკნილობასთან და $n^2 - \alpha$, როცა
$p_f - p_{se}$. მიღებულია დაბალსიხშირულ ზღვარში ფოროვან
გარემოში მყოფი ზედენადი სითხის ჰიდროდინამიკურ
განტოლებათა სისტემა, რომლის ტალღური ამოხსნის,
მეოთხე ბგერის სიჩქარეც მცირდება n-ჯერ.

USE OF FEED-BACKS FOR DEFINITION OF A MODE OF METEOROLOGICAL SIZES IN SURFACE LAYER OF THE ATMOSPHERE

Z. Khvedelidze, A. Chitaladze, R. Danelia, N. Ramishvili

ABSTRACT. The connection between radiation balance of the Earth and air temperature was established on the basis of feedback between meteorological elements. The singularity of relief of Georgia with an angular variation of exposure was stipulated. The findings of investigation will be utilized for an improvement of problems of solar power of Georgia.

For the solution of many practical problems (diurnal variation of air temperature, radiation balance of a surface of the Earth, night frost, air pollution) it is necessary to establish intercommunications in a surface layer (10 – 100 m) between meteorological elements, turbulence of air, cloudiness and the Earth's surface roughness.

Internal factors which cause a formation and modification of meteorological elements, are in tight correlation, strengthen and loosen the influence on the basis of feed-backs [1]. Of feed-back systems for mountain regions (Caucasus) the following connections are selected:

a) Temperature – (dampness – cloudiness). Naturally, the increase of air temperature mass ($\Delta T > 0$) increments an absolute dampness ($\Delta a > 0$). The cloudiness ($\Delta n > 0$) is incremented. Dampness - the water vapor intensively swallows an energy in infrared band, and the clouds reflect an incident solar radiation and decrease it ($\Delta R < 0$).

Simultaneously, the increase of cloudiness ($\Delta n > 0$) causes the increase of an absorption of long wavelength effective radiation going out from surface ($\Delta E < 0$). All this at last causes abatement of temperature ($\Delta T_s < 0$) This process can be presented under the following scheme:

$$\rightarrow \Delta T > 0 \rightarrow \Delta a > 0 \rightarrow \Delta T < 0 \rightarrow \leftarrow$$

$$\Delta T_s > 0 \rightarrow \Delta n > 0 \begin{cases} \rightarrow \Delta R < 0 \rightarrow \Delta T_s < 0 \\ \rightarrow \Delta E_0 < 0 \rightarrow \Delta T_s < 0 \end{cases}$$
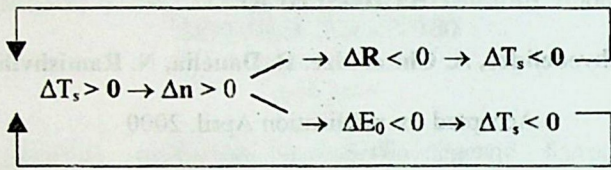
b) Temperature - albedo. The abatement of temperature of cover of the Earth causes the increase of precipitation ($\Delta T_s < 0$), formation of snowfalls and ices. All this increments an albedo ($\Delta A_s > 0$). The increase of an albedo decreases a solar radiation, what causes abatement of temperature ($\Delta T_s < 0$). In that way a positive feed-back is formed, which causes an increase of initial perturbation

On the basis of reduced feed-backs we shall consider mathematical model of diurnal variation of temperature in connection with a radiation balance and albedo for locality of Georgia. In model the relief originality of region with entering an angle of exposure will be stipulated. That represents physico-mathematical novelty of this model.

Assume that in an equation of motion advective terms, force effect of Coriolis and vertical component of the wind speeds are small and it is possible to neglect them. In that case it is possible to write a main system an equation of a task as follows [2]:

$$\frac{\partial U}{\partial t} = -\frac{1}{\rho}\frac{\partial p}{\partial x} + \frac{\partial}{\partial z}\left(k\frac{\partial U}{\partial z}\right), \qquad \frac{\partial q}{\partial t} = \alpha_q \frac{\partial}{\partial z}\left(k\frac{\partial q}{\partial z}\right),$$

$$\frac{\partial v}{\partial t} = -\frac{1}{\rho}\frac{\partial p}{\partial y} + \frac{\partial}{\partial z}\left(k\frac{\partial v}{\partial z}\right), \qquad \frac{\partial b}{\partial t} = k\Psi + \alpha_b \frac{\partial}{\partial z}\left(k\frac{\partial b}{\partial z}\right) - \varepsilon, \qquad (1)$$

$$\frac{\partial \theta}{\partial t} = \alpha_\theta \frac{\partial}{\partial z}\left(k\frac{\partial \theta}{\partial z}\right), \qquad \frac{\partial T_l}{\partial t} = \alpha \frac{\partial^2 T_l^2}{\partial z^2}.$$

For closure of a system (where 8 unknowns) are possible to use semiempirical relations of Kolmogorov:

$$k = l\sqrt{b}, \qquad \varepsilon = \frac{b\sqrt{b}}{l}, \qquad L = 2\kappa lc^{1/4}\frac{\Psi}{\partial\Psi/\partial z},$$

$$\Psi = \left(\frac{\partial u}{\partial z}\right)^2 + \left(\frac{\partial v}{\partial z}\right)^2 - \alpha_T\frac{g}{T}\frac{\partial\theta}{\partial z}, \tag{2}$$

where U, V are horizontal components of wind speed, accordingly on an axis and ρ air density; P atmospheric pressure; k turbulence coefficient; Z vertical coordinates; Θ potential temperature; q specific humidity; l scale of turbulence; ε a dissipation energy; b kinetic energy of a turbulence; $\alpha_b = k_b/k$, $\alpha_\theta = k_\theta/k$, $\alpha_q = k_q/k$ - turbulence coefficient of heat, damp and momentum; κ constant of Karman, $c^{1/4}$ the stationary value is introduced as a matter of convenience.

On the physical basis the solution of a problem should have periodic character. Therefore in the initial moment (t = 0) values can not be obtained. As to a boundary requirement, they will be posed for a level Z = 0.

Concretely, these requirements look like:

when Z = 0

$$u(z) = v(z) = 0, \tag{3}$$

$$\Theta(Z)\big|_{Z\to 0} = T_1(Z)\big|_{Z\to 0} = \Theta_0. \tag{4}$$

when $Z \to \infty$

$$U = U_g, \quad V = V_g,$$

$$\Theta(Z) = \Theta_H, \quad T_1(\zeta)\big|_{\zeta\to\infty} = T, \tag{5}$$

$$q(Z) = \big|_{z\to\infty} = 0, \quad b(z)\big|_{Z\to\infty} = 0.$$

Here U_g and V_g the values of a geostrophic wind, are considered. (5) indicates that daily fluctuation of meteorological elements gradually decreases on the altitudes and in high altitudes they are

29

constant. Let's consider a feed-back of air temperature and radiation balance, taking into account a relief singularity of Georgia. It is admissible, that the turbulence factor k is a non-constant magnitude and depends on an angle of exposure of a mountain:

$$k = k_0 \cos \alpha \qquad (6)$$

where α is changed in interval 0^0 - 50^0. Let's take model gradient magnitudes depending on - α. In boundary conditions the total of streams of heat, of dampness and quantity of movement is equal to a radiation balance [3,4] of the Earth.

$$-k\rho c_p \cos\overline{\alpha} \frac{\partial\Theta}{\partial Z}\Big|_{z\to 0} - Lk\rho\cos\overline{\alpha}\frac{\partial q}{\partial z}\Big|_{z\to 0} - a\rho_1 c_1 \frac{\partial T_1}{\partial\zeta}\Big|_{\zeta\to 0} =$$

$$= \overline{R} + \sum_{n=1}^{\infty}(R_n' \cos n\omega t + R_n'' \sin n\omega t) \qquad (7)$$

where $\overline{R}$ is daily average magnitude of a radiation balance, R_n' amplitude of its daily fluctuation, C_p specific heat capacity at constant pressure, ρ_1 density of soil, C_1 heat capacity of soil, $\omega = 2\pi/T$ frequency of oscillation, a constant, L specific vaporization heat. It is admissible, that the daily fluctuation of a radiation balance is described by a cosine, and the influence of an albedo is envisioned in effective radiation of the Earth. Taking into account physical properties of a ground surface and above-stated assumptions, the problem reaches a solution of a following set of equations [2,5]:

$$\frac{\partial\Theta}{\partial t} = k\cos\overline{\alpha}\,\frac{\partial^2\Theta}{\partial Z^2}, \qquad (8)$$

$$\frac{\partial T_1}{\partial t} = a\frac{\partial^2 T_1}{\partial z^2}. \qquad (9)$$

Boundary conditions:

$$\theta(t,z)\big|_{z=0} = T_1(t,\zeta)\big|_{\zeta=0} \quad \zeta = 0,$$ (10)

$$\theta(t,z)\big|_{z\to 0} = \Theta_H, \qquad T_1(t,\zeta)\big|_{\zeta\to\infty} = T_1(\zeta),$$ (11)

$$-k\rho c_p \cos\overline{\alpha}\,\frac{\partial\Theta}{\partial Z}\Big|_{z\to 0} - a\rho_1 c_1 \frac{\partial T_1}{\partial\rho\varsigma}\Big|_{\zeta\to 0} -$$

$$-Lk\rho\cos\overline{\alpha}\,\frac{\partial q}{\partial z}\Big|_{z\to 0} = \overline{R} + R_1\cos\omega t.$$ (12)

The theoretical solution of this problem is yielded [2; 4; 5]. For daily variation of air temperature the following association is obtained

$$T(0,t) = T_0 + A_1 \cos\left(\omega t - \frac{T}{2}\eta_0 - \varphi\right)$$ (13)

where φ is initial phase; η_0 parameter of detention, which depends on the form of a relief and from an altitude of sea level, T is period (day). Solution of the given problem was carried out by the numerical methods and the outcomes were compared to actual values.

For establishment of feed-back between radiation of the Sun and the air temperatures in various regions of Georgia (Telavi, Tbilisi, Sukhumi, Anaseuli) were taken the data of temperature and cloudiness (in central months of a season). On the basis of the formulas (8) and (9) the daily variation of radiation and temperature, and also their extreme values were calculated. In Figs. 1.2 these dependences are given. The appropriate precise values are applied. The error of radiation amounts to 20 %, and for temperature - 10 - 15 %. (the dampness and stream of heat was not stipulated to the formula (8)). As it is visible on the graphs and in calculations, a feed-back between these meteorological magnitudes are obvious (coefficient of correlation does not exceed 0,75). In calculations of gradient values of

31

Tbilisi

27 January, cloudiness 2 ball
max R_1=0.25, t=12hr. R_2=0.29, t=12hr
min R_1=-0.05, t=3hr. min R_2=-0.07, t=1hr

18 April, cloudiness 2 ball
max R_1=0.51, t=12hr. R_2=0.62, t=12hr
min R_1=-0.001, t=6hr. min R_2=-0.03, t=18hr

5 July, cloudiness 2 ball
max R_1=0.64, t=12hr. R_2=0.63, t=12hr
min R_1=-0.03, t=21hr. min R_2=-0.03, t=24hr

15 September, cloudiness 0 ball
max R_1=0.54, t=12hr. R_2=0.54, t=12hr
min R_1=-0.03, t=24hr. min R_2=-0.03, t=18hr
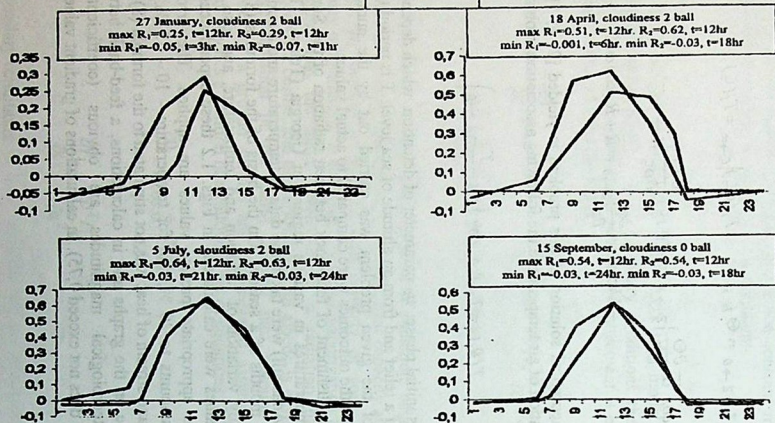
Fig.1. R_1 - calculated data; R_2 - experimental data

Anaseuli

1 December, cloudiness 0 ball
max R_1=0.35, t=15hr. R_2=0.35, t=12hr
min R_1=-0.04, t=24hr. min R_2=-0.07, t=18hr
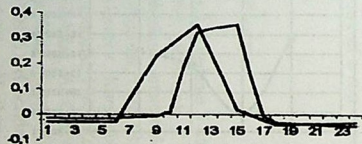
27 April, cloudiness 0 ball
max R_1=0.83, t=12hr. R_2=0.84, t=12hr
min R_1=-0.05, t=21hr. min R_2=-0.06, t=1hr
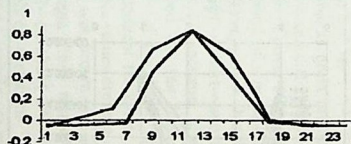
6 August, cloudiness 0..2 ball
max R_1=0.46, t=15hr. R_2=0.46, t=15hr
min R_1=-0.05, t=21hr. min R_2=-0.07, t=1hr
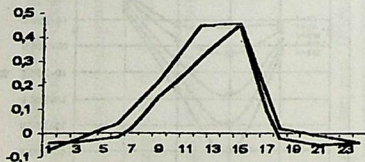
10 October, cloudiness 2 ball
max R_1=0.61, t=12hr. R_2=0.38, t=12hr
min R_1=-0.04, t=18hr. min R_2=-0.07, t=18hr
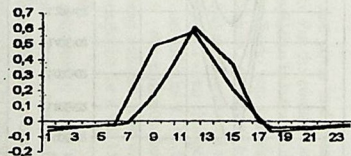
Fig.2. R_1 - calculated data; R_2 - experimental data.

33
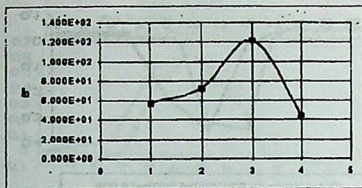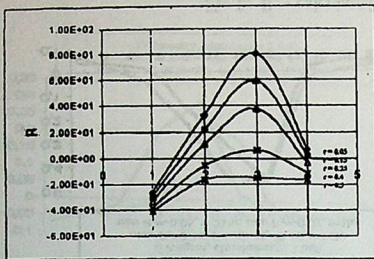
Fig.3
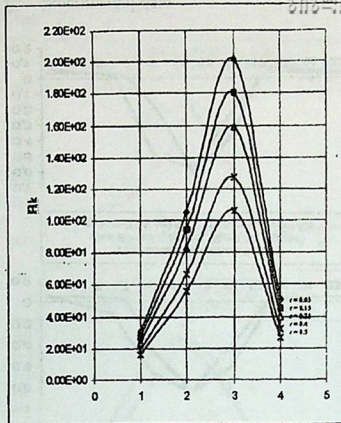
Fig.4

meteorological magnitudes the account of relief features with importation of an angle of exposure has increased an accuracy of connection on 5 -7 %.

For feed-backs great importance has also cover and grain of the Earth's surface and difference of an albedo. For the count of influence a modification of cover of the Earth, the radiation balance of the Earth for a broad band of a modification of an albedo was calculated [6]. From Fig. 3.4 is apparent, that the less reflection property of a surface, the more sharply a short-wave part of a radiation balance and radiation balance R_S and R increase. The considerable seasonal change R_S and R is observed for the least value of an albedo r = 0,05. At magnification of an albedo up to = 0,5 the radiation balance is practically identical for spring, summer and autumn. The calculated and observable values are in good correspondence for r = 0,15 and r = 0,85 (Tbilisi, wet, brown soil, small forest).

In Georgia the meteorological magnitudes are observed approximately on about 60 meteorological stations, but performance of the Sun all on 6 stations. The reduced technique ground of feedbacks gives the possibility to calculate performances of the Sun for all territory of Georgia and to develop the recommendations for possible usage of the use of a non-conventional energy, that has a large value in future.

REFERENCES

1. I. L. Karol. Vvedenie v dinamiku klimata Zemli. L. Gidrometeo-izdat, 1988, (Russian).
2. Dinamicheskaia meteorologia – Ed. D. L. Laikhtmana, L. Gidrometeoizdat, 1976, (Russian).
3. L. T. Matveev. Kurs obshei meteorologii-fizika atmosferi. L. Gidrometeoizdat, 1985,(Russian).
4. Z. Khvedelidze, A. Chitaladze. Sakartvelos regionis atmosferos micispira fenis sitburi rejimis buneba. Metsniereba da Teknika, 10-12, 1999. 52, (Georgian).
5. Z. Khvedelidze, N. Ramishvili. Bull. Georg. Acad. Sci. 159, 3, 1999. 421.

6. Z. Khvedelidze, A. Topchishvili. Uchet reliefnoi osobennosti pri vichiclenii radiatsionnogo balansa. Bull. Georg. Acad. Sci 160, 2. 1999. 259.

Tbilisi State University

ზ. ხვედელიძე, ა. ჩიტალაძე, რ. დანელია, ნ. რამიშვილი

ატმოსფეროს მიწისპირა ფენაში შექცევადი კაპურების გამოყენება მეტეოროლოგიური სიდიდეების რეჟიმის განსაზღვრისათვის

დასკვნა

საქართველოს ტერიტორიაზე მზის რადიაციაზე დაკვირვებები წარმოებს მარტო ექვს სადგურზე, ხოლო ტემპერატურის ცვლილებაზე - სამოცზე მეტ სადგურზე.

ჩვენს მიერ გამოყენებული მეთოდის საშუალებით შესაძლებელია ყველა იმ წერტილში, სადაც დაკვირვება წარმოებს ტემპერატურაზე, განსაზღვრულ იქნეს რადიაციული ბალანსის ყველა შესაკრები და ჯამური რადიაცია რთული და ძვირადღირებული აპარატურის გარეშე.

გათვლებში მხედველობაში იქნა მიღებული დედამიწის რელიეფი და ზედაპირის ალბედო. რელიეფის გავლენა გათვალისწინებულია ახალი მიდგომით, კერძოდ ექსპოზიციის კუთხის შემოტანით. აღმოჩნდა, რომ კარგი თანხვედრა გამოთვლილ და დაკვირვებულ სიდიდეებს შორის მიიღება, როდესაც ექსპოზიციის კუთხე იცვლება 10-დან 50⁰ -მდე, ხოლო ალბედოს მნიშვნელობა 0.15 -დან 0.85 -მდე.

მიღებული შედეგებით შეიძლება დაზუსტდეს ჰელიოენერგიის გამოყენების შესაძლებლობა მიკრორეგიონებისათვის და მიეცეს შესაბამისი რეკომენდაციები.

CALCULATION OF THE AVERAGE VERTICAL VELOCITY OF THE CONVECTION MOTION
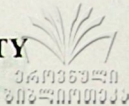
Z.V.Khvedelidze, A.D.Topchishvili

ABSTRACT: The vertical velocities of ascending aerial streams under the convection motion in the atmosphere have been calculated in this paper. Known dependency of vertical velocity upon temperature was used, and value of w for dry and wet air on the territory of Tbilisi during May was calculated.

Due to orographical features of our country almost 70% of land is represented by mountains, the height of which varies from 400 m and even more. In addition to this, almost every day different type of clouds can be observed on the territory of Georgia, where maximum recurrence is seen on Ci, Ac, Sc and St.

It's known that type of nebulosity is greatly dependent on solar radiation distribution on the Earth's surface. Modification of radiation balance is conductive to formation of ascending streams in the atmosphere [1].

Taking into consideration the above mentioned it's necessary to study velocities of ascending convection motion, which represent significant base in the formation of clouds.

During the tenfold, a lot of experimental researches of atmosphere convection were conducted by virtue of ordinary and installed radar-sets, meteorological artificial satellites and airplanes.

These researches improved the notion concerning vertical and horizontal scope of convection motion, its spatial structure and typical period of existence, the frequency of motion itself.

Convection motion in the atmosphere is known to appear under the force of floatation during superadiabatic vertical gradient of temperature, when single elemental scopes (aerial parts) are warmer, and consequently, light the surrounding air [2]. Velocity of lifting the aerial parts increases, until force of floatation is equal to force of tenacity. Current convection motion ensures such mixing of aerial

parts in the stream that the majority can be characterized by gradient similar to adiabatic.

Extremely simple and based on a physical conception way to calculate convection motion is to appraise basic force of convection force of floatation by virtue of data found through vertical probing of the atmosphere and to calculate vertical velocity of convection motion based on atmosphere dynamics equations.

Omitting convection pulsation of pressure and turbulent exchange, the static equation for vertical component of velocity w can be expressed by (2,3)

$$\frac{dw}{dt} = g\frac{T' - T}{T},\tag{1}$$

where T' is temperature of ascending aerial part, T temperature of surrounding air, t period, g acceleration of free incidence.

In specific experimental case $\partial w / \partial t = w\, \partial w / \partial z$, therefore the equation (1) will be modified:

$$\frac{1}{2}\frac{\partial(w^2)}{\partial z} = g\frac{T' - T}{T}.\tag{2}$$

Integrating it from level z_0 to level z, we will have:

$$w_{kz}^2 = w_{kz_0}^2 + \int_{z_0}^{z}\frac{T' - T}{T}dz,\tag{3}$$

where index k implies calculation of convection stream vertical velocity.

Taking into consideration equations of statics and conditions, the following formula will be applied for definition of vertical velocity of aerial part on level p [3]:

$$w_{kp}^2 = w_{k0}^2 + 2\int_{p}^{p_0} R(T'-T)d\ln p,$$

$$\overline{w_{kp}} = \sqrt{w_{k0}^2 + 2R\overline{(T'-T)}\ln\frac{p_0}{p}},\qquad (4)$$

where p_0 and p are pressures on the lowest and highest points of the given atmosphere stratum, w_{ko} velocity of convection on the lowest level (p_0) of stratum, R universal gas constant.

Average velocity for aerial parts, ascending from level p_0 up to level p, when $(T' - T) = 0$, suggesting that on level of the Earth (p_0) due to friction $w_{ko} = 0$, can be defined by the following equation [4]:

$$\overline{w_k} = \sqrt{R\overline{(T'-T)}\ln\frac{p_0}{p}}.\qquad (5)$$

Dew-point temperature and parts temperature values on isobar surfaces 1000, 850, 700, 500, 400, 300 and 200 mb for 1986, provided by the National Center of Hydro-Meteorological Department, were used in this paper in order to calculate average vertical velocity of convection. Month May was chosen for calculations, because in this month Georgia can be distinguished by frequent rains in comparison with other months. For each day of this month average vertical velocities were calculated taking into consideration that each aerial part ascended not only in dry, but also in wet air (calculations were done separately for case $R = 287$ m^{2}c^2/K and $R = 461.5$ m^{2}c^2/K).

Values T' and T were obtained after examining materials for vertical probing of the atmosphere. Difference $(T' - T)_{aver.}$ implies average temperature in the stratum of the defined thickness. Module $(T' - T)_{aver.}$ was used while calculating, because otherwise we have not only ascending, but also descending streams. After researching these descending streams we can assume that their charts are absolutely symmetrical with those of ascending streams concerning initial coordinates.

Vertical velocities of ascending streams were calculated based on equation of hydro-thermodynamics, which perfectly coincide with these values. However, this method is more flexible for calculations, because it's the simplest one and it requires shortest time for calculation.

39

The results of calculations are shown in the Tables 1 and 2 and charts. Table 1 (Table 2) contains average temperature differences $(T' - T)_{aver}$ and corresponding average vertical velocities, convection w_k, calculated for wet (dry) air for the 3 – 10 May 1986 time periods. For 3rd May the charts, describing the dependence of average velocity w_k on $(T' - T)_{aver}$, have been built, using data from the Tables. Charts were done taking into consideration that for each particular chart on each initial level p_0 vertical velocity of convection $w_{k_0} = 0$.

For example at the chart for 1000 mb we have:

The initial level is 1000 mb,

the curve 850 – describes the lifting of the particle from level 1000 to 850. ....

the curve 700 – describes the lifting of the particle from level 1000 to 700. ....

the curve 500 – describes the lifting of the particle from level 1000 to 500. ....

the curve 400 – describes the lifting of the particle from level 1000 to 400. ....

the curve 300 – describes the lifting of the particle from level 1000 to 300. ....

the curve 200 – describes the lifting of the particle from level 1000 to 200.

At the chart for 500 mb we have:

the initial level is 500 mb,

the curve 400 – describes the lifting of the particle from level 500 to 400. ....

the curve 300 – describes the lifting of the particle from level 500 to 300. ....

the curve 200 – describes the lifting of the particle from level 500 to 200. ....

Taking into consideration Tables and charts we can assume that:

1. In the initial stage velocity of ascending stream increases significantly.

2. While increasing difference of temperatures $(T' - T)_{aver}$ yields of average vertical velocity slowly becomes stationary.

3. While comparing the same charts for different R (R = 287, R = 461.5) during ascending of aerial part from initial level up to the last level (for example, for the chart 850 mb initial level shall be

Tab. 1.

H (mbar)	03-May		04-May		05-May		06-May	
_R=461.5_	(T''-T)aver	wk	(T''-T)aver	wk	(T''-T)aver	wk	(T''-T)aver	wk
1000-850	10.55	28.12963	7.7	24.03163	5.75	20.766904	8.7	25.544503
1000-700	8.45	37.29499	11.35	43.22352	8.7	37.842671	10.1	40.773955
1000-500	15.45	70.30121	23.6	86.88696	18.1	76.091802	11.1	59.588173
1000-400	19.05	89.75321	16.2	82.76753	25.6	104.0453	17.8	86.758593
1000-300	27.2	122.9359	22.25	111.1883	26.6	121.57241	24.75	117.26861
1000-200	32.3	154.8903					27.75	143.56695
	(T''-T)aver	wk	(T''-T)aver	wk	(T''-T)aver	wk	(T''-T)aver	wk
850-700	4	18.93177	7.15	25.31129	3.95	18.813077	7.3	25.575416
850-500	11	51.9012	19.4	68.92581	13.35	57.17704	8.3	45.083755
850-400	14.6	71.26597	12	64.60951	20.85	85.164544	15	72.235623
850-300	22.75	104.5675	18.05	93.14177	21.85	102.47822	21.95	102.71246
850-200	27.85	136.3705					24.95	129.07533
	(T''-T)aver	wk	(T''-T)aver	wk	(T''-T)aver	wk	(T''-T)aver	wk
700-500	8.9	37.17538	23.05	59.82682	16.3	50.309995	9.7	38.810241
700-400	12.5	56.81799	15.65	63.57524	23.8	78.400586	16.4	65.080781
700-300	20.65	89.85949	21.7	92.11572	24.8	98.475852	23.35	95.553665
700-200	25.75	122.0138					26.35	123.42713
	(T''-T)aver	wk	(T''-T)aver	wk	(T''-T)aver	wk	(T''-T)aver	wk
500-400	19.5	44.8121	27.9	53.60189	33.2	58.471881	17.4	42.330427
500-300	27.65	80.73647	33.95	89.46272	34.2	89.791503	24.35	75.765531
500-200	32.75	117.6815					27.35	107.54276

ერაევერი
ბიგ≈ხიიიგეე

H (mbar)	07-May		08-May		09-May		10-May	
R=461.5	(T"-T)aver	wk	(T"-T)aver	wk	(T"'-T)aver	wk	(T"'-T)aver	wk
1000-850	5.95	21.12498	6.45	21.99468	9.85	27.180406	9.85	27.180406
1000-700	9.7	39.95839	7.5	35.13604	7.05	34.065653	6.5	32.709871
1000-500	15.85	71.20545	16.45	72.54067	14	66.921028	16.65	72.98031
1000-400	17.55	86.14718	23.4	99.47419	18.9	89.399152		
1000-300	25	117.8594	32.4	134.1735	26.15	120.53968		
1000-200	32.35	155.0101	32.25	154.7704	36	163.52126		
	(T"-T)aver	wk	(T"-T)aver	wk	(T"'-T)aver	wk	(T"'-T)aver	wk
850-700	4.05	19.04973	3.65	18.08455	4.6	20.302064	4.05	19.049728
850-500	10.2	49.97826	12.6	55.54773	11.55	53.182902	14.2	58.969196
850-400	11.9	64.33974	19.55	82.46681	16.45	75.646484		
850-300	19.35	96.43759	28.55	117.141	23.7	106.72841		
850-200	26.7	133.5253	28.4	137.7105	33.55	149.67671		
	(T"-T)aver	wk	(T"-T)aver	wk	(T"'-T)aver	wk	(T"'-T)aver	wk
700-500	13.95	46.54227	13.65	46.0391	8.75	36.860778	10.85	41.046425
700-400	15.65	63.57524	20.6	72.93978	13.65	59.374116		
700-300	23.1	95.04076	29.6	107.5845	20.9	90.401794		
700-200	30.45	132.6826	29.45	130.4857	30.75	133.3346		
	(T"-T)aver	wk	(T"-T)aver	wk	(T"'-T)aver	wk	(T"'-T)aver	wk
500-400	21.8	47.38122	29.55	55.16413	20.6	46.058695		
500-300	29.25	83.03958	38.55	95.33105	27.85	81.027938		
500-200	36.6	124.4065	38.4	127.429	37.7	126.26215		

Tab. 2.

H (mbar) $R=287$	03-May (T''-T)aver	wk	04-May (T''-T)aver	wk	05-May (T''-T)aver	wk	06-May (T''-T)aver	wk
1000-850	10.55	22.182943	7.7	18.951269	5.75	16.376717	8.7	20.144317
1000-700	8.45	29.410716	11.35	34.085933	8.7	29.842615	10.1	32.154217
1000-500	15.45	55.439323	23.6	68.518789	18.1	60.005764	11.1	46.991052
1000-400	19.05	70.779108	16.2	65.270224	25.6	82.04981	17.8	68.417562
1000-300	27.2	96.946858	22.25	87.682777	26.6	95.871629	24.75	92.477672
1000-200	32.3	122.14602					27.75	113.21646
	(T''-T)aver	wk	(T''-T)aver	wk	(T''-T)aver	wk	(T''-T)aver	wk
850-700	4	14.929538	7.15	19.960407	3.95	14.835935	7.3	20.168695
850-500	11	40.929126	19.4	54.354687	13.35	45.08964	8.3	35.552912
850-400	14.6	56.20013	12	50.95086	20.85	67.1605	15	56.964793
850-300	22.75	82.461583	18.05	73.451314	21.85	80.814016	21.95	80.998734
850-200	27.85	107.54139					24.95	101.78841
	(T''-T)aver	wk	(T''-T)aver	wk	(T''-T)aver	wk	(T''-T)aver	wk
700-500	8.9	29.316395	23.05	47.17925	16.3	39.674309	9.7	30.605638
700-400	12.5	44.806491	15.65	50.13524	23.8	61.826464	16.4	51.322506
700-300	20.65	70.862918	21.7	72.64218	24.8	77.657757	23.35	75.353329
700-200	25.75	96.219704					26.35	97.334256
	(T''-T)aver	wk	(T''-T)aver	wk	(T''-T)aver	wk	(T''-T)aver	wk
500-400	19.5	35.338688	27.9	42.270289	33.2	46.110747	17.4	33.381646
500-300	27.65	63.668534	33.95	70.550025	34.2	70.809306	24.35	59.748467
500-200	32.75	92.803263					27.35	84.80789

H (mbar)	07-May		08-May		09-May		10-May	
$R=287$	$(T''-T)$aver	wk	$(T''-T)$aver	wk	$(T''-T)$aver	wk	$(T''-T)$aver	wk
1000-850	5.95	16.659095	6.45	17.344939	9.85	21.434386	9.85	21.434386
1000-700	9.7	31.511068	7.5	27.708172	7.05	26.86407	6.5	25.794905
1000-500	15.85	56.152399	16.45	57.205348	14	52.773719	16.65	57.55205
1000-400	17.55	67.935403	23.4	78.445046	18.9	70.499899		
1000-300	25	92.943557	32.4	105.8088	26.15	95.057225		
1000-200	32.35	122.24052	32.25	122.05144	36	128.95237		
	$(T''-T)$aver	wk	$(T''-T)$aver	wk	$(T''-T)$aver	wk	$(T''-T)$aver	wk
850-700	4.05	15.022558	3.65	14.261421	4.6	16.010146	4.05	15.022558
850-500	10.2	39.412703	12.6	43.80477	11.55	41.939874	14.2	46.502929
850-400	11.9	50.73812	19.55	65.033072	16.45	59.654587		
850-300	19.35	76.050391	28.55	92.377036	23.7	84.1657		
850-200	26.7	105.29765	28.4	108.5981	33.55	118.0346		
	$(T''-T)$aver	wk	$(T''-T)$aver	wk	$(T''-T)$aver	wk	$(T''-T)$aver	wk
700-500	13.95	36.703093	13.65	36.306292	8.75	29.068297	10.85	32.369086
700-400	15.65	50.13524	20.6	57.520087	13.65	46.822247		
700-300	23.1	74.948853	29.6	84.84082	20.9	71.29058		
700-200	30.45	104.63309	29.45	102.90063	30.75	105.14726		
	$(T''-T)$aver	wk	$(T''-T)$aver	wk	$(T''-T)$aver	wk	$(T''-T)$aver	wk
500-400	21.8	37.364688	29.55	43.502264	20.6	36.321747		
500-300	29.25	65.484757	38.55	75.177776	27.85	63.898385		
500-200	36.6	98.10658	38.4	100.49008	37.7	99.569946		

3 May 1986 R=287m2c2/K.

1000 mb

850 mb

45

700 mb

Wкr m/s vs (T'-T)aver

w500 — w400 — w300 — w200

500 mb

Wкr m/s vs (T'-T)aver

w400 — w300 — w200

3 May 1986 R=461m2c2/K.

1000 mb

850 mb

w850   w700   w500
w400   w300   w200

w700   w500   w400
w300   w200

700 mb

500 mb
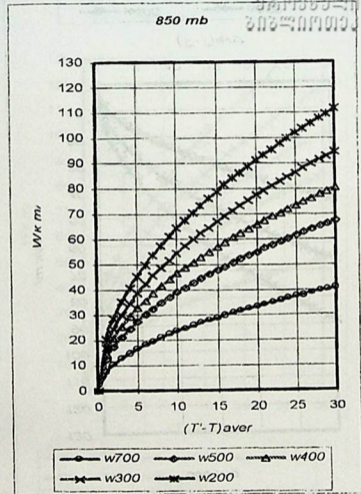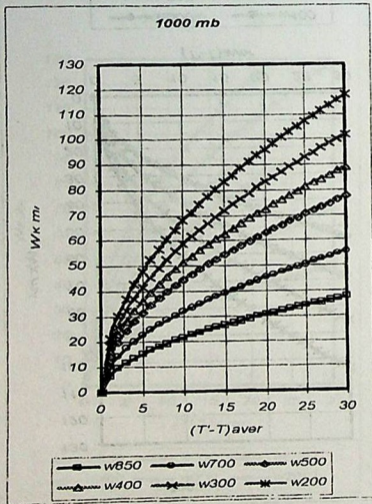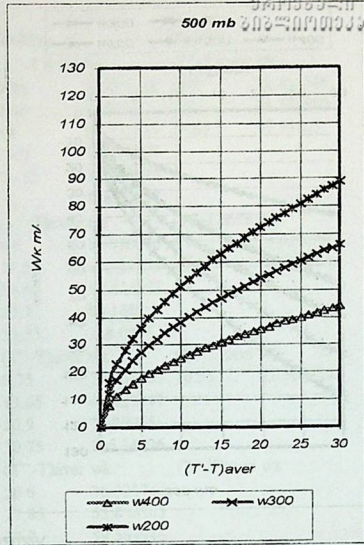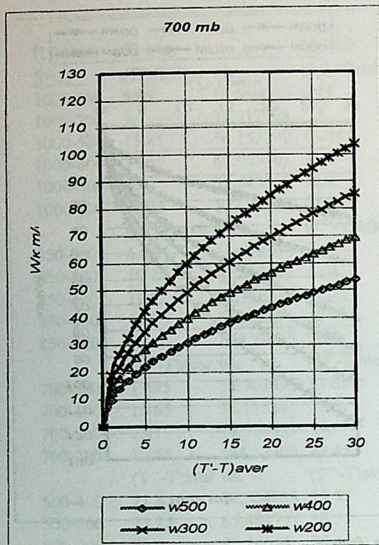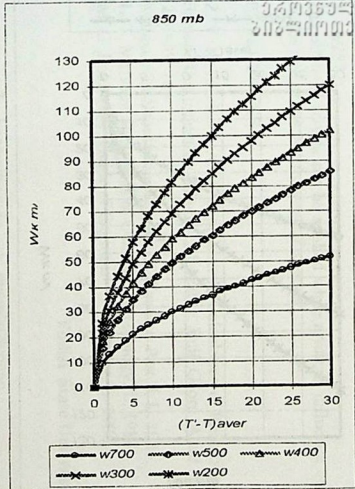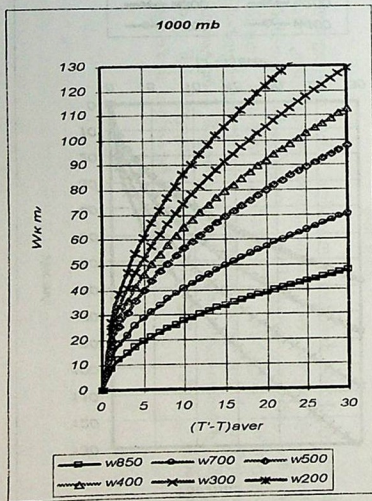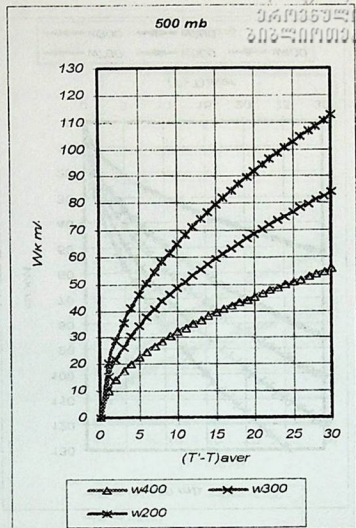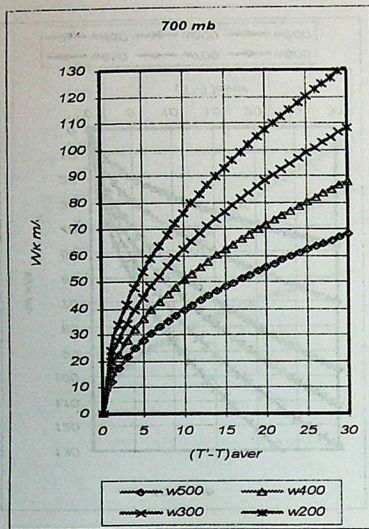
considered as yield $w700$, and last level – as $w200$) the difference $w461 - w287 \cong 20$.

The obtained results can be applied while artificial influence over the clouds and practicing forecast of weather.

REFERENCES

1. Z. V. Khvedelidze, A. D. Topchishvili. Calculation of Radiation Balance Dependent on Albedo of Locality. Bull. Georg. Acad. Sci. **2**, 1999, 160.
2. Manuals for Short-term Forecast of Weather. Part. I, L. 1986.
3. L. T. Matveev. Principles of General Meteorology. L. 1984.
4. M. G. Prikhodko. Guide of Engineer – Forecaster, L. 1986.

Tbilisi State University

ზ. ხვედელიძე,   ა. თოფჩიშვილი

კონვექციური მოძრაობის საშუალო ვერტიკალური სიჩქარის გამოთვლა

დასკვნა

დათვლილი იქნა ადმავალი დინების სიჩქარე ღრუბლებში კონვექციური მოძრაობისას ორ მშრალ და ნოტიო ჰაერისათვის. მიღებულია, რომ ვერტიკალური სიჩქარე ადმავალ ნაკადში დასაწყისში სწრაფად იზრდება; განსაზღვრული სისქის ატმოსფერული ფენის საშუალო ტემპერატურის მატებით ნელა გადის სტაციონარზე. შედეგები შესაძლებელია გამოყენებულ იქნეს ამინდის პროგნოზის სამსახურში.

NON-LINEAR LINKED OSCILLATION OF THE ELECTRONIC AND NUCLEAR MAGNETIZATION IN THIN FERROMAGNETIC PLATE

L. Chotorlishvili, B. Shergelashvili, P. Kurashvili,
G. Kutivadze

ABSTRACT. Non-linear dynamics of the nuclear and electronic magnetization by the linked superthin field in the thin ferromagnetic plate under the influence of the weak external magnetic fields is researched.

Recent years are witnesses of a rapid research development of the nuclear magnetic resonance in the magnetically-arranged materials. Under ordinal conditions, at which the experiment is carried out, a frequency of an electronic magnetic resonance exceeds by far a frequency of a nuclear magnetic resonance. So, many of the articles deal with analysis of such situation. Nevertheless, a growing interest is stirred by examination of a phenomenon occurred during coincidence of the frequencies of an electronic and nuclear magnetic resonance, which essentially (because of its experimental condition) is an electronic-nuclear magnetic system. The interest in many respects is stirred by an opportunity of applying a model of linked oscillators to explain experimental results. As it is known, at temperatures far below Curie point of ferromagnetic, electronic spins are arranged and nuclear ones are in paramagnetic condition. Respectively, movement equation electronic magnetization and nuclear magnetization are equations of Landau-Lipchitz [1] and Bloch [2]. When external magnetic fields are strong, an impact of a nuclear magnetization is negligible and we can consider an equation of Landau-Lipchitz only. Just such situation has been dealt with in the works [3-5]. Particularly in [5] with an application of disturbance theory [6] a short-wave solitary solution has been gotten without taking into account an impact of damping. On the other hand, with a decrease of an amplitude of an external magnetic fields (both direct and alternating) leading to diminishment of

frequency of electronic resonance $\omega_s = \gamma_e H$ role of superthin interaction increases and as a result it becomes necessary to consider Landau-Lipchitz and Bloch equations as a system of differential equations which describe a linked oscillation of an electronic and nuclear magnetization (a frequency of a nuclear magnetic resonance $\omega_s = \gamma_e H_0$ is determined by a superthin field and does not depend on external fields). A linear approximation to electronic magnetization

$$M(t) = M + m(t) \qquad |m| \ll M$$

allowing to get an analytical solution for a system of oscillators [7-8] according to authors is not sufficient to describe adequately a real physical process.

For this a dynamics of an electronic and nuclear magnetization has been researched in the thin plate magnetized perpendicularly to its plane (which is the best optimal sample to achieve a condition $\omega_n = \omega_s$ [9]) in the weak external direct H~10Gs and alternating $|h(t)|$ ~ 10Gs fields. For that purpose let's consider Landau-Lipchitz and Bloch equations as a system of equations which are linked by superthin field:

$$
\begin{cases}
\dot{\vec{M}} = -\gamma_e[\vec{M}\vec{H}_e] + \dfrac{\lambda}{M}[M\dot{M}] - \dfrac{\vec{k}M_z}{T_1^e} - \dfrac{\vec{i}M_x + \vec{j}M_y}{T_2^e}, \\[2ex]
\dot{\vec{\mu}} = \gamma_n[\vec{\mu}\vec{H}_n] - \dfrac{\vec{k}(\mu_z + \mu)}{T_1^n} - \dfrac{\vec{i}\mu_x + \vec{j}\mu_y}{T_2^n}, \\[2ex]
\vec{H}_e = -\dfrac{\delta H}{\delta \vec{M}}, \quad \vec{H}_n = -\dfrac{\delta H}{\delta \vec{\mu}},
\end{cases}
\qquad (1)
$$

where T_1 and T_2 are the times of longitudinal and transverse relaxation, γ_n and γ_e are gyromagnetic ratio for nuclei and electrons, H_{int} is a phenomenological Hamiltonian with an appearance:

$$H_{int} = -\vec{H}_0\vec{M}(t) - \vec{h}(t)\vec{M}(t) + \vec{H}_0\vec{\mu}(t) + \vec{h}(t)\vec{\mu}(t) + A\vec{M}\vec{\mu}$$

51

where $\vec{H}_0(0,0,H_0)$ and $\vec{h}(h\cos\omega t;0;0)$ are an external direct and alternating field respectively, $A\vec{M}\vec{\mu}$ is Hamiltonian of superthin interaction (we have neglected an anisotropy of the tensor $A^{\alpha\beta}$). An item relaxation is added to the Landau-Lipchitz equation in order to get a damping oscillation.

In order to apply numerical methods and give a standard appearance, which allows numerical integration, to system (1), an algebraic transformation should be performed upon the Landau-Lipchitz equation. Considering the Landau-Lipchitz equation as an algebraic equation towards $\dot{\vec{M}}$ and applying standard methods [10], we will have:

$$\begin{cases} \dot{M}_y = \dfrac{\Delta_2}{\Delta}, \\[2mm] \dot{M}_z = \dfrac{\Delta_3}{\Delta}, \\[2mm] \dot{\vec{\mu}} = \gamma_n[\vec{\mu}\vec{H}_n] - \dfrac{\vec{k}(\mu_z+\mu)}{T_1^n} - \dfrac{\vec{i}\mu_x + \vec{j}\mu_y}{T_2^n}, \end{cases} \qquad (2)$$

where

$$\Delta_1 = \begin{vmatrix} f_1 & \gamma M_x & -\gamma M_y \\ f_2 & 1 & \gamma M_x \\ f_3 & -\gamma M_x & 1 \end{vmatrix}, \qquad \Delta_2 = \begin{vmatrix} 1 & f_1 & -\gamma M_y \\ -\gamma M_x & f_2 & \gamma M_x \\ \gamma M_y & f_3 & 1 \end{vmatrix},$$

$$\Delta_3 = \begin{vmatrix} 1 & \gamma M_x & f_1 \\ -\gamma M_x & 1 & f_2 \\ \gamma M_y & -\gamma M_x & f_3 \end{vmatrix},$$

$$\Delta = \begin{vmatrix} 1 & \gamma M_x & -\gamma M_y \\ -\gamma M_x & 1 & \gamma M_x \\ \gamma M_y & -\gamma M_x & 1 \end{vmatrix} = 1 + \gamma^2 M^2$$

are the respective determinants, f_i not containing $\dot{M}$ is right part of the Landau-Lipchitz equation respective to M_i ($I = x,y,z$), $\gamma = \dfrac{\lambda}{M}$. Though for the items of relaxation containing the times of longitudinal T_1^e and transverse T_2^e relaxations, a condition $|M| = $ const. is no longer valid, we still assume that approximately $\gamma = $ const.

The results of reckoning for a system [2] with standard values of parameters $H_0 \sim |h(t)| \sim 10$ Gs, $\gamma_e H_0 \sim 10^8$ Hz, $\gamma_n H_0 \sim 10^5$ Hz, $A\gamma_e \sim 10^8$ Hz/Gs, $A\gamma_e \sim 10^5$ Hz/Gs, $\gamma \sim 10^3$ Gs^{-1}, $T_1^e \sim 10^9$ Hz, $T_1^n \sim 10^7$ Hz, $T_2^e \sim 10^{10}$ Hz, $T_2^n \sim 10^8$ Hz at starting conditions $M(t = 0) = (0; 0; M_0)$ $\mu(t = 0) = \mu(0; 0; \mu_0)$, $M_0 \sim 10^3$ Gs, $\mu \sim 1$ Gs are reflected in the graphs (Figs.1-3). On the graph in Fig.1 dependence of longitudinal $M^z(t)$ and transverse $M^+(t)$ components of electronic magnetization on time is reflected. The graph shows how after turning on alternating field at the moment $t = 1$ μs a longitudinal magnetization turns into transverse magnetization. The graph in Fig.2 reflects dependence of longitudinal component $\mu^z(t)$ of nuclear magnetization on time. The graph presents that a nuclear magnetization arranges in anti-parallel position with direct field H according to (1). The graph in Fig.3 illustrates the possibility of formation of forced non-linear linked oscillations and as the graph in Fig.3 tells the oscillations of M^+ and μ^+ happen at the counterphase in accordance with [8], but unlike linear linked oscillations [8] a difference of phases is a little displaced relatively $\dfrac{\pi}{2} + \pi k$ (minimum of M^+ does not exactly match maximum of μ^+). As it has been mentioned in [5] through an application of disturbance theory a short-wave solitary solutions of Landau-Lipchitz equations has been gotten without taking into account nuclear

53
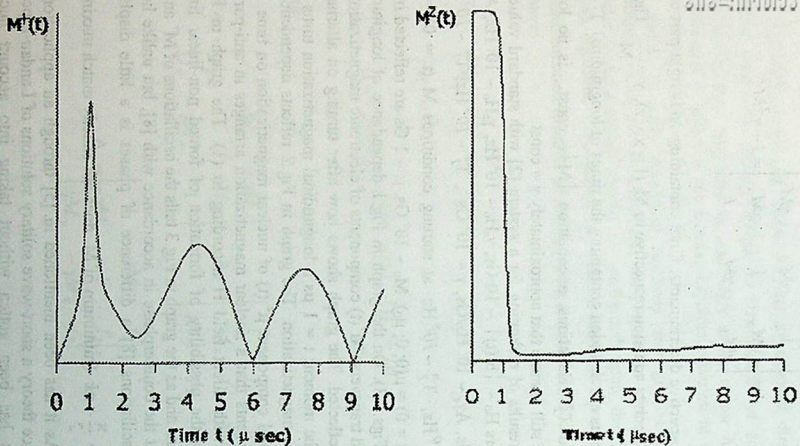
Fig.1. Electron magnetization as a function of time.
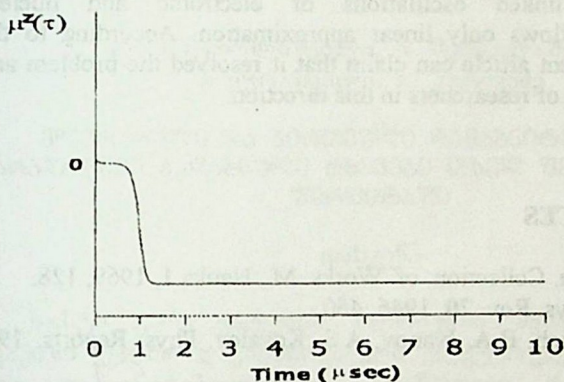
Fig.2. Nuclear magnetization as a function of time.
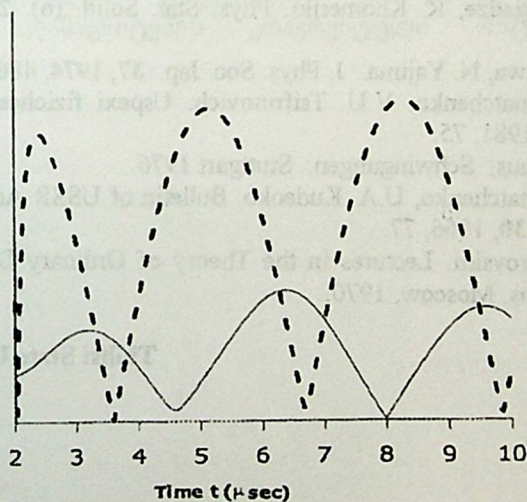
Fig.3. Coherent oscillation of the transversal electron
(dashed line) and nuclear (solid line) magnetization
as a function of time.

magnetization and relaxation process. On the other hand, analytical solutions for linked oscillations of electronic and nuclear magnetization allows only linear approximation. According to the authors the present article can claim that it resolved the problem and can arise interest of researchers in this direction.

REFERENCES

1. L.D. Landau. Collection of Works. M., Nauka **1**, 1969, 128.
2. F. Bloch. Phys. Rev. **70**, 1946, 460.
3. A.M. Kosevich, B.A. Ivanov, A.S. Kovalev. Phys. Reports. **194**, 1990, 117.
4. A.M. Kosevich, B.A. Ivanov, A.S. Kovalev. Nonlinear Waves of Magnetization. Dynamical and Topological solitons, Naukova Dumka, Kiev, 1983.
5. N. Giorgadze, R. Khomeriki. Phys. Stat. Solid. (b). **207**, 1998. 249.
6. M. Oikawa, N. Yajima. J. Phys. Soc. Jap. **37**, 1974, 486.
7. V.A. Ignatchenko, V.U. Tsifrinovich. Uspexi fizicheskix nauk. **133**, 1, 1981, 75.
8. K. Magnus, Schwingungen. Stuttgart 1976.
9. V.A. Ignatchenko, U.A. Kudenko. Bulletin of USSR Academy of Siences **30**, 1966, 77.
10. I.G. Petrovskii. Lectures in the Theory of Ordinary Differential Equations. Moscow, 1970.

Tbilisi State University

ლ. ჯოტორლიშვილი, ბ. შერგელაშვილი
პ. ყურაშვილი, გ. კუტივაძე

ელექტრული და ბირთვული დამაგნიტებულობის
არაჯერივი გადაბმული რხევები თხელ ფერომაგნიტურ
ფირფიტაში

დასკვნა

სუსტი გარე ველების პირობებში შესწავლილია ზე-
ფაქიზი ველით დაკავშირებული ელექტრული და ბირთვუ-
ლი დამაგნიტებულების არაჯერივი რხევები თხელ
ფერომაგნიტურ ფირფიტაში. მანქანური ინტეგრების
საშუალებით მიღებულია ბირთვული დამაგნიტების დროზე
დამოკიდებულების მრუდი, ბირთვული და ელექტრონული
განივი დამაგნიტების კოჰერენტული ოსცილაციების
მრუდები.

NATURE OF SINGLE-PULSE NUCLEAR SPIN ECHO AND ITS MULTIPULSE ANALOGUES IN MULTIDOMAIN MAGNETIC MATERIALS

A.M.Akhalkatsi, Gr.I.Mamniashvili[*], G.A.Sakhelashvili, Z.G.Shermadini

ABSTRACT. Different analogues of the multipulse Hahn echo excitation in the single-pulse echo method were experimentally realized in multidomain magnetic materials. Experiments were performed in conditions of a sufficiently fast change of the effective magnetic field direction in the rotating coordinate system at the displacement of domain walls by the pulses of magnetic field and also at the stepwise change of frequency or amplitude of the radio frequency pulse. The experimental results are in the favour of the edge mechanism of the single-pulse echo formation.

A number of works [1,2] were devoted to the investigation of the nature of single-pulse (SP) echo but this question has not been finally clarified so far.

The SP echo formation mechanisms could be subdivided into the following two groups: the first group concerns the so-called edge-type mechanisms like nonresonance mechanism [3] and the pulse distortion mechanism [1] (when edges of the RF pulse act as two resonance RF pulses), the second one is the mechanism of intrinsic nature of the SP echo formation [2].

The important role of RF pulse edges is caused by the fact that just at these time moments the change of direction of the effective magnetic field H_{eff} in the rotating coordinate system (RCS) occurs and as a result of this the RF pulse edges play the role of two RF pulses in the Hahn method. Then, as it was shown in [4], an analog of the multipulse excitation of the Hahn echo in the single-pulse echo method is the action of an RF pulse of complex shape when, during the length of the pulse, discrete, sufficiently fast changes of the direction of H_{eff} occur in RCS. The direction of H_{eff} is changed by changing RF pulse frequency, amplitude or phase during its action.
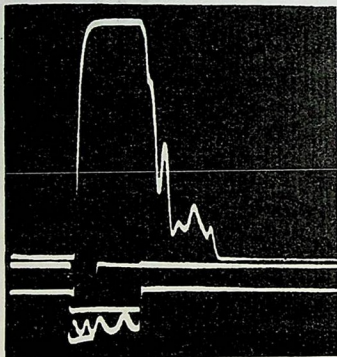
Fig.1. ^{59}Co spin echo signals in hexagonal cobalt at the stepwise change of frequency of the RF pulse - upper beam, the form of modulating voltage pulse applied to the varicap system of RF generator- the middle beam, the wavemeter beating signals - the lower beam.
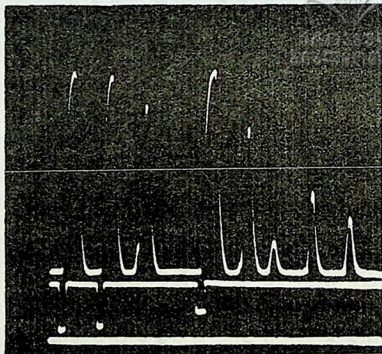
Fig.2. Multiple ^{59}Co nuclear spin echo signals in hexagonal cobalt at the three-pulse Hahn echo excitation.

In work [5] multipulse analogues were realized causing the nonadiabatically fast changes of H_{eff} at the displacement of domain walls in multidomain magnetic materials by a magnetic field pulse applied in combination with the RF pulse. Similar signals were also obtained at the stepwise change of frequency or amplitude of the RF pulse.

In Fig.1 the spin-echo signals of ^{59}Co at the stepwise change of RF pulse frequency in hexagonal cobalt were shown, and Fig.2 shows multiple echo signals of ^{59}Co in the same sample at three-pulse Hahn echo excitation.

Similar single-pulse analogues were realized in a number of multidomain magnetic materials with considerably different physical properties, such as Co, Co_2MnSi, $MnSb$, $LiFe_2O_4$ and others.

The above considered different ways of excitation of echo signals present essentially the realization of the new mechanism of spin echo formation in magnetic materials related with the nonadiabatically fast change of H_{eff} direction in RCS.

REFERENCES

1. I.G. Kiliptari, V.I. Tsifrinovich. Phys. Rev. B. 57, 1998, 11554.,
2. L.N. Shakhmuratova, D.K. Fowler, D.H. Chaplin. Phys. Rev. B. 55, 1997, 2955.
3. V.P. Chekmarev, M.I. Kurkin, S.I. Goloshapov. Sov.Phys., JETP. 49, 1979, 851.
4. V.P. Chekmarev, G.I. Mamniashvili. Fiz. Met. Metalloved. 51, 1981, 685.
5. A.M. Akhalkatsi, G.I. Mamniashvili, T.I. Sanadze. Appl. Magn. Reson. 15, 1998, 393.

Tbilisi State University
* Georgian Academy of Sciences
Institute of Physics

ა. ახალკაცი, გ. მამნიაშვილი, გ. სახელაშვილი,
ზ.შერმადინი

მრავალდომენიან მაგნეტიკებში ერთიმპულსიანი ბირთვული სპინური ექოს ბუნება და მისი მრავალრიცხოვანი ანალოგი

დასკვნა

ექსპერიმენტულად რეალიზებულია ერთიმპულსიანი ზემოქმედების სქემა, რომელიც წარმოადგენს პანის ექოს მრავალიმპულსიანი აგზნების ხარისხობრივ ანალოგს. დამატებითი ექო სიგნალები დაიმზირებოდა რადიო-სიხშირული იმპულსების მოქმედების არეში იმპულსური მაგნიტური ველების ზემოქმედებით, აგრეთვე სიხშირისა და იმპულსის ნახტომისებური ცვლილებით. ექსპერიმენ-ტული რეზულტატები მიანიშნებს ერთიმპულსიანი ექო ფორმირების კიდურა მექანიზმის ეფექტურობის სასარგებ-ლოდ.

ON REVERSILIBITY OF INTERACTING SPIN SYSTEMS EVOLUTION

A. Ugulava, S. Chkhaidze

ABSTRACT. On the basis of consideration of dynamics of two interacting moments the conditions, in which spin system is locally unstable are found. Spin-spin interaction is taken for dipole-dipole interaction. It's shown, that the separatrix curve, separating the topologically different trajectories, expressing various oscillations of z-component of these spins, corresponds to the instantons solutions of the motion equation on the phase plane.

Locally unstable are called such trajectories, which diverge exponentially even in one direction. It can be shown, that from the properties of local unstability tends the property of mixing. The well known paradox of Loschmidt contradiction between reversible laws of mechanics and unreversible ones of thermodynamics following [2] can be interpreted using the notion of local unstability.

Indeed, reflecting the time with any finite accuracy, we reverse the beam of trajectories in the phase. If this time, the system is locally stable, the beam of trajectory going to the reversal direction will be slightly distorted and, after some time the system will return to the initial state. If the system is locally unstable, then reflecting the time the beam of trajectories will diverge exponentially and thus the initial state will not be restored.

Reversibility of time practically is possible only for spin systems with the aid of well known sequences of RF pulses, for example, by means of π-pulse in the Hahn echo and "magic sandwich" in the experiments of Waugh [3,4]. Below the system of interacting spins, in which reversibility of time is achieved by means of "magic sandwich" will be considered. The main idea of the experiment of Waugh is as following. After action of short RF pulse and some delay exceeding T_2 – transverse relaxation time – during which transverse component of magnetization seem to disappear for good, "magic sandwich" is given. Action of "magic sandwich" is nearly equal to reverse of time in the

given system. Later, after reflecting time the restortion of transverse component of magnetization "magic echo" is noted. Initially, this phenomenon seemed to be contradictional and was perceived as "revival to the new life of already buried one" [4]. Long before the experiment of Waugh, describing various phenomena on paramagnetic resonance for the system of interacting spins, conception of spin temperature was used successfully, which was based on the assumption that in the spin-system, during the time T_2 the thermodynamical equilibrium is being set i.e. it's meant, that during the time T_2 – the system "forgets" its initial conditions.

Following the above mentioned interpretation of Loschmidt paradox, we can conclude that there are no contradictions in the experiments with "magic sandwich". Indeed, investigated spin-system is quantum, and can be well described by the stationar equation of Schrödinger. Such system (far from classical) in the presence of any finite number of particles is locally stable and hence reversible by "magic sandwich". These properties of spin-system, according to the experiment of Waugh are kept even at macroscopically great number of interacting particles.

Locally unstable system of interacting spins can be stood only at quasiclassical limit. In the conditions of local stability the initial state must not be restored even by means of "magic sandwich".

This paper aims to find the conditions, at which the system of interacting spins is locally unstable. As in the case of [3] we take dipole-dipole interaction for spin-spin one.

As analytical investigation of N interacting moments (spins) is practically impossible, we'll consider the dynamics of two interacting moments. In the case of small concentrations of spins, when the existence of spin in the sphere of interaction is scarcely probable, the principle conclusions about stability can be made on the basis of a simplified model. Directing the z-axis along the constant magnetic field, Hamiltonian system can be written as

$$\mathcal{H} = \mathcal{H}_0 + \mathcal{H}, \qquad \mathcal{H} = \mathcal{H}_z + \mathcal{H}_d^{(0)},$$

$$\mathcal{H}_z = \omega S^z, \qquad S^z = S_1^z + S_2^z, \qquad \omega = \gamma H,$$

$$\mathcal{H}_d^{(0)} = A S_1^z S_2^z + B(S_1^+ S_2^- + S_1^- S_2^+),$$

63

$$\mathscr{H}_d' = C(S_1^z S_2^+ + S_1^+ S_2^z) + E S_1^+ S_2^+ + \text{c.c.}$$

where γ is a gyromagnetic ratio, H intensity of magnetic field, S^z, S^-, S^+ coordinates of spin vector,

$$A = -4B = \frac{\gamma^2}{r^3}(1 - 3\cos\vartheta), \quad S_{1,2}^\pm = S_{1,2}^x \pm S_{1,2}^y,$$

$$C = -\frac{3}{4}\frac{\gamma^2}{r^3}\sin 2\vartheta\, e^{-i\alpha}, \quad E = -\frac{3}{4}\frac{\gamma^2}{r^3}\sin^2\vartheta\, e^{-2i\alpha}, \tag{1}$$

$r = |\vec{r}|$, $\vec{r}$ denotes vector connecting spin points, Q and α are polar and azimuth angles of vector $\vec{r}$. Below we'll consider an approximation of strong field - H >> A, C, D. Hamiltonian of perturbation $\mathscr{H}_d'$ in the equations of Hamilton gives fast-oscillating contribution, which disappears at averaging during the time $2\pi/\omega$. The equations produced by Hamiltonian $\mathscr{H}_0$ can be seen in the form

$$\begin{cases} \dfrac{d\sigma}{dt} = A S_1^\perp S_2^\perp \sin\varphi, \\[2mm] \dfrac{d\varphi}{dt} = -A\sigma + \dfrac{1}{2}A\left(S_2^\perp \dfrac{S_1^z}{S_1^\perp} - S_1^\perp \dfrac{S_2^z}{S_2^\perp}\right)\cos\varphi, \end{cases} \tag{2}$$

where $\sigma = S_1^z - S_2^z$, $\varphi = \varphi_1 - \varphi_2$, $S_{1,2}^\perp$ and $\varphi_{1,2}$ are transverse component and azimuth angles of vectors $\bar{S}_1$ and $\bar{S}_2$ properly.

$$S_{1,2}^x = S_{1,2}^\perp \cos\varphi_{1,2}, \qquad S_{1,2}^y = S_{1,2}^\perp \sin\varphi_{1,2},$$

$$S_{1,2}^z = \frac{1}{2}(S^z \pm \sigma), \quad S_{1,2}^\perp = \frac{1}{2}\sqrt{4S^2 - (S^z \pm \sigma)^2}, \quad S \equiv |\bar{S}_1| = |\bar{S}_2|.$$

64

The system of equations (2) has two integrals of motion - z-component of summary spin S^z and the resonance part of interaction

$$\mathcal{H}_d^{(0)} = A(S_1^z S_2^z - \frac{1}{2} S_1^\perp S_2^\perp \cos \varphi). \tag{3}$$

Excluding variable φ by means of (3) from the first equation of the system (2) we'll obtain

$$\frac{d\sigma}{dt} = -\sqrt{-(\sigma^2 - \sigma_+^2)(\sigma^2 - \sigma_-^2)}, \tag{4}$$

where

$$\sigma_{+,-}^2 = -\frac{2^4}{3}\left[d + \frac{1}{4}\left(S^2 - \frac{3}{4}S_z^2\right)\right] \pm$$

$$\pm \left\{ \frac{2^8}{3^2}\left[d + \frac{1}{4}\left(S^2 - \frac{3}{4}S_z^2\right)\right]^2 + \frac{2^4}{3}\left(S^2 - \frac{1}{4}S_z^2\right)^2 - 4\left(d - \frac{1}{4}S_z^2\right)^2 \right\}^{1/2}$$

$$t' = -\left(\sqrt{3}/4\right)At, \quad d = \mathcal{H}_d^0/A, \tag{5}$$

The solution (4) can be written as

$$\sigma(t') = \sigma \, dn\left\{\sigma_- t'; \sqrt{1 - (\sigma_+/\sigma_-)^2}\right\}, \quad \sigma_{+,-}^2 \geq 0, \tag{6}$$

where $dn\left\{\sigma_- t'; \sqrt{1 - (\sigma_+/\sigma_-)^2}\right\}$ is eliptical function of Jacobi - delta amplitude.

Of great interest for us is the motion corresponding to the initial conditions $S_1^z(-\infty) = S_2^z(-\infty) = \varphi(-\infty) = 0$ (e.i. $S^z = 0$, $d = -S^2/2$). In such initial values, according to (5) and (6) $\sigma_- \equiv \sigma_0 = (2/3)^{1/2} 2S$, $\sigma_+ = 0$, and solution takes the form of instantones

$$\sigma(t) = \sigma_0 / ch(\sqrt{2}ASt) . \tag{7}$$

It can be shown, that the separatrix curve, separating the topologically different trajectories corresponds to the instantone solution on the plane (σ, φ). Indeed, substituting corresponding values $S_{1,2}^z$, $S_{1,2}^{\perp}$ in (3) and accounting, that $\mathscr{H}_d^{(0)}/A = d$, after some transformation for $S_z = 0$ we'll obtain

$$\sigma = \pm 2\sqrt{\frac{2d + S^2 \cos\varphi}{\cos\varphi - 2}} . \tag{8}$$

This dependence is shown in the Fig.1, from which is seen that the curves a, b and d are separated by separatrix c. The curves of type a express an oscillation of z-component of spins at which $S_1^z > S_2^z$, but the curves of type d - on the contrary - express an oscillation of z-component of spins at which $S_1^z < S_2^z$. For the curves of type b relations between S_1^z and S_2^z change periodically.
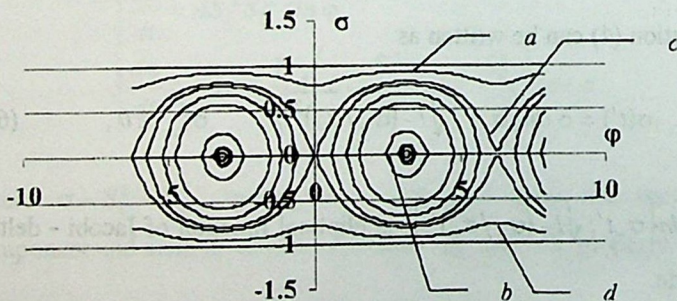
Fig.1. "Phase" picture of motion of two magnetics, connecting with dipole-dipole interaction ($S = 0.5$; $d = -0.25 \div 0.25$).

66

The motion in the range of separatrix is very unstable, because slight perturbations can sharply change the type of motion. Usually, near the separatrix, local unstability is generated and "layer" of chaotic motion is arisen, the so-called stochastic layer.

To study the generation of stochastic layer, it must be studied the system of equations, which will be created by full Hamiltonian $\mathcal{H}$. This system is unintegrated and its full analysis can be done only using the methods of numerical integration.

In the future with the aid of these methods we'll study the influence of unsecular members of dipole-dipole interaction, which in our opinion leads to creation of the "stochastic layer" near the separatrix and we also investigate influence of "magic sandwich" on the system.

REFERENCES

1. G.M. Zaslavsky. Stokhastichnost dinamicheskikh sistem. Nauka, Moscow, 1984, (Russian).
2. A. I. Anselm. Osnoyy statisticheskoi fiziki. Nauka, Moscow,
3. 1972, (Russian).
4. J.S. Waugh. New NMR methods in solid state physics. Cambridge, 1978.
5. A. Adragam, M. Goldman. Nuclear Magnetizm: Order and Disorder. Oxford, 1982.

Tbilisi State University

ა. უგულავა, ს. ჩხაიძე

ურთიერთქმედი სპინური სისტემის ევოლუციის შექცევადობის საკითხისათვის

დასკვნა

ურთიერთქმედი სისტემების ევოლუციის შეუქცევადობა წარმოიშვება ტოპოლოგიურად განსხვავებული ტრაექტორიების სეპარატრისების მიდამოებში.

ორი ურთიერთმოქმედი მომენტის დინამიკის განხილვის საფუძველზე ნაჩვენებია პირობა, რომლის დროსაც სპინური სისტემა ლოკალურად არამდგრადია. სპინ - სპინურ ურთიერთქმედებად მიჩნეულია დიპოლ - დიპოლური ურთიერთქმედება. ნაჩვენებია, რომ მომრაობის განტოლების ინსტანტონურ ამოხსნას ფაზურ სივრცეში შეესაბამება სეპარატრისული მრუდი, რომელიც ერთმანეთისგან მიჯნავს ტოპოლოგიურად განსხვავებულ ტრაექტორიებს, რომლებიც ასახავენ ამ სპინების z —კომპონენტის სხვადასხვაგვარ რხევებს.

68

FORMATION OF EXCITED HYDROGEN ATOM AT COLLISIONS H_3^+ - He: ROLE OF INTERNAL EXCITATION OF H_3^+

M.R.Gochitashvili, N.R.Dzhaliashvili, R.V.Kvizhinadze,
B.I.Kikiani

ABSTRACT. We have presented results of experimental measurements of the excitation function of hydrogen atomic line L_α ($\lambda = 121.6$ nm), emitted during dissociation of H_3^+ molecular ion, at collisions H_3^+ - He in the energy interval 3 - 9 keV of ion. It is determined, that the intensity of the given radiation lines depends on internal (vibrational) excitation of H_3^+ molecular ion in the initial (ground) electronic state.

1. INTRODUCTION

The molecule H_3^+ was detected by Thompson [1] still in 1912. However more or less full understanding of structure and property of this molecule is far from being completed. In experimental research of H_3^+ dissociation on a thin foil was determined that H_3^+ had the structure of an equilateral triangle [2]. The band system in the infrared range of the absorption spectrum of this ion was detected by Oka et al [3]. Binding energy of H_3^+ ion was defined experimentally [4,5] on research of a threshold of H_3^+ dissociation at collisions H_3^+ - He. The energy surfaces appropriate to various electronic states H_3^+ were calculated in articles [6-9]. Many parameters of H_3^+ molecular ion (binding energy, energy of electronic-vibration excitation, symmetry of state, dissociation limit etc.) were defined in collisional experiments. For example, in articles on electronic recombination of a molecule H_3^+ the thresholds of excitation of various electronic state [10,11] were defined, the cross section of formation of dissociation products H, H^+, H^-, H_2^+ was measured and the excited states of a molecule which at decay gave these products were determined [12-16]. The research of processes of H_3^+ dissociation with formation of excited atoms of hydrogen is of special interest. It is stipulated by that

69

the appropriate excited electronic state has not been investigated enough. For example, the excited H atoms in a state $(2p)$ at dissociation of H_3^+, will be formed at decay [17] of $1A_2''$ molecular state, which till now practically is not investigated experimentally. The definition of polarization degree of L_α emission in coincidence with dissipated ion H_2^+, at collisions H_3^+ - He, has allowed the authors of article [17] to study the mechanism of H_3^+ dissociation and the role of molecular orientation in the excitation process. The radiation cross section of L_α lines (transition 2p-1s) of hydrogen atom was measured by Dunn et al. [18] at collisions of ions H_3^+ with H_2 and He.

The research of H_3^+ molecular ion has independent theoretical and practical interest. There is some theoretical and experimental evidence that H_3^+ is an important catalyst in the stellar medium [19-21]. Large concentrations of H_3^+ in dense stellar clouds provide one of the important mechanisms of molecular formation in stellar medium according to the reaction

$$H_3^+ + X \rightarrow XH^+ + H_2, \tag{1}$$
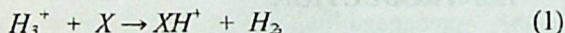
where X may be CO, N_2, H_2O, NH_3, Si, S, H_2S, etc. Seventy-seven reactions involving H_3^+ in stellar clouds were studied with their rate coefficients by Suzuki [21].

The experimental investigations of the dissociation processes showed dependence of the cross section of various inelastic channels on the vibrational excitation of these ions [10,11,16] in the ground electronic state $1A_1'$. The purpose of the present article was to study the role of vibrational excitation of an initial electronic state of H_3^+ ions in the process of L_α emission at dissociation of these ions .

2. EXPERIMENTAL TECHNIQUE

The H_3^+ ion beam leaving the Toneman type ion source was accelerated to a predetermined energy, then focused by the quadruple lenses and analyzed by the magnet mass analyzer (with resolution ~30). The emerging ions passed through collimating slits and finally entered collision chamber. The radiation emitted as a result of the

excitation of hydrogen atom was observed at the angle 90^0 to the direction of the beam. The spectroscopic analysis of the emission was performed with a Seya-Namioka vacuum monochromator incorporating a toroidal diffraction grating. Radiation was registered by the secondary electronic multiplier in the pulse – counting conditions.

The photon signal was linear with pressure and ion beam current $(0.1-0.5\eta A)$, showing the relative unimportance of secondary processes. The experimental set-up and calibration procedures of the light-recording system have been described previously [22].

An estimate of the uncertainty in the absolute values of the cross sections is about ~30% and main by defined by an error of calibration.

The used experimental device allows to carry out research of the excitation processes in various conditions of experiment. In particular, by changing the pressure of working gas - hydrogen in an ion source it was possible to vary relative fraction of the output of H^+, H_2^+, H_3^+ ions depending on the value of pressure and to investigate influence of internal excitation degree of a molecule on efficiency of the process of L_α line excitation . The relatively high value of a current of H_3^+ ions was obtained, when pressure in the ionic source reached ~ 0.1 Torr. In this case, the H_3^+ ions with inappreciable internal energy was extracted from the source (mainly in v = 0 vibrational state) [10,11]. In these conditions, vibrationally - excited ions H_3^+ participate in quenching collisions with molecules H_2

$$(H_3)^+ * + H_2 \rightarrow H_3^+ + H_2^*. \tag{2}$$
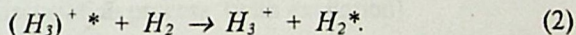
The H_3^+ ions in the ionic source will be formed in the following reaction [10]

$$H_2^+ + H_2 \rightarrow H_3^+ + H . \tag{3}$$
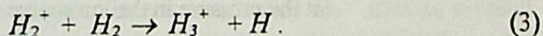
The number of quenching collision is defined from a relative output of H_2^+ and H_3^+ ions. Therefore, it is necessary to measure dependence of a relative output H_2^+ ions on the pressure of hydrogen inside the source, as it was offered in article [10]

71

$$R = I(H_2^+) \, / \, I(H_2^+) + I(H_3^+).\qquad(4)$$

$I(H_2^+)$ and $I(H_3^+)$ are currents of (H_2^+) and (H_3^+) ions extracted from the source. From this dependence follows, that in the investigated range, the relative fraction of H_3^+ ions was decreased with increasing of pressure in the source (Fig.1). The coefficient R reaches at least value 0.05. This value is comparable with the value 0.06, which was obtained in article [10] in the Penning type source, at the same values of the pressure ~ 0.1 Torr. It is necessary to note, that the coefficient R essentially varies depending on the type of the source. However researches of various types of the source indicate [10], that the minimum value of R in all cases is reached approximately at the same pressure ~ 0.1 Torr. Our results are well agreed with results of the authors of ref. [10].
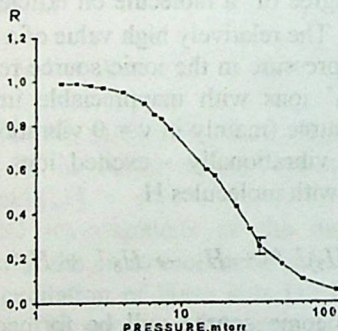
Fig.1. Dependence of a relative output R of ions H_2^+ and H_3^+
at the pressure in the ion source.

We have presented a result of the measurement of the excitation efficiency (normalized counting rate on a current of a primary beam) of L_α lines in the collision H_3^+ - He (at the energy E = 4 keV of ion) at various pressures of a source (Fig.2). The excitation efficiency decreases (approximately 2 times) with increasing of pressure and $\rightarrow$

72
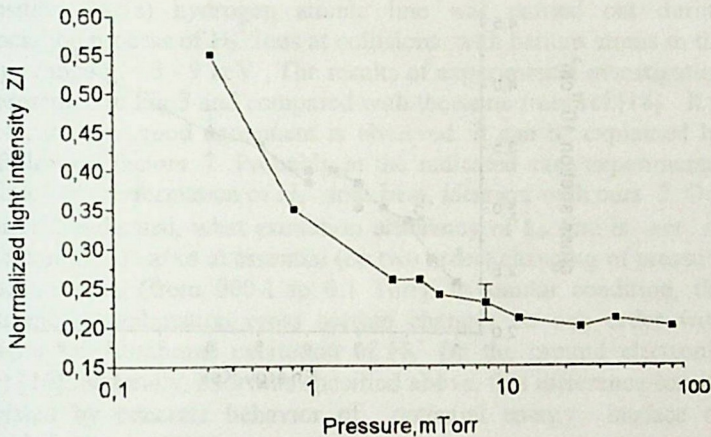
Fig.2. Dependence of the efficiency Z / I (Z- light intensity, I – ion beam intensity) on the pressure in the ion source .

achieves saturation at pressure of hydrogen 0.06 - 0.08 Torr. (Fig.2). It means, that at rather low pressures ~ 0.0003 Torr., the internal (vibrational) excitation of H_3^+ ions essentially influences on the probability of the dissociation process (with excitation).

3.RESULTS AND DISCUSSION

The analysis of our experimental results indicates, that excitation efficiency of hydrogen atomic line is less, when H_3^+ ions as a result of quenching collision become de-excited. It can be explained on the basis of following fact: the vibrational excitation (~ 0.3 - 1 eV) in the ground electronic state reduces to the considerable change (a few eV) of inelastic threshold amount of excitation energy of an excited electronic state. In our case this is the electronic state ($^1A_2''$). Such type of investigation was carried out earlier [10,11,16]. However they

73
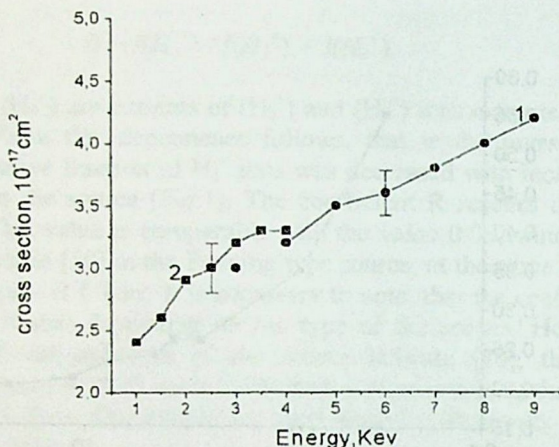
Fig.3. Emission cross section of the hydrogen atomic line
HI (121.6 nm) 1-Our results, 2-G.H. Dunn et al. [18].

concerned inelastic channels of dissociation, producing the hydrogen atoms in the ground state. Consequently excited states, studied in these articles, differ from those surveyed by us. It is necessary to note, that the research of excitation efficiency of various inelastic channels depending on vibration excitation of H_3^+ ion (in a ground electronic state) contains the important information sort of a surface of potential energy of various excited electronic states. Our results specify that the concrete behavior of energy surfaces in area Franck-Kondon (is meant saving a principle Franck-Kondon) is those, that the energy difference between vibrational level v = 0 (of the ground electronic state $1A_1{}'$) and vibrational level of excited electronic state $1A_2{}''$ at vertical transition (in frameworks of principle Franck-Kondon) on some eV is more than for transition from excited v = 1, v = 2 or v = 3 vibrational levels (of the ground electronic state of H_3^+). Investigation of authors of ref. [11] indicates that in various ionic sources at pressures 10^{-3} mTorr there can be a sufficient amount of ions H_3^+ in excited v = 1, v = 2 or 3 vibrational states. Probably, in our conditions when pressure inside a source reaches $P = 8 \cdot 10^{-2} - 10^{-1}$ Torr, from a source the ions are extracted in the ground v = 0 vibrational state. In these conditions,

74

the measurements of the emission cross section of $\lambda = 121.6$ nm (transition 2p-1s) hydrogen atomic line was carried out during dissociation process of H_3^+ ions at collisions with helium atoms in the energy range $E = 3 - 9$ keV . The results of experimental investigation are presented in Fig.3 and compared with the same from ref.[18]. It is visible, that the good agreement is observed. It can be explained by the following factors: 1. Probably in the indicated case experimental condition of the formation of H_3^+ ions beat, identical with ours 2. Our researches indicated, what excitation efficiency of L_α line is not so significant (~ 2) varies at essential (on two order) changing of pressure inside a source (from 000.1 to 0.1 Torr). In similar condition, the electronic recombination cross section changes on one order with changing of vibrational excitation of H_3^+ (in the ground electronic state) [16]. Naturally, as it was specified above, this difference can be stipulated by concrete behavior of potential energy surface of excited electronic state.

REFERENCES

1. J.J. Thompson. Philos. Mag. **24**, 1912, 209.
2. M. J. Gailard, D.S. Gemmel, G. Goldring, L. Levine, W.J. Pietch, J.C. Poizat, R.J. Ratkowski, J. Remilleux, Z. Vager, B.J. Zabrowsky. Phys. Rev. **A17**, 1978, 1797.
3. T. Oka. Phys. Rev. Lett. **45**, 1980, 531.
4. S.C. Goh, J.B. Swan. Phys. Rev. A **24**, 1981, 1624.
5. H. Martinez, I. Alvarez, J. De Urquijo, C. Cisneros, A. Amaya-Tapia. Phys. Rev. A **36**, 1987, 5425.
6. G.D. Carney, R.N. Porter. J. Chem. Phys. **60**, 1974, 4251.
7. G.D. Carney, R.N. Porter. J. Chem.Phys. **65**, 1976, 3547.
8. C.E. Dykstra, W.C. Swope. J. Chem.Phys. **70**, 1970, 1.
9. L.J. Schaad, W.V. Hicks. J. Chem. Phys. **61**, 1974, 1934.
10. B. Peart, K.T. Dolder. J. Phys. **B7**, 1974, 1567.
11. H. Hus, F. Youssif, A. Sen, J.B. A. Mitchell. Phys. Rev. **A38**, 1988, 658.
12. O. Yenon, L.M. Miese, D.Golabrese, D. H. Jaecks. Phys. Rev. **A42**, 1990, 324.

13. D.L. Montgomery, D.H. Jaecks. Phys. Rev. Lett. **51**, 1983, 1862.
14. J.B.A. Mitchell, J.L. Forand, C.T. Ng, D.P. Levac, R.E. Mitchell, P.M. Mul, W. Claeys, A. Sen, J .Wm. McGovan. Phys. Rev. Lett. **51**, 1983, 885.
15. I. Alvarez, C. Cisneros, J. DeUrquaijo, T.G. Morgan. Phys. Rev. Lett. **53**, 1984, 740.
16. I. Alvarez, F. Youssif, G. Hinojosa, C. Cisneros, J. DeUrquaijo. XXI - ICPEAC, abstr. of conf. papers **II**, 1999, 601.
17. O.Yenon, D.H. Jaecks, L.M. Wiese. Phys. Rev. **A39**, 1989, 1767.
18. G.H. Dunn, R. Geballe, D. Pretzer. Phys. Rev. **128**, 1962, 2200.
19. E. Herbst, W. Klemperer. Astrophys. J. **185**, 1973, 505.
20. W.D. Watson. Rev. Mod. Phys. **48**, !976, 513.
21. H. Suzuki. Prog. Theor. Phys. **62**, 1979, 936.
22. M.R. Gochitashvili, R.V. Kvizhinadze, N.R.Dzhaliashvili, B.I.Kikiani, JTF. **63**, 1993, 35.

Tbilisi State University

მ. გოჩიტაშვილი, | ნ. ჯალიაშვილი, | რ.კვიჟინაძე, ბ.კიკიანი

ატომური წყალბადის აღგზნება H_3^+ - He დაჯახების პროცესში: შინაგანი (რხევითი) აღგზნების წვლილი

დასკვნა

მოცემულ სამუშაოში წარმოდგენილია წყალბადის ატომური ხაზის L_α ($\lambda = 121.6$ ნმ) გამოსხივების სრული კვეთის ექსპერიმენტული გაზომვის შედეგები იონების 3 - 9 კევ ენერგეტიკულ არეში. ნაჩვენებია, რომ H_3^+ იონების რხევითი დონეების დასახლება მნიშვნელოვან გავლენას ახდენს მოცემული ოპტიკური ხაზის აღგზნების ეფექტურობაზე. აღნიშნული მოლეკულური იონის რხევითი დონეების დასახლების ხასიხი დამოკიდებულია იონურ წყაროში იონების წარმოქმნის პირობებზე. კერძოდ წყალბადის წნევაზე იონურ წყაროში.

STUDY OF COSMOGENIC RADIOCARBON CONCENTRATION VARIATIONS IN THE EARTH'S ATMOSPHERE DURING SOLAR ACTIVITY OF MOUNDER MINIMUM (1645-1715)

S. Tsereteli, V. Bochorishvili, M. Samkharadze, G. Khoriauli

ABSTRACT. Variations of radiocarbon concentration have been studied in annual rings for the last 350 years (1600-1950) on the basis of our experimental research using methods of spectral analysis. From this interval of time special attention is paid to the so-called period of Maunder minimum (1645-1715) of solar activity. In the experimental series of corresponding period of cosmogenic radiocarbon concentration of Maunder minimum two types of periodicity are revealed: ~20 year and ~8 year.

The establishment of the dynamics of solar activity, regularity of its cyclicing is one of the actual problems of contemporary astrophysics. Correspondingly the study of those intervals in the coarse of history of the Sun's existence when solar activity is sharply changed is of particular significance, namely: in 1100-1250 "maximum of Middle Ages", in 1282-1342 "Volf minimum", 1416-1534 "Shperer minimum", 1645-1715 "Mounder minimum", etc.

The period of Maunder minimum solar activity has particular attention of scientists also by the fact that this last one puts forward a lot of new and unexpected problems. Really, one of the main characteristics of solar activity - spots on the surface of the Sun are long known to scientists and therefore the notes about the spots disappearance on the Sun during Mounder minimum are reliable but due to the absence of regular observations on the Sun in the mentioned period it is difficult to say something about solar activity, about the parameters of this minimum.

It should be noted that the anomalies are found in differential rotation of the Sun's surface at the beginning of Maunder minimum. In the opinion of the different scientists, it might indicate that global characteristics of the Sun's inner parts at that time change even before "dynamo" mechanisms of the Sun's spots. In this connection the following questions can be put: what are the mean parameters of Maunder minimum and radioactive state in the Earth's space in that epoch? What is the character of those processes which cause such a sharp fall of solar activity? To what extent are our imaginations about solar activity in general right?

For the mentioned direction of the study of special attention are cosmogenic isotopes ^{14}C ($T_{1/2}$ = 5730 year), ^{10}Be ($T_{1/2}$ = 1.5 mln. year) by which it is possible to obtain much information about the dynamics of solar activity.

At present the most complete data about the solar activity and the intensity of cosmic rays in the past are obtained by means of the above mentioned cosmogenic isotopes (^{14}C and ^{10}Be) formed in the Earth's atmosphere. The main peculiarity of these isotopes and advantage as compared with other isotopes is the fact that in nature there exist objects (e. g. tree rings, Arctic and Antarctic ices, algae with long life time, etc.) which can "fix" i.e. "memorize" annual concentration of the mentioned isotopes is that period of time which prevails in great extent the period of isotopes half-life.

To study the influence of solar activity(modulation) in the Earth's atmosphere on radiocarbon concentration during Maunder minimum of solar activity we use experimental data obtained at the laboratory of nuclear physics of the TSU [1,2] (Fig. 1).

First of all, it should be noted that experimental data contain both Maunder minimum itself (1645-1720) (Fig. 2) and its neighboring sections (1600-1645 and 1715-1800). It should be also marked that the measurements in [1] were performed with one-year step, or ^{14}C concentration is increased in every calendar year of corresponding tree ring

The experimental data illustrated in Fig. 1 were obtained in Lithua as a result of ^{14}C concentration measurement in annual ring. The value

of ^{14}C concentration in relation to International standard scale is calculated by the following formula

$$\Delta^{14}C_0(\%) = \frac{N_S - N_{ST}}{N_{ST} - N_B},$$

where N_S, N_{ST}, N_B represent reference velocity of experimental installation during measurement of sample (S), standard (ST) and background (B). Measurement error didn't exceed 0.2-0.3%.

Due to the fact that first of all we are interested in variations of ^{14}C concentration only of "comic" sources, it is necessary from the data of ^{14}C concentration data to exclude the share of the Earth's magnetic field. Numerous authors consider the problems of geometric field effect on ^{14}C concentration. At present the most accurately established one can be considered global change of geomagnetic field with period ≈ 10 thousand year causes about $\approx 10\%$ change ^{14}C concentration.

The account of geomagnetic field effect on ^{14}C concentration is realized by formula

$$\Delta^{14}C(t) = \Delta^{14}C_0(t) - 4.27 - 4.97 \cdot \sin\left[\frac{2\pi}{10402} \cdot (t + 7388)\right]\%,$$

where t is a current calendar year (t is negative B C).

To study the dynamics of solar activity in the Earth's atmosphere by means of determination of ^{14}C concentration in the period of Maunder minimum it is necessary to reveal the existed cyclings (periodicities in experimental data of given in Fig.2 of ^{14}C time dependence or to establish the character of variations. For this we have used the method of spectral analysis of experimental data processing [4], the results of which are shown in Fig.3. The mentioned diagram expresses the dependence between the calculated values of the intensity of radiocarbon curves spectrum and frequency. As is seen from the Table the main peak is marked by high reliability interval (95%) on frequency ~0.05 (corresponding period ~20 min). Besides comparatively weak

peak is observed on frequency ~0.12 (corresponding period ~ 8 min). The reliability of this last one is comparatively low.

Thus the following conclusions can be done:

1) With the help of the method of spectral analysis we have studied variations of cosmogenic radiocarbon concentration in the Earth's atmosphere in the period of Maunder minimum of solar activity.

2) Periodicity of two types has been revealed in experimental curves of cosmogenic radiocarbon concentration of Maunder minimum corresponding period.

3) The source of the above mentioned can be considered the solar activity. This means that in Maunder minimum period of solar activity modulating action of the Sun becomes weak but cycling is preserved. It can be also said that in period of Maunder minimum the mechanism of solar dynamo still continues the work and sharp reduce of spots on the Sun during Maunder minimum can be caused by the fact that minimum of any other long-period wave coincides with the period of Maunder minimum.
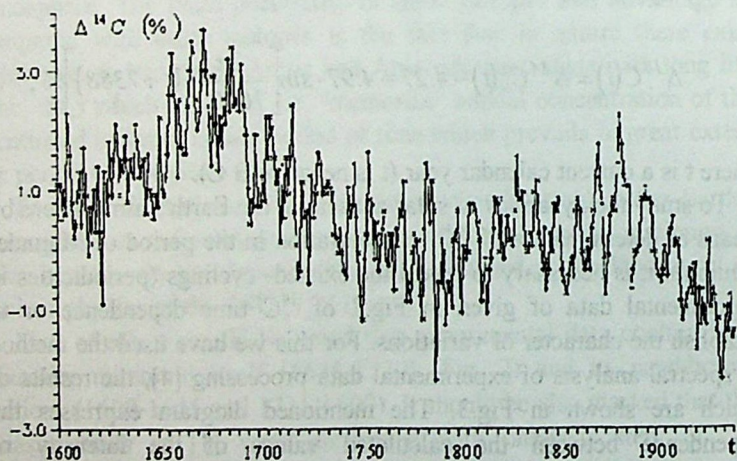
Fig.1. ^{14}C concentration in the atmosphere in 1600-1940.
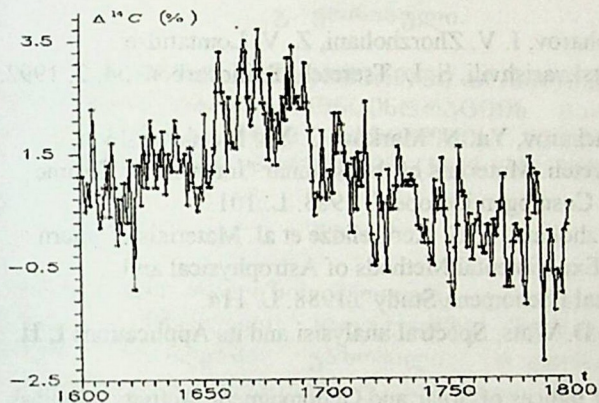
Fig. 2. ^{14}C concentration in the atmosphere in 1600-1800.
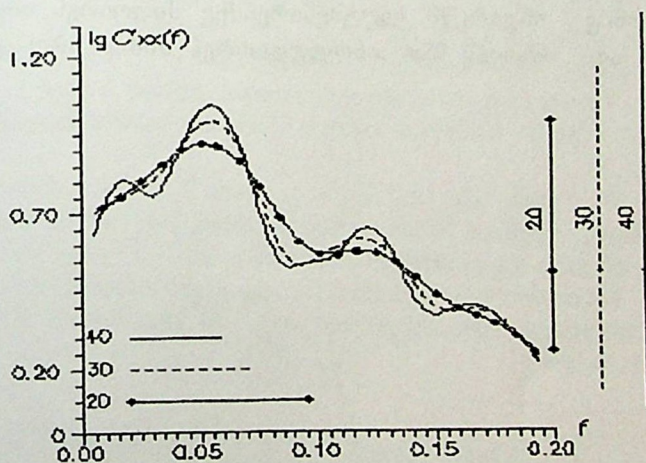
Fig. 3. Dependence of spectrum power $C_{xx}(t)$ on frequency (period).
For radiocarbon in 1645-1720.

REFERENCES

1. G. E. Kocharov, I. V. Zhorzholiani, Z. V. Lomtatidze,
   R. Y. Metskvarishvili, S. L. Tsereteli. Radiocarbon. **34**, 2, 1992,
   213.
2. G. E. Koncharov, Yu. N. Markov, G. Ya. Metskvarishvili,
   S. L. Tsereteli. Materials of the Seminar "Intensity of Cosmic
   Rays and Cosmogen Isotopes". 1983. L. 101.
3. I. V. Zhorzholiani, P. G. Kereselidze et al. Materials of Intern.
   Seminar "Experimental Methods of Astrophysical and
   Geophysical Phenomena Study". 1988. L. 114.
4. G. Jekins, D. Wats. Spectral analysisi and its Applications **I, II**.
   M. 1971.
5. Catalog of Indices of Solar and Geliomagnetic Activity. Obninsk.
   1976.

Tbilisi State University

ს. წერეთელი, ვ. ბოჯორიშვილი, მ. სამხარაძე,
გ. ყორიაული.

დედამიწის ატმოსფეროში კოსმოგენური რადიონახშირბადის კონცენტრაციის ვარიაციების შესწავლა მზის აქტივობის მაუნდერის მინიმუმის პერიოდში (1645-1715 წლები)

დასკვნა

სპექტრული ანალიზის მეთოდის გამოყენებით ჩატა-
რებული გამოკვლევის საფუძველზე შესწავლილია ხის
წლიურ რგოლებში გაზომილი რადიონახშირბადის
კონცენტრაციის ვარიაციები უკანასკნელი 350 წლის მან-
ძილზე (1600-1950წ.) დროის ამ ინტერვალიდან განსა-
კუთრებული ყურადღება ეთმობა მზის აქტივობის ე. წ.
მაუნდერის მინიმუმის პერიოდს (1645-1715წ.). კოსმოგენური
რადიონახშირბადის კონცენტრაციის მაუნდერის მინიმუმის
შესაბამისი პერიოდის ექსპერიმენტულ მწკრივში გამოვ-
ლენილია ორი სახის პერიოდულობა: ≈20 წლიანი და ≈8
წლიანი.

ON THE PROBLEM OF PHONON AVALANCHE

K.Nikoladze

ABSTRACT. The nonlinear system of differential equations is obtained and solved analytically which describes an interaction of the spin system with the phonon one (the lattice modes of crystal) immersed in the heat reservoir. Comparison with the well-known results of numerical calculations and experiments of Brya and Wagner [5], devoted to the study of the phonon avalanche phenomenon, shows their rather good agreement. The suggested formulas allow to describe the problem with a sufficiently high accuracy.

Recently the radiofrequency radiation from the spin system, particularly superradiance and stationary lasing, is experimentally and theoretically intensively investigated [1-7].

The numerical methods of problems solution is used for explanation of the results of the experimental investigations of paramagnetic relaxation impurities in crystals immersed in the heat reservoir.

The original analytical approximate method is used in the present work for the analytical solution of the nonlinear differential equations [2, 8].

We consider the case $T_2 \ll \tau$, where T_2 is the spin-spin relaxation time, τ - phonon-phonon relaxation time. This case corresponds to the well-known experimental situations.

Let us derive the equations for spin-phonon dynamics. There are two subsystems: spin and phonon ones. The Hamiltonian of the integrate system is:

$$H = \sum_k^n \omega_s S_{zk} + \sum_k^n \omega_k a_k^+ a_k + \frac{1}{2}\sum_{ki}(L_k^+ S_i^- + L_k^- S_i^+), \qquad (1)$$

where the first term is the Zeeman energy of spin-system, second the phonon's Hamiltonian in harmonic approximation, third - the

Hamiltonian of spin-phonon interaction; a_k^+, a_k are creation and annihilation operators of phonons with wave vector $\bar{k}$ and cyclic frequency ω_k; $L_k^{\pm}$ are lattice operators which would be represented in the single-phonon relaxation form:

$$L_k^+ = (A\omega_k)^{1/2} a_k^+, \quad L_k^- = (L_k^+)^+,$$

where A is a constant of spin-phonon coupling [9].

Equations of motion for spin operators S_x, S_y, S_z and phonon ones a_x and a_y are obtained by application of the rule for operator's derivative

$$\frac{d\hat{Q}}{dt} = \frac{i}{\hbar}[H, \hat{Q}]$$ (in the equation (1) and below everywhere signs of operators is omitted and it is supposed that $\hbar = 1$). Taking into consideration the spin-spin relaxation time T_2 and τ - the time of phonon–phonon relaxation one obtains the system of five coupled differential equations for every spin (subscript i) and phonon (subscript k):

$$\dot{S}_{ix} + \frac{S_{ix}}{T_2} + \omega_s S_{iy} = \sum_k (A\omega_k)^{1/2} a_{ky} S_{iz} ,$$

$$\dot{S}_{iy} + \frac{S_{iy}}{T_2} - \omega_s S_{ix} = -\sum_k (A\omega_k)^{1/2} a_{kx} S_{iz} ,$$

$$\dot{S}_{iz} = \sum_k (A\omega_k)^{1/2} a_{kx} S_{iy} - \sum_k (A\omega_k)^{1/2} a_{ky} S_{ix} , \quad (2)$$

$$\dot{a}_{kx} + \frac{a_{kx}}{\tau} - \omega_k a_{ky} = \frac{1}{2}\sum_i (A\omega_k)^{1/2} S_{ix} ,$$

$$\dot{a}_{ky} + \frac{a_{ky}}{\tau} - \omega_k a_{kx} = \frac{1}{2}\sum_i (A\omega_k)^{1/2} S_{ix} .$$

Taking into account that $T_2 \ll \tau$ and isotropy of the sample and going over into component of the magnetization $\bar{M}$, the system (2) is symplified to a considerable extent

$$\dot{M}_x + \frac{1}{T_2} M_x + \omega_s M_y = 0,$$

$$\dot{M}_Y \frac{1}{T_2} M_Y - \omega_s M_x + M_z \sum_k (A\omega_k)^{1/2} a_{kx} = 0,$$

$$\dot{M}_z = M_Y \sum_k (A\omega_k)^{1/2} a_{kx} = 0, \tag{3}$$

$$\dot{a}_{lx} + \omega_l a_{ly} + \frac{(A\omega_l)^{1/2}}{2\gamma} M_y = 0,$$

$$\dot{a}_{ly} - \omega_l a_{lx} - \frac{1}{2\gamma} (A\omega_l)^{1/2} M_x = 0,$$

where $M_x = \gamma \sum_i S_{ix}$, $M_y = \gamma \sum_i S_{iy}$, γ is the gyromagnetic relation; M_y and a_y are eliminated from the system (3) and one obtains the new system of equations

$$\ddot{M}_x + \frac{2}{T_2} \dot{M}_x + \omega_s^2 M_x - \omega_s M_z \sum_k (A\omega_k)^{1/2} a_{kx} = 0,$$

$$\dot{M}_z = -\frac{1}{\omega_s} \dot{M}_x \sum_k (A\omega_k)^{1/2} a_{kx}, \tag{4}$$

$$\ddot{a}_{lx} + \frac{2}{\tau} \dot{a}_{lx} + \omega_l^2 a_{lx} = -\frac{\omega_l (A\omega_l)^{1/2}}{2\gamma} M_x.$$

To solve the system (4) it is applied the method of slow changing amplitudes.

The solution is found in the form:

$$M_x = \frac{1}{2}(\tilde{M}_x e^{i\omega t} + c.c.), \quad a_x = \frac{1}{2}(\tilde{a}_x e^{i\omega t} + c.c.).$$

One obtains the first order differential equations system for amplitudes.

$$2i\omega - \omega^2 M_x + \frac{2i\omega}{T_2}\tilde{M}_x + \omega_s^2\tilde{M}_x = \omega_s M_z \sum_k (A\omega_k)^{1/2}\tilde{a}_{kx},$$

$$\dot{M}_z = \frac{i}{4}\sum_k (A\omega_k)^{1/2}(\tilde{a}_{kx}\tilde{M}_x^* - \tilde{a}_{kx}^*\tilde{M}_x), \tag{5}$$

$$2i\omega\,\tilde{a}_{lx} - \omega\omega^2\tilde{a}_{lx} + \frac{2i\omega}{\tau}\tilde{a}_{lx} + \omega\omega^2\tilde{a}_{lx} = -\frac{\omega\omega_l(A\omega_l)^{1/2}}{2\gamma\gamma}\tilde{M}_x.$$

Using the condition $\frac{d}{dt} \ll \frac{2}{T_2}$ and simplifying the first equation of the system (5) one obtains

$$-\omega^2\tilde{M}_x + \frac{2i\omega}{T_2}\tilde{M}_x + \omega_s^2\tilde{M}_x = \omega_s M_z \sum_k (A\omega_k)^{1/2}\tilde{a}_{kx}.$$

Then

$$\tilde{M}_x = \frac{(\omega_s M_z / 2i\omega)\sum_k (A\omega_k)^{1/2}\tilde{a}_{kx}}{1/T_2 + (\omega_s^2 - \omega^2)/2i\omega}.$$

Substituting $\tilde{M}_x$ into the second and third equations of the system (5) one obtains respectively

$$\dot{M}_z = -T_2 \left| \sum_k (A\omega_k)^{1/2} \right|^2 |\widetilde{a}_{kx}|^2 M_z,$$

$$2\dot{a}_{lx} + \frac{2}{\tau}\widetilde{a}_{lx} = \frac{(A\omega_l)^{1/2}}{4\gamma} T_2 \sum_k (A\omega_k)^{1/2} \widetilde{a}_{kx} M_z. \tag{6}$$

It was supposed that $\omega = \omega_l = \omega_s$ in previous calculations. Let us proceed to the equation for $|\widetilde{a}_x|^2$ instead of the equation for $\widetilde{a}_x$ using the relation:

$$\frac{d}{dt}|\widetilde{a}_x|^2 = \frac{d}{dt}(\widetilde{a}_x \widetilde{a}_x^*) = a_x^* \frac{d\widetilde{a}_x}{dt} + \widetilde{a}_x \frac{d\widetilde{a}_x}{dt}.$$

A little manipulations yield:

$$\frac{d}{dt}\widetilde{a}_{lx}^2 + \frac{2|\widetilde{a}_{lx}|^2}{\tau} = \tag{7}$$

$$= \frac{M_z/(8T_2)\left[(A\omega_l)^{1/2}\widetilde{a}_{lx}^* \sum_k (A\omega_k)^{1/2} + (A\omega_l)^{1/2}\widetilde{a}_{lx} \sum_k (A\omega_k)^{1/2} a_{kx} \right]}{(1/T_2)^2}$$

The multiplier in brackets containing sums was transformed. The equation (7) takes the form:

$$\frac{d}{dt}|\widetilde{a}_{lx}|^2 + \frac{2}{\tau}|\widetilde{a}_{lx}|^2 = \frac{T_2}{4\gamma}(A\omega_l)^{1/2}|\widetilde{a}_{lx}|^2 \sum_k (A\omega_k)^{1/2} M_z. \tag{8}$$

Summation of the equation (8) with respect to l gives

$$\frac{d}{dt}\sum_l |\tilde{a}_{lx}|^2 + \frac{2}{\tau}\sum_l |\tilde{a}_{lx}|^2 = \frac{T_2}{4\gamma}|\tilde{a}_{lx}|^2 \sum_k A\omega_k M_z .\qquad (9)$$

One replaces the sum by integral

$$\sum_k \omega_k = \int_\Delta \omega \frac{3\omega^2}{2\pi^2 U^3}d\omega = \frac{3}{2\pi^2 U^3}\int_\Delta \omega^3 d\omega \approx \frac{3\omega_s^3}{2\pi^2 U^3}\frac{1}{T_2} .\qquad (10)$$

One takes integral over the range of half-breadth of paramagnetic ion line. The sign $\sum = \frac{3\omega^2 d\omega}{2\pi^2 U^3}$ is the number of quantum states of phonons in unit volume in the given range of frequencies, here U is a sound velocity [7]. Let's introduce designation $P = |\tilde{a}_{ix}|^2$, which is mean-square amplitude of the lattice mode.

As $\sum_l |\tilde{a}_{lx}|^2 = p\sum$ the equation (9) takes the form:

$$\frac{dp}{dt} + \frac{2}{\tau}p = -\frac{1}{4\gamma\sum}\frac{3A\omega_s^3}{2\pi^2 U^3}M_z .\qquad (11)$$

One makes use of the expression for magnetization of spin system (s = 1/2, $\hbar = 1$):

$$M_{zo} = N\mu th\frac{\mu H}{kT_0} = N\frac{\gamma}{2}th\frac{\omega_s}{2kT_0} ,\qquad (12)$$

where N is the number of paramagnetic ions in unit volume; μ is magnetic moment of the single ion; T_0 is a bath temperature.

Taking into consideration (12) and the expression [10]:

$$\frac{1}{T_1} = \frac{3A\omega_s^3}{4\pi U^3}cth\frac{\omega_s}{2kT_0} ,\text{ the system (6) takes the form:}$$

89

$$\frac{dM_z}{dt} = -\frac{\omega_s}{\pi k T_0 T_1} p M_z,$$

$$\frac{dp}{dt} = -\frac{p}{\tau_c}\left[1 + \frac{T_2}{T_R}\frac{M_z}{|M_{z0}|}\right], \tag{13}$$

where T_1 is the longitudinal relaxation time, $T_R = \dfrac{8\pi T_1 T_2 \sum}{\tau N \, th^2\left(\dfrac{\omega_s}{2kT_0}\right)}$ the

radiation damping time of spin system [11], T_2 the transversal

relaxation time or the spin-spin relaxation time, $\tau_c = \dfrac{\tau}{2}$, where τ is the

phonon-phonon relaxation time, T_0 is a bath temperature. One

introduces the designation $\rho = \dfrac{\omega_s}{\pi k T_0 T_1}$, where ω_s is the Larmor

precession frequency.

The system (13) takes the form:

$$\frac{dM_z}{dt} = -\rho M_z p, \tag{14a}$$

$$\frac{dp}{dt} = -\frac{p}{\tau_c}\left(1 + \frac{T_2}{T_R}\frac{M_z}{|M_{z0}|}\right). \tag{14b}$$

The solution of (14b) is found in the form :

$$p = AS \, ch^2 (Bt - C). \tag{15}$$

The parameters A, B and C will be determined below. Let's divide (14a) into (14b):

$$\frac{dM_z}{dp} = \frac{\rho M_z \tau_c}{1 + \dfrac{T_2}{T_R}\dfrac{M_z}{|M_{z0}|}}. \qquad (16)$$

One designates $z \equiv ln\left(-\dfrac{M_z}{|M_{z0}|}\right)$; here z < 0, as $|M_z| < |M_{z0}|$. The

equation (14a) takes the form

$$\dot{z} = -\rho\, p. \qquad (17)$$

One presents (16) in the form:

$$\rho\tau_c dp = \frac{dM_z}{M_z} + \frac{T_2}{T_R}\frac{dM_z}{|M_{z0}|}. \qquad (18)$$

Let's integrate (18) with initial conditions: $M_z(0) = -|M_{z0}|$ and $p(0) = p_0$, where p_0 is quadratic mean value of a lattice resonance mode's amplitude in the initial moment.

As a result one obtains:

$$p = \frac{1}{\rho\tau_c}\left\{ ln\left(-\frac{M_z}{|M_{z0}|}\right) + \frac{T_2}{T_R}\left(\frac{M_z}{|M_{z0}|}+1\right)\right\} + p_0. \qquad (19)$$

Let's substitute (19) into (17) and determine $\dfrac{M_z}{|M_{z0}|}$:

$$\frac{M_z}{|M_{z0}|} = -1 - \frac{\tau_c T_R}{T_2}\left[\dot{z} + \frac{1}{\tau_c}z + \rho p_0\right]. \qquad (20)$$

Substituting the value $p = AS\, ch^2\,(Bt - C)$ into (17), at the initial condition: z(0) = 0, after integration respective equation for z, one obtains

91

$$z = -\frac{\rho A}{B}[th(Bt - C) - th(-C)]. \qquad (21)$$

From (20) and (21) it follows that

$$\frac{M_z}{|M_{z0}|} =$$

$$-1 + \frac{\tau_c T_R}{T_2}\rho A\left\{S\,ch^2(Bt - C) + \frac{1}{\tau_c B}\left[th(Bt - C) - th(-C)\right] - \frac{p_0}{A}\right\} \quad (22)$$

To determine the parameter B the values $\dot{p}$, p and $\dfrac{M_z}{|M_{z0}|}$ are substituted into (14b) at $t = 0$:

$$B = -\frac{(T_2/T_R)(1 - T_R/T_2)}{2\tau_c\ th(-C)}. \qquad (23)$$

The solution of the system getting generation of the superradiation is found when $T_R/T_2 < 1$, i.e. $1 - \dfrac{T_R}{T_2} > 0$. For $th(-C) < 0$, $C > 0$ and B > 0. At $t = 0$, $S\,ch^2(-C) = \dfrac{p_0}{A} \ll 1$, i.e. $S\,ch^2(-C) = 1 - th^2(-C) \approx$ 0, or $th^2(-C) \approx 1$, i.e. $th(-C) \approx -1$.

Analogically to determine the parameter A the values $\dot{p}$, p and $\dfrac{M_z}{|M_{z0}|}$ are substituted into (14b) but at $t \to \infty$: because $B > 0$,

$$\lim_{t \to \infty} th(Bt - C) = 1, \text{ and } \lim_{t \to \infty} S\,ch(Bt - C) = 0.$$

Then

92

$$A = \frac{(T_2/T_R)^2(1-T_R/T_2)^2}{2\tau_c\rho \; th^2(-C)} + \frac{1-T_R/T_2}{4(T_R/T_2)}p_0. \qquad (24)$$

Using designation $x = T_R/T_2$, from (15), (22)-(24)

$$\frac{M_z}{|M_{z0}|} = -1 + (1-x)\left\{th\left[\frac{1-x}{2x\tau}(t-T_m)\right] + th\left(\frac{1-x}{2x\tau}T_m\right)\right\} \qquad (25)$$

and

$$p = \left\{\frac{Nth\left(\dfrac{\omega_s}{2kT_0}\right)(1-x)^2}{16x\Sigma} + \frac{1-x}{4x}p_0\right\}S\,ch^2\left\{\frac{1-x}{\tau x}(t-T_m)\right\}, \qquad (26)$$

where $T_m = C/B$ is time when p reaches its maximum.

For finding T_m it is used the initial condition for p (see (15) at $t = 0$): $p/A \ll 1$. A little manipulation yield:

$$T_m = \frac{\tau x}{1-x}ln\left\{2\left[\frac{N\,th(\omega_s/2kT_0)(1-x)^2}{16xp_0\Sigma} + \frac{1-x}{4x}\right]^{1/2}\right\}. \qquad (27)$$

The width of the phonon pulse is

$$\Delta t = \frac{\tau x}{1-x}ln(1+\sqrt{2}). \qquad (28)$$

In calculations we used parameters from experiments of Brya and Wagner [5] carried out for dilute cerous magnesium nitrate at Zeeman frequencies of 11 GHz and nominal cerium concentration of 0.2%: density of paramagnetic ions $N = 3 \cdot 10^{18}$ cm^{-3}, a temperature of 1.4^{0}K,

a sound velocity $\sim 2.5 \cdot 10^5$ cm/sec, bandwidth approximately equal to the resonance linewidth, 15 MHz, the phonon lifetime $\tau = 1 \mu sec$.

Results of numerical calculations of T_m, P_m, p/p_m and $-M_z/|M_{z0}|$ for different values of x in interval 0.5 through 0.9 according to formulas (25) - (27) are present in Table and Figs. 1 and 2. Here the parameter $1/x$ is the "bottleneck factor" [5].

Table. Values of moments of phonon's maximum excitation, (T_m), and maximum of phonon excitation, (p_m), as a function of x according to (27) and (26).

x	0.5	0.51	0.55	0.6	0.7	0.8	0.9
T_m	4.44	4.59	5.22	6.2	8.76	13.2	22.9
p_m	4000.6	3750.5	2906.9	2100.4	1000.2	390.1	95.2
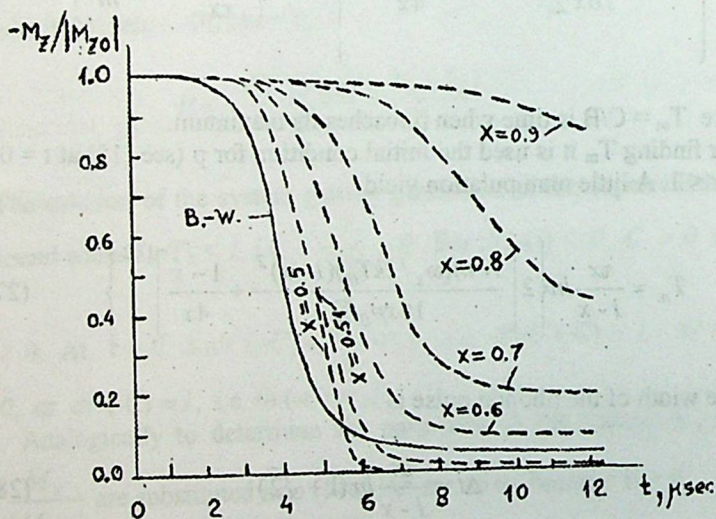
Fig. 1. Magnetization, $-M_z/|M_{z0}|$, as a function of time t according to (25) for different values of x. Solid line – numerical solution of Brya and Wagner [5].
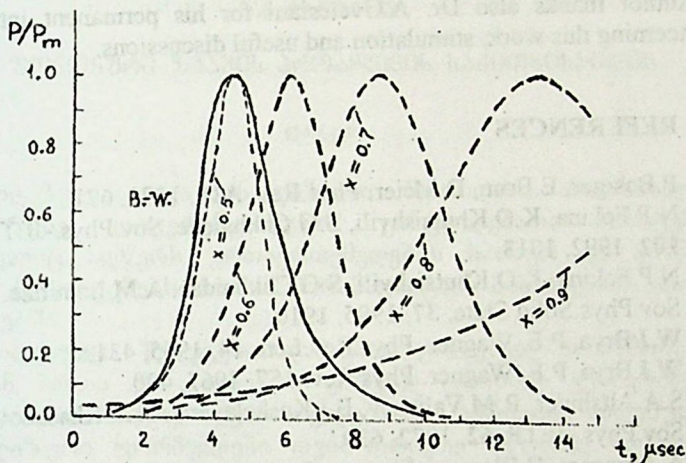
Fig. 2. Phonon excitation as a function of time t according to (26) for different values of x. Solid line -- numerical solution of Brya and Wagner [5].

The analysis of Table and Figs. 1 and 2 shows that when $x \rightarrow 1$ branches of phonon excitation curves are expanded and both moments of excitation maximums and most fast decays of curves are shifted to the right side and, in addition, their values are decreased. Physically this is explained by weakening of phonon avalanche when the "bottleneck factor" is decreased. In case when $x = 0.5, 0.51$, the analytical curve almost coincides with numerical and experimental curves [4,5]. Thus, the suggested analytical formulas with a sufficiently high accuracy describe the well-known experiments of Brya and Wagner on the phonon avalanche.

ACKNOWLEDGEMENTS.

Author thanks also Dr. A.Gvelesiani for his permanent interest, concerning this work, stimulation and useful discussions.

REFERENCES

1. P.Bosiger, E.Brun, D.Meier. Phys.Rev. **A18**, 1978, 671.
2. N.P.Fokina, K.O.Khutsishvili, S.G.Chkhaidze. Sov.Phys.-JETP. **102**, 1992, 1013.
3. N.P.Fokina, K.O.Khutsishvili, S.G.Chkhaidze. A.M.Lomidze. Sov.Phys.Solid State. **37**, 1995, 1910.
4. W.J.Brya, P.E. Wagner. Phys.Rev.Lett. **14**, 1965, 431.
5. W.J.Brya, P.E. Wagner. Phys.Rev. **157**, 1967, 400.
6. S.A.Altshuler, R.M.Valishev, B.I.Koshelayev, A.Kh.Khasanov. Sov.Phys.-JETP. **62**, 1972, 639.
7. A.Abragam, B.Bleaney. Electron Paramagnetic Resonance of Transition Ions Oxford, 1970.
8. K.Khutsishvili, M.Meladze. Materials of 28th congress Ampere. Canterburry, UK, **28** 1996.
9. N.P.Georgadze, M.D.Zviadadze, A.I.Ugulava. Sov.Phys.-JETP. **67**, 1974, 665.
10. L.L.Buishvili, N.P.Fokina. Sov.Phys.Solid State. **25**, 1983, 1961.
11. N.P.Pomerantsev, V.M.Rizhkov, G.V.Skrotski. Fizicheskie osnovi kvantovoi magnitometrii. Moscow, 1972.

Tbilisi State University

კ. ნიკოლაძე

ფონონური ზვავის პრობლემის საკითხისათვის

დასკვნა

მიღებულია და ანალიზური მეთოდით ამოხსნილია არაწრფივ დიფერენციალურ განტოლებათა სისტემა, რომელიც აღწერს ურთიერთქმედებას სპინურ და ფონონურ ქვესისტემებს შორის პარამაგნიტურ მინარევიან კრისტალებში.

მიღებული შედეგები დამაკმაყოფილებელ თანხმობაშია ბრაია და ვაგნერის კარგად ცნობილ ექსპერიმენტებთან და რიცხვით გამოთვლებთან. ამრიგად, მიღებული ანალიზური ფორმულები თვისობრივად სწორად აღწერენ ფონონური ზვავის მოვლენას.

DIFFERENTIAL CROSS SECTION FOR DOUBLE IONIZATION OF HELIUM-LIKE IONS IN 2^1S AND 2^3S METASTABLE STATES BY ELECTRON IMPACT

P. Defrance[*], T. Kereselidze, I. Noselidze, M. Tsulukidze

ABSTRACT. Fully differential cross sections for double ionization of helium-like ions by electron impact are calculated in the first Born approximation. The results are found in the case when helium-like ions are in 2^1S and 2^3S metastable states. It is obtained that the shape of angular distributions of the ejected electrons strongly depends on the symmetry of wave function describing the bound electrons.

1. INTRODUCTION

Double ionization (DI) of atoms or ions by electron impact is at present the subject of an increasing number of theoretical investigations. Various processes can contribute to DI of atoms and ions, depending on the incident electron energy and on the structure of parent and intermediate atomic or ionic states. For ejection of electrons from *He* atom and helium-like ions only two types of mechanisms are identified: the so-called shake-off [1] and two-step mechanisms [2].

In case of DI via shake-off mechanism, the incident electron interacts with one of the two bound electrons and ejects it. The other bound electron being left in a state which is not an eigenstate of the residual ion. In the subsequent relaxation process there is a finite probability of a second ionization. This mechanism is formally first order in the interaction potential [3]. Unlike shake-off the two-step mechanisms are formally second order in the interaction potential [3].

Electron impact DI of *He* atom or helium-like ions is a four particle (one nucleus and three electrons) problem. In the final channel these four charged particles interact with each other via the long-range Coulomb potential. It makes the correct treatment

of this many-body problem extremely difficult. For this reason it is still impossible to carry out exact theoretical calculations for these processes. The most detailed description of the process is given by means of fully differential cross section (eightfold differential cross section) allowing the analysis of angular and energy distributions for each one of the ejected or scattered electrons.

Eightfold differential cross sections (8DCS) have been calculated for the H^- ion [4,5], for the He atom [6-10] and for the Li^+ ion [11]. All these calculations have been carried out for DI of two-electron atomic systems from their ground state. To the author's knowledge electron impact DI of excited He atom have been considered only in [12]. The most important conclusion resulting from the above-mentioned theoretical studies is that the 8DCS are very sensitive to the choice of wave functions in the initial and especially in the final state. Experimentally the fully differential cross sections are determined by detecting the three outgoing electrons in coincidence in coplanar or non-coplanar geometry [13-15].

In the present paper we calculate the fully differential cross sections for DI of helium atom and helium-like ions being in the excited 2^1S and 2^3S metastable states. The main attention is paid to the investigation of the influence of kinematical conditions and excitation on the shape and magnitude of angular distributions of the ejected electrons.

2. THEORY

For given wave vectors $\vec{k}_i$, $\vec{k}_s$, $\vec{k}_1$, $\vec{k}_2$ describing the incident, scattered and ejected electrons, respectively, the 8DCS of helium-like ions from its metastable 2^1S and 2^3S states may be written (in atomic units) as:

$$\frac{d^8\sigma^{(\pm)}}{d\Omega_s d\Omega_1 d\Omega_2 d(k_1^2/2) d(k_2^2/2)} = \frac{(2\pi)^4 k_s k_1 k_2}{k_i} \left| T_{fi}^{(\pm)} \right|^2. \tag{1}$$

Here Ω and k represent, respectively, the solid angles and the moduli of the different wave vectors, $T_{fi}^{(\pm)}$ represents the matrix element given by

$$T_{fi}^{(\pm)} = \int \Psi_f^{(\pm)} V_i \Psi_i^{(\pm)} d\vec{r} d\vec{r}_1 d\vec{r}_2. \qquad (2)$$

The sign $(\pm)$ indicates that the total spin of two bound electrons may be zero or one.

In (2) V_i describes the interaction between the incident electron and the helium-like ion

$$V_i = -\frac{Z}{r} + \frac{1}{|\vec{r} - \vec{r}_1|} + \frac{1}{|\vec{r} - \vec{r}_2|} \qquad (3)$$

$(\vec{r}, \vec{r}_1, \vec{r}_2$ are the position vectors of the incident and two bound electrons), $\Psi_i^{(\pm)}$ and $\Psi_f^{(\pm)}$ represent the wave functions of the colliding system in the initial and in the final states, respectively; $\Psi_i^{(\pm)}$ is the solution of the Shrödinger equation where $V_i = 0$ and $\Psi_f^{(\pm)}$ is a solution of the complete Shrödinger equation.

The conservation of energy requires

$$k_i^2/2 = I^{(\pm)} + k_s^2/2 + k_1^2/2 + k_2^2/2, \qquad (4)$$

where $I^{(\pm)}$ represents the binding energy of electrons in helium-like ion.

This study is restricted to the high-energy domain, where the scattered electron is always fast and the ejected electrons leave the ion with small energies. These kinematical conditions allow us to use plane waves for the description of both the incident and the scattered electron. Thus the wave function of the colliding system may be written in the initial state as the product of a plane wave describing the incident electron and the wave function $\Phi_i^{(\pm)}(\vec{r}_1, \vec{r}_2)$ describing the two

100

bound electrons in the singlet and triplet metastable states in helium-like ion

$$\Psi_i^{(\pm)}(\vec{r},\vec{r}_1,\vec{r}_2) = \frac{e^{i\vec{k}_i\vec{r}}}{(2\pi)^{3/2}} \Phi_i^{(\pm)}(\vec{r}_1,\vec{r}_2). \qquad (5)$$

The best way to have an appropriate description of the electron motion in the metastable 2^1S and 2^3S states in helium-like ions is to use correlated wave functions of the Hylleraas type [16].

$$\Phi_i^{(\pm)}(\vec{r}_1,\vec{r}_2) = C_i^{(\pm)}\left[e^{-\alpha r_1-\beta r_2}\left(1-\beta r_2\right) \pm e^{-\alpha r_2-\beta r_1}\left(1-\beta r_1\right)\right] \times$$

$$\times \left(1 + \gamma|\vec{r}_1 - \vec{r}_2| + ...\right). \qquad (6)$$

Here $\alpha, \beta, \gamma, ...$ are the variational parameters and $C_i^{(\pm)}$ is a normalization constant. This wave function describes both the radial and angular correlation of electrons in helium-like ions.

In our present study we completely ignore the angular correlation and consider only the radial correlation of electrons in the target. It means that we employ wave functions (6) where only α and β variational parameters differ from zero. This simplification allows us to obtain an analytical expression for the matrix element $T_{fi}^{(\pm)}$ and accordingly to write the 8DCS in the explicit form. Numerical values of the variational parameters α and β together with the calculated values of the binding energy of electrons are given in Tables 1 and 2 for He atom and helium-like ions $Li^+, Be^{2+},...,N^{5+}$.

In the final state the scattered electron is described by a plane wave as in the initial state (the first Born approximation), and the two ejected electrons by the double-continuum wave function orthogonalized with respect to the initial state wave function $\Phi_i^{(\pm)}$:
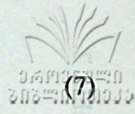
Hylleraas-type wave function parameters for the 2^1S metastable state of He atom and helium-like ions Li^+, Be^{2+},..., N^{5+}. $I^{(+)}$ is the calculated value of the binding energy of electrons.

	$He(2^1S)$	$Li^+(2^1S)$	$Be^{2+}(2^1S)$	$B^{3+}(2^1S)$	$C^{4+}(2^1S)$	$N^{5+}(2^1S)$
α	1.955	2.953	3.951	4.950	5.950	6.949
β	0.940	1.439	1.938	2.438	2.938	3.438
$I^{(+)}$	2.058	4.952	9.095	14.481	21.131	29.025

Hylleraas-type wave function parameters for the 2^3S metastable state of He atom and helium-like ions $Li^+, Be^{2+}, ..., N^{5+}. I^{(-)}$ is the calculated value of the binding energy of electrons.

	$He(2^3S)$	$Li^+(2^3S)$	$Be^{2+}(2^3S)$	$B^{3+}(2^3S)$	$C^{4+}(2^3S)$	$N^{5+}(2^3S)$
α	1.994	2.994	4.002	5.004	6.006	7.006
β	0.775	1.285	1.789	2.291	2.793	3.295
$I^{(-)}$	2.167	5.103	9.289	14.726	21.413	29.350

$$\Psi_f^{(\pm)} = \frac{e^{i\vec{k}_s\vec{r}}}{(2\pi)^{3/2}}\left[\Phi_f^{(\pm)}(\vec{r}_1,\vec{r}_2) - S^{(\pm)^*}\Phi_i^{(\pm)}(\vec{r}_1,\vec{r}_2)\right], \qquad (7)$$

where

$$\Phi_f^{(\pm)} = \frac{1}{\sqrt{2}}\left(\varphi_f(\vec{r}_1,\vec{r}_2) \pm \varphi_f(\vec{r}_2,\vec{r}_1)\right) \qquad (8)$$

and

$$S^{(\pm)} = \int \Phi_f^{(\pm)^*}\Phi_i^{(\pm)}d\vec{r}_1 d\vec{r}_2.$$

The most sophisticated Coulomb double-continuum wave function has been proposed by Brauner, Briggs and Klar [17]. This wave function (called the BBK wave function) is the product of two exact Coulomb wave functions $f_{\vec{k}}(\vec{r})$ with a third one $f(\vec{r}_{12})$ describing the interaction between the electrons. In our study we will use the approximated BBK wave function [4,5]. This wave function takes into account the Coulomb interaction between each ejected electron and the nucleus, and includes in an approximate way repulsion between the ejected electrons

$$\varphi_f(\vec{r}_1,\vec{r}_2) = f_{\vec{k}_1}(\vec{r}_1)f_{\vec{k}_2}(\vec{r}_2)f(k_{12}), \qquad (9)$$

where

$$f_{\vec{k}}(\vec{r}) = \frac{1}{(2\pi)^{3/2}}e^{\frac{Z\pi}{2k}}\Gamma(1+iZ/k)e^{i\vec{k}\vec{r}}F(-iZ/k,1,-i(kr+\vec{k}\vec{r})), \qquad (10)$$

$$f(k_{12}) = e^{-\frac{\pi}{4k_{12}}}\Gamma(1-i/k_{12}), \qquad (11)$$

and $\quad k_{12} = \left|\vec{k}_1 - \vec{k}_2\right|/2$.

Substituting wave functions of the initial and final states (5) and (7) into (2) and performing the integration over $\vec{r}$ the matrix element $T_{fi}^{(\pm)}$ is written as:

$$T_{fi}^{(\pm)} = \frac{1}{2\pi^2 q^2}\left[\int \Phi_f^{(\pm)^*}(\vec{r}_1,\vec{r}_2)(e^{i\vec{q}\vec{r}_1} + e^{i\vec{q}\vec{r}_2}) \times \right.$$

$$\left. \times \Phi_i^{(\pm)}(\vec{r}_1,\vec{r}_2)d\vec{r}_1 d\vec{r}_2 - S^{(\pm)}G(q)\right], \tag{12}$$

where $\vec{q} = \vec{k}_i - \vec{k}_s$ is the momentum transfer and

$$G^{(\pm)}(q) = \int \Phi_i^{(\pm)^*}(\vec{r}_1,\vec{r}_2)(e^{i\vec{q}\vec{r}_1} + e^{i\vec{q}\vec{r}_2})\Phi_i^{(\pm)}(\vec{r}_1,\vec{r}_2)d\vec{r}_1 d\vec{r}_2. \tag{13}$$

Now substituting the wave function (6) (where only $\alpha, \beta \neq 0$) together with the approximated BBK wave function (9) into (12) the matrix element $T_{fi}^{(\pm)}$ can be written in the following form:

$$T_{fi}^{(\pm)} = \frac{C_i^{(\pm)} f(k_{12})}{\sqrt{2}\pi^2 q^2}\left\{I_\alpha^{(0)}(\vec{k}_1)\left[J_\beta^{(0)}(k_2) - \beta J_\beta^{(1)}(k_2)\right] \pm \right.$$

$$\pm I_\alpha^{(0)}(\vec{k}_2)\left[J_\beta^{(0)}(k_1) - \beta J_\beta^{(1)}(k_1)\right] +$$

$$\left. + \left[I_\beta^{(0)}(\vec{k}_2) - \beta I_\beta^{(1)}(\vec{k}_2)\right]J_\alpha^{(0)}(k_1) \pm \left[I_\beta^{(0)}(\vec{k}_1) - \beta I_\beta^{(1)}(\vec{k}_1)\right]J_\alpha^{(0)}(k_2)\right., \tag{14}$$

where

$$I_\mu^{(n)}(\vec{k}_j) = \int f_{\vec{k}_j}^*(\vec{r})\left(e^{i\vec{q}\vec{r}} - \frac{1}{2}G^{(\pm)}(q)\right)e^{-\mu r}r^n d\vec{r}, \tag{15}$$

105

$$|f(k_{12})|^2 = \frac{2\pi}{\left|\bar{k}_1 - \bar{k}_2\right|\left(e^{2\pi/\left|\bar{k}_1 - \bar{k}_2\right|} - 1\right)} \qquad (20)$$

is the repulsive Gamov factor.

In (17) the first term corresponds to direct ejection of an electron from the strongly bound state and the subsequent ionization of an electron from the weakly bound state due to the sudden change in potential (process I). The second term corresponds to direct ejection of an electron from the weakly bound state followed by ionization of an electron from the strongly bound state (process II). The third term in (17) describes interference between these two processes. It should be noted that when $A_\beta^{(1)}(\bar{k}_j) = B_\beta^{(1)}(k_j) = 0$ the formulae (17)-(20) transform into the formulae for DI of helium-like ions from its ground state obtained in our previous work [18].

3. RESULTS OF THE NUMERICAL CALCULATIONS

Using formulae (17)-(20) we have calculated the fully differential cross sections corresponding to DI of He atom and helium-like ions $Li^+, Be^{2+}, ..., Ne^{5+}$ in 2^1S and 2^3S metastable states by electron impact. Calculations have been carried out for kinematical conditions usually used in electron impact DI experiments, namely at high incident energy ($E_i = 5$ keV), small scattering angle ($\vartheta_s = 0.5$) and low ejection energies ($E_1, E_2 \le 25eV$) in coplanar geometries. Results of calculations are shown in polar diagrams, where the polar axis is in the direction of the incident electron. The 5DCS results are plotted as a function of the direction $\bar{k}_2$ of one ejected electron for a fixed direction $\bar{k}_1$ of the other one.

In Figures 1 and 2 we present the 5DCS for DI of helium atom respectively for symmetric energy sharing ($E_1 = E_2 = 15eV$) and for non-symmetric energy sharing ($E_1 = 5eV, E_2 = 25eV$). The first outgoing electron comes out in a direction parallel (a), perpendicular (b) and anti-parallel (c) to the momentum transfer $\bar{q}$. The light full
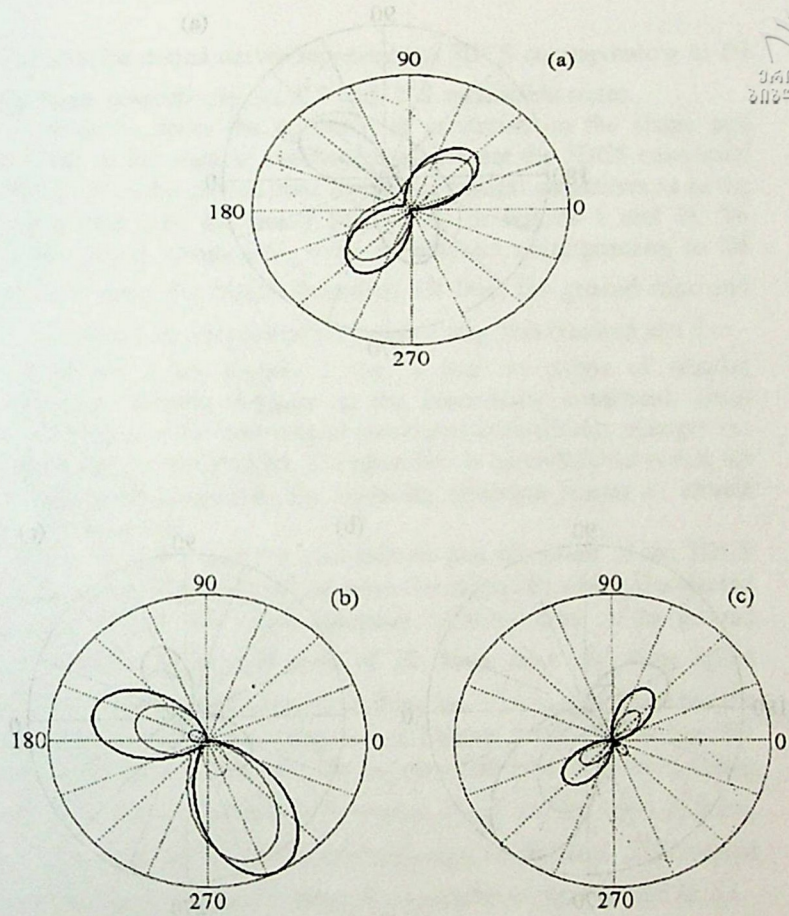
Fig.1. Angular distributions of the ejected electrons for symmetric energy sharing. The light full curves correspond to DI of the 2^1S excited state, the dotted curves correspond to DI of the 2^3S excited state. The angular distributions of the ejected electrons when the helium atom is in the ground state are represented by the heavy full curves.
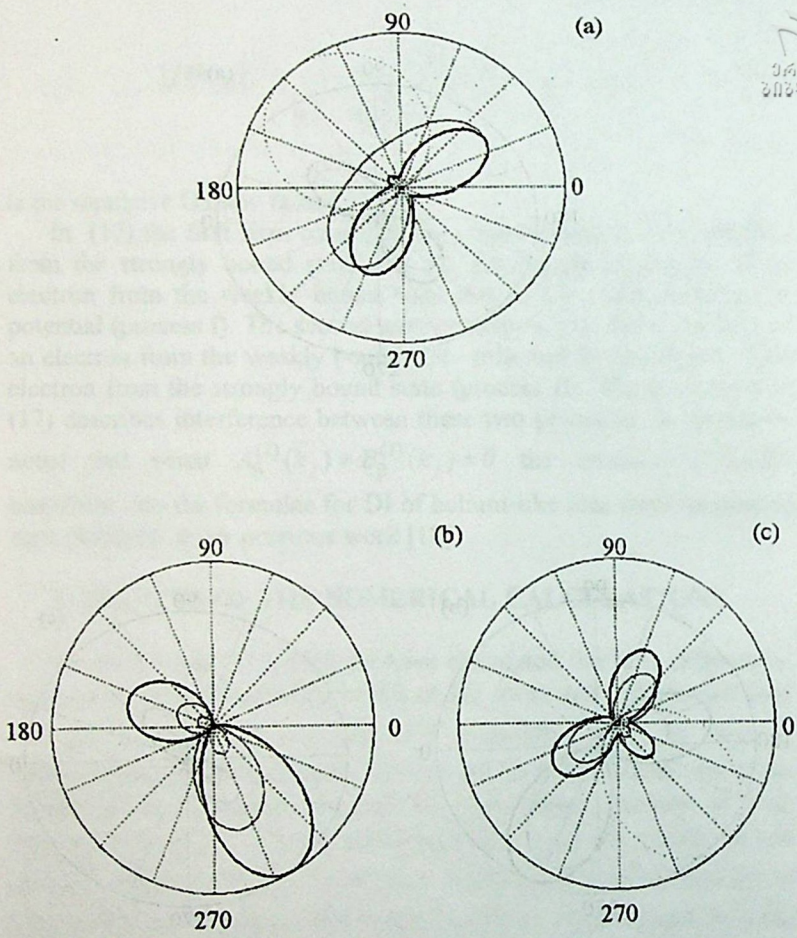
Fig. 2. Angular distributions of the ejected electrons for non-symmetric energy sharing. The light full curves correspond to DI of the 2^1S excited state, the dotted curves correspond to DI of the 2^3S excited state. The angular distributions of the ejected electrons when the helium atom is in the ground state are represented by the heavy full curves.

curves and the dotted curves represent the 5DCS corresponding to DI of the atom, respectively, in 2^1S and 2^3S metastable states.

In order to show the influence of excitation on the shape and magnitude of the angular distribution we present the 5DCS calculated for DI of He in the ground state at the kinematical conditions as in the previous case (see the heavy full curves in figures 1 and 2). To facilitate visual comparison with the diagram corresponding to DI from 2^3S state, the 5DCS describing DI from the ground state and 2^1S excited state are multiplied, respectively, two hundred and five.

It follows from Figures 1 and 2 that the shape of angular distributions strongly depends on the kinematical conditions. Even small variation of the kinematical conditions considerably changes the shape of angular distribution. The main fact to be underlined is that for all kinematical conditions the outgoing electrons depart in almost opposite directions.

From Figures 1 and 2 it also follows that the shape of the 5DCS depends on the symmetry of the wave functions describing the ejected electrons. Indeed, the wave functions corresponding to the ground state and the 2^1S excited state of He atom have the same space symmetry. The wave function describing the 2^3S excited state has the opposite space symmetry. Diagrams in Figures 1 and 2 show that, for given kinematical conditions, the angular distributions corresponding to DI from the ground and 2^1S excited states are the same in form, while the shape of the 5DCS corresponding to DI from 2^3S excited state is different (especially when $\bar{k}_1$ is parallel or anti-parallel to $\bar{q}$).

We do not consider here the 5DCS corresponding to DI of the other members of the helium sequence $Li^+, Be^{2+}, ..., N^{5+}$ because their properties are the same.

APPENDIX

The analytical expressions for $I_\mu^{(n)}(\vec{k}_j)$ and $J_\nu^{(n)}(k_j)$ $(n = 0,1)$ are

$$I_\mu^{(n)}(\vec{k}_j) = \frac{1}{(2\pi)^{3/2}} \Gamma\left(1 - iZ / k_j\right) e^{\pi Z / 2k_j} A_\mu^{(n)}(\vec{k}_j), \qquad (a.1)$$

$$J_\nu^{(n)}(k_j) = \frac{1}{(2\pi)^{3/2}} \Gamma\left(1 - iZ / k_j\right) e^{\pi Z / 2k_j} B_\nu^{(n)}(k_j), \qquad (a.2)$$

where

$$B_\nu^{(0)}(k_j) = -8\pi \frac{Z - \nu}{\left(\nu^2 + k_j^2\right)^2} e^{-\frac{Z}{k_j} arctg \frac{2\nu k_j}{\nu^2 - k_j^2}},$$

$$B_\nu^{(1)}(k_j) = \left[\frac{2(Z - 2\nu)}{\nu^2 + k_j^2} - \frac{1}{Z - \nu}\right] B_\nu^{(0)}(k_j), \qquad (a.3)$$

$$A_\mu^{(n)}(\vec{k}_j) = \left[\frac{a_\mu(q,k_j)}{\left(\mu^2 + q^2 + k_j^2 - 2qk_j x_j\right)^2} d_\mu^{(n)}(x_j) - \frac{1}{2} G^{(\pm)}(q) B_\mu^{(n)}(k_j)\right] +$$

$$+ i\left[\frac{a_\mu(q,k_j)}{\left(\mu^2 + q^2 + k_j^2 - 2qk_j x_j\right)^2} h_\mu^{(n)}(x_j)\right]. \qquad (a.4)$$

In the formulae given above $x_j = \cos\vartheta_j$, where ϑ_j is the angle between $\vec{q}$ and the wave vectors $\vec{k}_j$.

The functions $a_\mu(q,k_j)$ and $d_\mu^{(n)}(x_j), h_\mu^{(n)}(x_j)$ in (a.4) are determined as follows:

112

$$a_\mu(q,k_j) = -\frac{8\pi}{\left[\mu^2 + (q+k_j)^2\right]\left[\mu^2 + (q+k_j)^2\right]} e^{-\frac{Z}{k_j}arctg\frac{2\mu k_j}{\mu^2 + q^2 - k_j^2}}, \quad \text{(a.5)}$$

$$d_\mu^{(0)}(x_j) = \left[(\mu^2 + q^2 - k_j^2)w_\mu^{(1)}(x_j) - 4\mu^2 k_j w_\mu^{(2)}(x_j)\right]\cos\chi_\mu(x_j) -$$

$$- 2\mu\left[(\mu^2 + q^2 - k_j^2)w_\mu^{(2)}(x_j) + k_j w_\mu^{(1)}(x_j)\right]\sin\chi_\mu(x_j), \quad \text{(a.6)}$$

$$h_\mu^{(0)}(x_j) = \left[(\mu^2 + q^2 - k_j^2)w_\mu^{(1)}(x_j) - 4\mu^2 k_j w_\mu^{(2)}(x_j)\right]\sin\chi_\mu(x_j) +$$

$$+ 2\mu\left[(\mu^2 + q^2 - k_j^2)w_\mu^{(2)}(x_j) + k_j w_\mu^{(1)}(x_j)\right]\cos\chi_\mu(x_j), \quad \text{(a.7)}$$

where

$$w_\mu^{(1)}(x_j) = 2Zqk_j x_j - q^2(Z+\mu) + (Z-\mu)(\mu^2 - k_j^2),$$

$$w_\mu^{(2)}(x_j) = Zqx_j - (Z-\mu)k_j, \quad \text{(a.8)}$$

$$\chi_\mu(x_j) = \frac{Z}{k_j}ln\frac{\mu^2 + q^2 + k_j^2 - 2qk_j x_j}{\sqrt{(\mu^2 + q^2 - k_j^2)^2 + (2\mu k_j)^2}},$$

and

$$d_\mu^{(1)}(x_j) = \left[\frac{2Z(q^2 - k_j^2 - \mu^2) + 4\mu(\mu^2 + q^2 + k_j^2)}{(\mu^2 + (q+k_j)^2)(\mu^2 + (q-k_j)^2)} + \right.$$

113

$$+\left.\frac{4\mu}{\mu^2+q^2+k_j^2-2qk_jx_j}\right]d_\mu^{(0)}(x_j)+\frac{2\mu Z}{k_j}\left[\frac{1}{\mu^2+q^2+k_j^2-2qk_jx_j}\right.$$

$$\left.-\frac{\mu^2+q^2+k_j^2}{\left(\mu^2+(q+k_j)^2\right)\left(\mu^2+(q-k_j)^2\right)}\right]h_\mu^{(0)}(x_j)+$$

$$+Q_\mu(x_j)\sin\chi_\mu(x_j)-R_\mu(x_j)\cos\chi_\mu(x_j), \qquad\qquad (a.9)$$

$$h_\mu^{(1)}(x_j)=\left[\frac{2Z\left(q^2-k_j^2-\mu^2\right)+4\mu\left(\mu^2+q^2+k_j^2\right)}{\left(\mu^2+(q+k_j)^2\right)\left(\mu^2+(q-k_j)^2\right)}+\right.$$

$$+\left.\frac{4\mu}{\mu^2+q^2+k_j^2-2qk_jx_j}\right]h_\mu^{(0)}(x_j)+\frac{2\mu Z}{k_j}\left[\frac{1}{\mu^2+q^2+k_j^2-2qk_jx_j}-\right.$$

$$\left.-\frac{\mu^2+q^2+k_j^2}{\left(\mu^2+(q+k_j)^2\right)\left(\mu^2+(q-k_j)^2\right)}\right]d_\mu^{(0)}(x_j)-$$

$$-R_\mu(x_j)\sin\chi_\mu(x_j)-Q_\mu(x_j)\cos\chi_\mu(x_j), \qquad\qquad (a.10)$$

$$Q_\mu(x_j)=2Zqx_j\left(3\mu^2+q^2+k_j^2\right)-4Zk_jq^2,$$

$$R_\mu(x_j)=-4Zq\mu k_jx_j+4\mu Z\left(\mu^2+k_j^2\right)-4\mu^2\left(\mu^2+k_j^2+q^2\right)-$$

$$-\left(\mu^2+(q+k_j)^2\right)\left(\mu^2+(q-k_j)^2\right). \qquad\qquad (a.11)$$

The analytical expressions for $C_i^{(\pm)}$ and $G^{(\pm)}(q)$ are:

$$C_i^{(\pm)} = \frac{1}{4\pi}\left\{\frac{1}{8\alpha^3\beta^3} \pm \frac{8}{(\alpha+\beta)^6}\left[1 - \frac{6\beta}{(\alpha+\beta)} + \frac{9\beta^2}{(\alpha+\beta)^2}\right]\right\}^{-\frac{1}{2}}, \quad \text{(a.12)}$$

$$G^{(\pm)}(q) = 32\pi^2(C_i^{(\pm)})^2\left\{\frac{\alpha}{\beta^3(4\alpha^2+q^2)^2} + \frac{2\beta}{\alpha^3}\frac{8\beta^4 - 6\beta^2 q^2 + q^4}{(4\beta^2+q^2)^2} \pm\right.$$

$$\left.\pm\frac{8(\alpha-2\beta)}{(\alpha+\beta)^4}\frac{\left[(\alpha-2\beta)(\alpha+\beta)^2 + (\alpha+2\beta)q^2\right]^2}{\left[(\alpha+\beta)^2+q^2\right]^3}\right\} \quad \text{(a.13)}$$

REFERENCES:

1. M.H. Mittleman. Phys, Rev. Lett. **16**, 1966, 498.
2. T.A. Carlson, M.O. Krause. Phys. Rev. **A140**, 1965, 1057.
3. R.I. Tweed. Z. Phys. **D23**, 1992, 309.
4. P. Lamy, C. Dal Cappello, B. Joulakian, C.Le Sech. J.Phys. B: At. Mol. Opt. Phys. **27**, 1994, 3559.
5. P. Defrance, T.M. Kereselidze, Z.S. Machavariani, J.V. Mebonia. J. Phys. B: At. Mol. Opt. Phys. **32**, 1999, 2227.
6. B. Joulakian, C. Dal Cappello, M.Brauner. J. Phys. B: At. Mol. Opt. Phys. **25**, 1992, 2863.
7. J.Berakdar, H. Klar. J. Phys. B: At. Mol. Opt. Phys. **26**, 1993, 4219.
8. B. Joulakian, C. Dal Cappello. Phys. Rev. **A47**, 1993, 3788.
9. M.K. Srivastava, S. Gupta, C. Dal Cappello. Phys. Rev. **A53**, 1996, 4104.
10. A. Lahmam-Bennani, I. Taouil, A. Duguet, M. Lecas, L. Avaldi, J. Berakdar. Phys. Rev. **A59**, 1999, 3548.
11. R. Biswas, C. Sinha. Proc. 20th Int. Conf. on Physics of Electronic and Atomic Collisions, Book of Abstracts. Vienna, 23-29 July, 1997 ed.F.Aumayr, G.Betz and H.Winter 1997.
12. M.K. Srivastava. Proc.20th Int. Conf. on Physics of Electronic and

Atomic Collisions, Book of Abstracts (Vienna, 23-29 July, 1997) ed.F.Aumayr, G.Betz, H.Winter 1997.

13. A. Lahmam-Bennani. J. Phys. B: At. Mol. Opt. Phys. **24**, 1991, 2401.

14. B. El. Margy, C.Schroter, A.Duguet, A.Lahmam-Bennani, M. Lecas, L.Spielberger. J Phys B: At. Mol.Opt.Phys. **30**, 1997, 3677.

15. C. Schroter, B.El Marji. A. Lahmam-Bennani, A. Duguet, M. Lecas, L. Spielberger. J. Phys. B: At. Mol. Opt. Phys. **31**, 1998, 131.

16. E.A. Hylleraas, B. Undheim Zs. f. Phys. **65**, 1930, 759.

17. M. Brauner, J.S. Briggs, H. Klar. J. Phys. B: At. Mol. Opt. Phys. **22**, 1989, 2265.

18. P. Defrance, T.M. Kereselidze, Z.S. Machavariani, I.L. Noselidze. J. Phys.B: At.Mol. Opt. Phys. **33**, 2000, 4323.

*Universite' Catholique de Louvain, De'partment de Physique, Louvain-la-Neuve, Belgium
Tbilisi State University

ჰ. დეფრანსი, თ. კერესელიძე, ი. ნოსელიძე, მ. წულუკიძე

ელექტრონებით მეტასტაბილურ 2^1S და 2^3S
მდგომარეობაში მყოფი ჰელიუმისმაგვარი იონების
ორჯერადი იონიზაციის დიფერენციალური განივკვეთი

დასკვნა

ბორნის პირველ მიახლოებაში „შენჯდრევის" მექა-
ნიზმის გამოყენებით გამოთვლილია სწრაფი ელექტრონე-
ბით აღგზნებულ 2^1S და 2^3S მეტასტაბილურ მდგომარეო-
ბაში მყოფი ჰელიუმისმაგვარი იონების ორჯერადი იონი-
ზაციის სრული დიფერენციალური განივკვეთები. განხი-
ლულია ისეთი კინემატიკური პირობები, რომლებიც
წვეულებრივ რეალიზდებიან ექსპერიმენტებში, კერძოდ,
დამჯახებელი ელექტრონის ენერგია არის 5 კევ-ი,
გაბნევის კუთხე 0.5, ხოლო ამოტყორცნილი ელექტრონე-
ბის ჯამური ენერგია 30 ევ-ი. ნაჩვენებია, რომ ამო-
ტყორცნილი ელექტრონების კუთხური განაწილების
ფორმა ძლიერად არის დამოკიდებული როგორც კინე-
მატიკურ პირობებზე, ისე ბმული ელექტრონების მდგომა-
რეობაზე სამიზნეში.

ON DETERMINATION OF „RELAXATION TIME " BY MEASUREMENT DATA OF RADIO WAVE ABSORPTION IN IONOSPHERE

K. Tukhashvili, G. Entzian[*], V. Kandashvili, M. Devnozashvili, M. Miminoshvili

ABSTRACT. Due to sluggishness of ionosphere, diurnal variation curve maximum of radio waves absorption is shifted from midday to evening hours by τ time - „ relaxation time". To determine this time is very important for D region research of ionosphere.

Determination of „relaxation time" is possible by hourly absorption data, but such measurements are connected with great difficulties. That is why measurements in almost every ionosphere station of the earth is carried out only three times a day. Up till now it was not possible to determine τ by these data.

The present article deals with working out of the method and corresponding formula for calculation of τ, that enables us to study the nature of „ relaxation time" for different latidudes.

It is established by numerous experiments that ultra-violet and Roentgen radiation of the sun are main ionizing factors of ionosphere. The radiation results in photoionization of atmosphere. A simultaneous counter process in the form of recombination ends with a certain degree of ionization [1,2], but because of the sluggishness of the ionosphere the equilibrium is gained later on τ, the so-called "relaxation time". Relaxation time in the ionosphere is connected with the recombination coefficient (α) and electron density (N) [3]. One of the important parameters of ionosphere characterizing the scale of temporal variations of N in the ionosphere is recombination coefficient [2], therefore experimental measurement of τ is important for D region research of ionosphere.

It is usual to interpret the diurnal variation of ionospheric absorption of the radiowaves in terms of the well-known

$$L(t) = L_0(cos\,\chi(t - \tau))^n, \qquad (1)$$

where

$$cos\,\chi = sin\,\varphi \cdot sin\,\delta + cos\,\varphi \cdot cos\,\delta \cdot cos\,t, \qquad (2)$$

φ is latitude, δ -solar declination, t - hour angle of the sun.

If the absorption data is available on an hourly basis during a day it is possible to determine τ by (1) using computer [4] or graphic method [5].

There are valuable data of absorption measurements in the World Data Center (WDC), obtained during periods of International Geophysical Year and Quiet Sun Year as well as the data obtained by international projects: URSI, KAPG, MAP and MAC. Values of τ are found rare in these data, therefore it is not possible to research the seasonal and latitudinal variations of this parameter. τ is a small quantity, therefore it is difficult to calculate it by data of absorption: graphic method has big errors and τ often gets into the bounds of errors. In some points of globe, absorption measurement is carried out only at $cos\,\chi = 0,2$ (forenoon and afternoon) because of complexity of measurement. Thus, we can't take all the information from the rich data of absorption measurements, which is accumulated in WDC.

It is shown in this paper that it is possible to calculate τ just on the basis of values of absorption at midday and $cos\,\chi = 0,2$ (forenoon and afternoon). That means, that if WDC data enables us to calculate τ, it will play a great role in D region research by WDC data.

As above, when radiation of the sun influences the ionosphere the equilibrium establishes not at once but some time later, consequently, value of absorption measured at the zenith angle χ_0 corresponds not to this angle, but to the angle which was for τ time earlier (Fig.1).

119

sunrise   noon   sunset
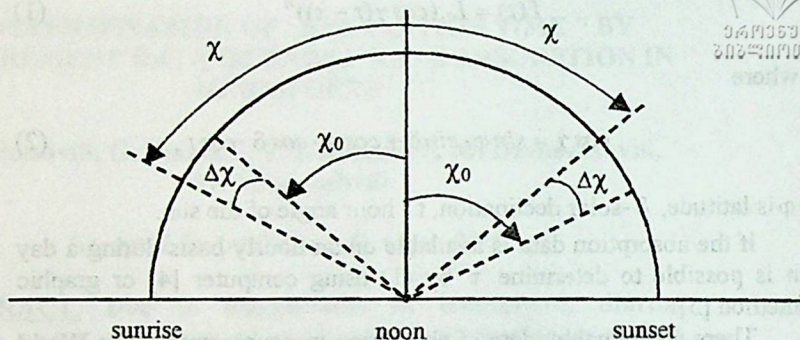
Fig.1

Forenoon $\chi = \chi_0 + \Delta\chi$ and afternoon $\chi = \chi_0 - \Delta\chi$

$$\Delta\chi = |V| \cdot \tau, \tag{3}$$

where V denotes the velocity of change of the sun zenith angle. For its part V is the function of χ

$$V(\chi) = \frac{\sqrt{Q^2 - (\cos\chi - p)^2}}{\sin\chi}, \tag{4}$$

where $p = \sin\varphi \cdot \sin\delta$ and $Q = \cos\varphi \cdot \cos\delta$ [6], but as τ is a small quantity, it is possible to count $v = const$ during this interval. In that way forenoon

$$L_1 = L_0 \cos^n(\chi_0 + \Delta\chi), \tag{5}$$

and afternoon

$$L_1 = L_0 \cos^n(\chi_0 - \Delta\chi), \tag{6}$$

where $L_1 = L(\cos\chi_0)$ forenoon and $L_2 = L(\cos\chi_0)$ afternoon.

120

Thus, from (5)

$$L_1 = L_0 (\cos \chi_0 \cdot \cos \Delta\chi - \sin \chi_0 \cdot \sin \Delta\chi)^n =$$

$$= L_0 (\cos \chi_0 \cdot \cos \Delta\chi)^n (1 - tg\chi_0 \cdot tg\Delta\chi)^n . \qquad (7)$$

If we decompose $(1 - tg\chi_0 \cdot tg\Delta\chi)^n$ by binomial theorem [7] and limit first three members (it is possible to neglect the rest of members for a trifle), we have

$$L_1 = L_0 (\cos \chi_0 \cdot \cos \Delta\chi)^n (1 - n tg\chi_0 \cdot tg\Delta\chi +$$

$$+ \frac{n(n-1)}{2} (tg\chi_0 \cdot tg\Delta\chi)^2) , \qquad (8)$$

analogically

$$L_2 = L_0 (\cos \chi_0 \cdot \cos \Delta\chi)^n (1 + n tg\chi_0 \cdot tg\Delta\chi +$$

$$+ \frac{n(n-1)}{2} (tg\chi_0 \cdot tg\Delta\chi)^2) . \qquad (9)$$

If we subtract (8) from (9), we have

$$L_2 - L_1 = 2L_0 (\cos \chi_0 \cdot \cos \Delta\chi)^n \cdot n \cdot tg\chi_0 \cdot tg\Delta\chi . \qquad (10)$$

$\Delta\chi$ is a small quantity, therefore $tg\Delta\chi \approx \Delta\chi$ and $\cos \Delta\chi \approx 1$, therefore (10) assumes

$$L_2 - L_1 = 2L_0 \cos^n \chi_0 \cdot n \cdot tg\chi_0 \cdot \Delta\chi \qquad (11)$$

Taking into account (3) we have

$$\tau = \frac{L_2 - L_1}{2n \cdot L_0 \cdot |V| \cdot \cos^n \chi_0 \cdot tg\chi_0}. \qquad (12)$$

Data of many points of globe show, that $L_2 > L_1$; this probably must be so: forenoon, when absorption was measured at the χ_0, due to the ionosphere sluggishness, the degree of ionization at a given moment corresponds to that zenith angle χ, which existed the τ time earlier, i. e. $\chi = \chi_0 + \Delta\chi = \chi_0 + |V| \cdot \tau$ (see Fig. 1).

Consequently, absorption at χ is smaller than at χ_0. In the afternoon $\chi = \chi_0 - \Delta\chi$ i.e. degree of ionization is more and consequently absorption is larger, than at χ_0 [6].

Parameters L_1, L_2, n and L_0 are given in data of absorption for many points. It is possible to calculate V by (4) and (12) enables to calculate τ.

If it is known only L_1, L_2, and L_n (value of absorption at noon), then at first we must calculate n and L_0:

$$L_n = L_0 \cdot (\cos\chi_n)^n, \qquad (13)$$

$$L_\chi = L_0 \cdot (\cos\chi)^n, \qquad (14)$$

where $L_\chi = \dfrac{L_1 + L_2}{2}$; from (13) and (14) follows that

$$\frac{L_n}{L_\chi} = \left(\frac{\cos\chi_n}{\cos\chi}\right)^n. \qquad (15)$$

It is possible to calculate n from (15) and then calculate L_0 from (13) or (14) and then - τ from (12).

On the other hand

$$L_1 = L_0\left[P + Q \cdot \cos(t_1 - \tau)\right]^n, \qquad (16)$$

122

$$L_2 = L_0 [P + Q \cdot \cos(t_2 - \tau)]^n, \qquad (17)$$

from (2)

$$t_{1,2} = \pm arccos \frac{\cos \chi - P}{Q}, \qquad (18)$$

where „ - " corresponds to forenoon (t_1) and „ + " to afternoon (t_2).

For considering (18) from (16)

$$\tau = arccos \frac{\left(\frac{L_1}{L_0}\right)^{\frac{1}{n}} - P}{Q} - arccos \frac{\cos \chi - P}{Q}, \qquad (19)$$

and from (17)

$$\tau = - arccos \frac{\left(\frac{L_2}{L_0}\right)^{\frac{1}{n}} - P}{Q} + arccos \frac{\cos \chi - P}{Q}, \qquad (20)$$

adding (19) and (20) we have

$$\tau = arccos \frac{\left(\frac{L_1}{L_0}\right)^{\frac{1}{n}} - P}{Q} - arccos \frac{\left(\frac{L_2}{L_0}\right)^{\frac{1}{n}} - P}{Q}. \qquad (21)$$

123

Experiments (Norddeich Radio (2614KHz) - Neustrelitz) show that difference between the values of τ calculated by (12) and (21) is negligible and corresponds to measured value of τ (Fig.2. a,b,c).

a)

This indicates that our reasoning above about $\Delta\chi$ is true.

The calculation of τ requires the shift to apparent solar time. The sun performs an uneven ecliptic go-round because of the Earth orbit, which is not circumference but ellipse, that is why the sun moves faster or slower in different months, though it goes through the locked annual cycle. The influence of the above mentioned unevenness is essential.

b)

The apparent solar body goes round the ecliptic rout, which is inclined towards celestial equator, while the hour angles are counted off according to the equator.

In order to have the solar time measured the scientists had to introduce a certain fictive point referred to as the „average

Fig.2.

solar body", that actually shifts the „apparent solar body". The „average solar body" moves evenly on celestial equator performing the entire annual detour and is considered by the scientists as an index for average solar time.

If we have an hour angle of the „average solar body" marked as t_m
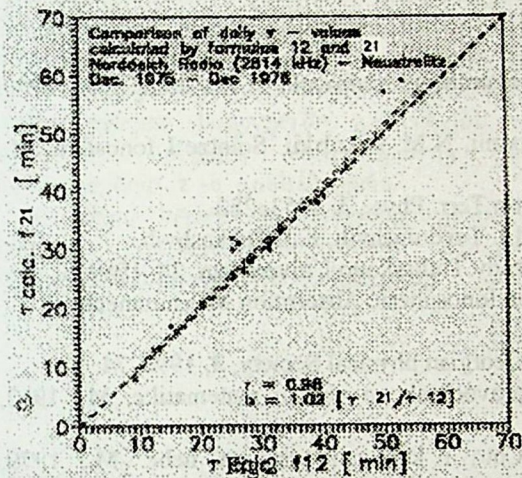
and the average local time as $T_m = 12^h + t_m$, the „average solar hour" is counted off according to the hour angle of the „average solar body", a certain fictive point.

$$t_m = t_0 + \alpha_0 - \alpha_m = t_0 + \eta.$$

t_0 is the hour angle of the apparent solar body, α_0 the actual sunrise, α_m the actual sunrise of the average solar body. η - difference. $\eta = \alpha_0 - \alpha_m$ the so-called time equation [8].

If η is ignored, it will definitely have a considerable influence on seasonal variation τ in D and E region of the ionosphere as τ and η on this level are of the same order [1,9].

125

REFERENCES

1. I.L. Alpert. Rasprostranenie radiovoln i ionosfera. M., 1960, (Russian).
2. G.S. Ivanov-Kholodnii, N.M. Nikolskii. Solntze I Ionosfera. M., 1969, (Russian).
3. E.V. Applton. J. Atm.Terr. Phys., 3, 1953, 282.
4. G.G. Zazashvili, M.I. Tevdorashvili, K.I. Tukhashvili, K.D. Kvavadze. Trudy Tbilisskogo Universiteta, 28, 1989, 5.
5. K.Raver. Manual on Ionospheric Absorption Measurements, 1976, 141.
6. K. Tukhashvili. J. Georgian physical Society, 3, 1996, 74.
7. M.I. Vigodskii. Spravochnik po visshei matematike, M., 1962, (Russian).
8. V.P. Tzesevich. Chto i kak nabliudat na nebe. M., 1979, (Russian).
9. Astronomicheskii kalendar. M., 1975, (Russian).

Tbilisi State University
*Institute of Atmosphere Physics
of Universitete Rostock, Germany

ქ. ტუხაშვილი, გ. ენციანი, ვ. იანდაშვილი,
მ. დევნოზაშვილი, მ. მიმინოშვილი

იონოსფეროში რადიოტალღების შთანთქმის ბაზომვის მონაცემებით „რელაქსაციის დროის" განსაზღვრის შესახებ

დასკვნა

იონოსფეროს ინერციის გამო, რადიოტალღების შთანთქმის დღედამური ცვლილების მრუდის მაქსიმუმი წანაცვლებულია სადამოს საათებისაკენ τ „რელაქსაციის დროით". ამ დროის განსაზღვრას დიდი მნიშვნელობა აქვს იონოსფეროს D გარემოს გამოკვლევისათვის.

„რელაქსაციის დროის" განსაზღვრა შესაძლებელია შთანთქმის ყოველსათიანი მონაცემების საშუალებით, მაგრამ ასეთი გაზომვების ჩატარება დიდ სიძნელეებთან არის დაკავშირებული. ამიტომ დედამიწის თითქმის ყველა იონოსფერულ სადგურში გაზომვებს აწარმოებენ დღეში მხოლოდ სამჯერ, რის გამოც ვერ ხერხდება ამ მონაცემებით τ-ს განსაზღვრა.

მოცემულ სტატიაში დამუშავებულია მეთოდი, რომელიც იძლევა „რელაქსაციის დროის" ბუნების შესწავლის საშუალებას სხვადასხვა განედებზე.

GRAPH METHOD OF QUANTITATIVE INTERPRETATION OF GRAVITATIONAL FORCE BY LOCALIZED FIELD APPROPRIATE TO SIMPLE SHAPE BODIES

G. Managadze, R. Managadze, S. Lomidze, R. Danelia, R. Gotsiridze.

ABSTRACT. On the basis of localized field appropriate to simple bodies a graph method for quantitative interpretation of gravitational force has been worked out.

The analytical method to interpret gravity anomaly Δg appropriate to simple bodies on localized function extremum x-intercepts and abscissas of the points where function gets meanings 1/2, 1/3, 1/4, etc, of extremum [1]. But the number of algebraic equations obtained this way is mostly more than two. It is the result of complicated form of localized functions and this makes them practically useless for determining geological and physical parameters of examined bodies [2]. That is why for solving the aimed problem by localized anomalous field we can use the method of quantitative interpretation in such cases when the exponent is more than two.

The sense of the method is following.

On the basis of localized function selected for examining, the appropriate graphs of anomalous field of investigating model are built. According to these graphs the function extremum, x-intercepts and abscissas of the points, where function gets meanings of 1/2, 1/3, 1/4, etc, of extremum are determined.

The following equations are obtained after putting the determined values into the localized function analytical expression where $X_{1/2}$ is the abscissa of localized function in 1/2, 1/3, 1/4

$$F[\Delta g(x,s,h)]_m = F[\Delta g(x_m,s,h)], \tag{1}$$

$$F[\Delta g(x,s,h)]_m = \frac{1}{n}[F\Delta g(x_{1/n},s,h)], \tag{2}$$

$$F[\Delta g(x,s,h)] = F[\Delta g(x_0,s,h)] = 0, \tag{3}$$

where X_m is the abscissa for which the localized function takes the extremal meaning, $X_{1/n}$ is the extremal meanings of X_o abscissas, where function equals to zero.

For determining the depth Δh of the simple shape body depression $X_{1/n}$ and X_o are determined from graphs, and the selection of S parameter is proceeded by giving S different meanings from 0 and a certain Δh interval is added until (1) or (2) equation is not satisfied.

After determining h parameter by using the above-mentioned method it is possible to figure out anomalous mass and in several cases even σ - excessive density of examining body. For example, if investigating localized function's graph is represented by an extremum, then h could be calculated by (1) equation. If besides the extremum localized function has X- intercepts, then for determining h it is necessary to use (1) and (2) equations and the real meaning is considered to be arithmetic average of all determined values.

To introduce this method in practice let's consider Andreev-Griphin's localized function's usage on the model of horizontal matter semi-plane and horizontal circular cylinder.

The profile variant of Andreev-Griphin localized function [1]

$$F[\Delta g(x,s)] = \Delta g(x) - \frac{1}{2}[\Delta g(x-s) + \Delta g(x+s)] \tag{4}$$

in the case of horizontal matter semi-plane [2] could be written in the following way:

$$F[\Delta g(x_m,s)] = 2f\mu\left[arctg\,\frac{x_m}{h} - \frac{1}{2}\left(arctg\,\frac{x_m-s}{h} + arctg\,\frac{x_m+s}{h}\right)\right], \tag{5}$$
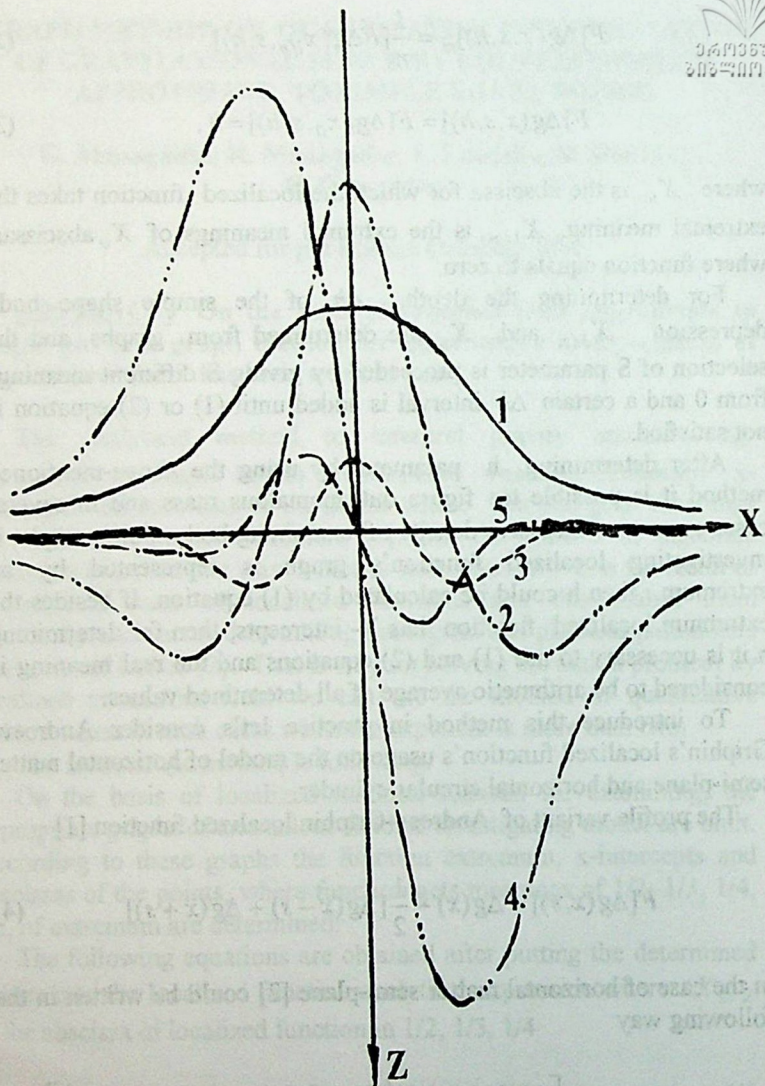
1

5

X

3

2

A

4

Z

Fig.1.

$$F\big[\Delta g(x_{1/n}, s)\big] =$$

$$= 2f\mu\left[\arctg\frac{x_{1/n}}{h} - \frac{1}{2}\left(\arctg\frac{x_{1/n}-s}{h} + \arctg\frac{x_{1/n}+s}{h}\right)\right], \quad (6)$$

$$F\big[\Delta g(x_0, s)\big] = 2f\mu\left[\arctg\frac{x_0}{h} - \frac{1}{2}\left(\arctg\frac{x_0-s}{h} + \arctg\frac{x_0+s}{h}\right)\right]. \quad (7)$$

Its corresponding form is shown in Fig.1. In this case the following expression is used to determine h:

$$F[\Delta g(x_{1/n}, s)] =$$

$$= \frac{1}{n}2f\mu\left[\arctg\frac{\overline{x_{1/n}}}{h} - \frac{1}{2}\left(\arctg\frac{\overline{x_{1/n}-s}}{h} + \arctg\frac{\overline{x_{1/n}+s}}{h}\right)\right], \quad (8)$$

which is constructed with $X_{1/2}, X_{1/3}, X_{1/4}$ using computer equipment for their calculations. The entire procedure is implemented by altering the meaning of h ascending it from 0 gradually adding Δh until (8) is fulfilled. $n = 1, 2, 3\ldots$ in (8) and the average of $\overline{X}_{1/2}$ is defined by the following formula:

$$\overline{F[\Delta g]}_m = \frac{\big|F[\Delta g(-x_m, s)]\big| + \big|F[\Delta g(x_m, s)]\big|}{2},$$

$$\overline{X}_m = \frac{|-x_m| + |x_m|}{2}, \quad \overline{X}_0 = \frac{|-x_0| + |x_0|}{2}, \quad \overline{X}_{1/2} = \frac{|-x_{1/n}| + |x_{1/n}|}{2}. \quad (9)$$

Then the obtained value of h is introduced into

131

$$F[\Delta g(\overline{x_{1/n}}, s)]_{1/n} =$$

$$= \frac{1}{n} 2f\mu \left[arctg \frac{\overline{x_m}}{h} - \frac{1}{2} \left(arctg \frac{\overline{x_m - s}}{h} + arctg \frac{\overline{x_m + s}}{h} \right) \right], \quad (10)$$

the mass and in some opportunity cases σ - excessive density of examined body is found out.

For horizontal circular cylinder

$$F[\Delta g(x, s)] =$$

$$= 2f\lambda \left[\frac{h}{x^2 + h^2} - \frac{1}{2} \left\{ \frac{h}{(x-5)^2 + h^2} + \frac{h}{(x+5)^2 + h^2} \right\} \right] \quad (11)$$

the graphical form of it is presented in Fig.1.

As shown by the graph, function is represented by the central extremum and two symmetrical minimums.

On the model example we used $\overline{X}_o$, $\overline{X}_m$ and $\overline{X}_{1/n}$ abscissas and solutions of (1) and (2) equations defined on the basis of expression (2) to determine h parameter. And then we used the arithmetic average of all calculated values to figure out the meaning of h as it was mentioned above.

$$F[\Delta g(x_m, s)] = 2f\lambda \left\{ \frac{h}{x_m^2 + h^2} - \frac{1}{2} \left[\frac{h}{(x_m - s)^2 + h^2} + \frac{h}{(x_m + s)^2 + h^2} \right] \right\}$$

$$F[\Delta g(x_o, s)] =$$

$$= 2f\lambda \left\{ \frac{h}{\overline{x_0} + h^2} - \frac{1}{2} \left[\frac{h}{(\overline{x_0 - s})^2 + h^2} + \frac{h}{(\overline{x_0 + s})^2 + h^2} \right] \right\}, \quad (12)$$

132

$$F[\Delta g(x_{1/n}, s) =$$

$$= 2f\lambda \left\{ \frac{h}{x_{1/n} + h^2} - \frac{1}{2} \left[\frac{h}{(x_{1/n} - s)^2 + h^2} + \frac{h}{(x_{1/n} + s)^2 + h^2} \right] \right\}.$$

Finally, we note that, the work presents the gravity reverse problem solving method by using localized field appropriate to simple shape body. The method was implemented by means of Andreev-Griphin's localized function considering the samples of horizontal matter semi-plane and cylinder. The method is common and can be used in the case of any localized function and any simple shape body.

REFERENCES

1. B.A. Andreev, I.G. Klushin. The Geological Interpretation of Gravity Anomaly. L. 1965, (Russian)
2. The Building and Dynamic of Lithosphere of Caucasus. On the 85-birthday of academic B.K. Balavadze. Institute of Geophysics. Georgian Academy of Sciences. 1996.
3. L. Nettletone. Geophysical prospecting for oil. N.Y.1940.

Tbilisi State University

გ. მანაგაძე, რ. მანაგაძე, ს. ლომიძე, რ. დანელია,
რ. გოცირიძე

მარტივი ფორმის სხეულის შესაბამისი ლოკალიზებული ველით სიმძიმის ძალის ანომალიის ოდენობითი ინტერპრეტაციის გრაფიკული ხერხი

დასკვნა

მარტივი ფორმის სხეულის შესაბამისი ლოკალიზე-
ბული ველით სიმძიმის ძალის ანომალიის ოდენობითი
ინტერპრეტაციის წარმოებისას საქმე გვაქვს ალგებრულ
განტოლებებთან, რომელთა ხარისხის მაჩვენებელი რამო-
დენიმეჯერ აღემატება ორს. ამიტომ მისი გამოყენება სა-
ვლევი სხეულის გეოლოგიური პარამეტრების დასადგენად
შეუძლებელია. აღნიშნული სიძნელის თავიდან ასაშორებ-
ლად ნაშრომში შემოტანილია გრავიმეტრიის შებრუ-
ნებული ამოცანის ამოხსნის ახალი ხერხი დაფუძნებული
სალოკალიზაციო ფუნქციის ანალიზური სახის გამოყენე-
ბაზე. მეთოდი უნივერსალურია და მისი გამოყენება
შეიძლება ნებისმიერი სტაციონარული გეოფიზიკური
ველის მიხედვით მარტივი ფორმის სხეულთა გეოლოგი-
ური პარამეტრების დასადგენად.

134

THE SYNTHESIS TECHNOLOGY INFLUENCE ON THE ELECTRIC AND MAGNETIC PROPERTIES OF THE BI(PB)SR-CA-CU-O SUPERCONDUCTORS

R. Kokhreidze, A. Mestvirishvili, G. Mumladze, S. Odenov, N. Papunashvili, J. Sanikidze, M. Chubabria

ABSTRACT. In this article, the influence of the thermoprocessing conditions on the Bi-based superconductors properties is studied. The magnetic properties are investigated by the crossed fields method, which allows to get the necessary information about the samples quality change during the thermoprocessing. The two-stage processing of the powder during the synthesis and the following annealing at different temperatures permits to improve essentially the samples quality. The results are analyzed in connection with the thermo differential curves. The current-voltage characteristics of the samples in magnetic fields are investigated too.

The investigations of the Bi-containing superconducting ceramics is being carried out for a long time already [1].

It is known, that such materials have a number of peculiarities, which makes them rather promising for application in some power appliances [2,3], and the textured samples use permits to raise significantly their critical parameters[4]. Simultaneously these materials have another peculiarities – a strong flux creep at the nitrogen boiling temperature, sensitivity to an annealing regime, etc.

Earlier [5,6] we have investigated electric and magnetic characteristics of the system Bi-(Pb)-Sr-Ca-Cu-O. There was investigated a magnetic hysteresis of the samples and their main physical properties. It was shown [6], that the bismuth superconductor qualities (in the powder form) were strongly dependent on the temperature and the duration of the synthesis process. In particular, the additional processing of the powder, obtained after the 845-855^{0}C annealing for 30-40 hours at the relatively low temperature of 820-

840°C leads to the strong (almost 2 times) enhancement of the magnetic susceptibility of the material.

In this paper the influence of the processing regime temperature both of the powder and of the pressed samples on the electric and magnetic properties of these samples is investigated.

$$Bi_{1.7}(Pb_{0.3})Sr_2Ca_2Cu_nO_x$$
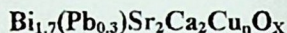
Table1 n=3

The samples	The thermal processing duration					
	The powder			The samples		
	855°C	840°C	The sum	855°C	840°C	The sum
8	50	-	50	-	4	4
8'				4	-	4
8''				4	9	13
8'''				4	22	26
9	50	20	70	-	4	4
9'				4	-	4
9''				4	9	13
9'''				4	22	26

n=4

The samples	850°C	840°C	The sum	850°C	840°C	The sum
4	30	-	30	-	4	4
4'				-	17	17
5	30	20	50	-	4	4
5'				-	17	17
6	50	-	50	-	4	4
6'				4	-	8
6''				4	17	21
7	50	20	70	-	4	4
7'				4	-	9
7''				4	17	22

For this purpose the powder of the reacting mixture of the optimal composition $Bi_{1.7}(Pb_{0.3})Sr_2Ca_2Cu_nO_x$ (n = 3 and n = 4) was annealed in the two-stage temperature regime [6]. At the first stage the powder was processed at the synthesis temperature of 850-855°C for 30-50 hours, and at the second stage there was an additional annealing at

840^0C then this powder was pressed into the samples (the pressure of $\sim7\cdot10^3$ MPa) and annealed at the temperature 850^0C (n = 4) and 855^0C (n = 3), and also at 840^0C for both cases during 4-30 hours. The thermal processing regime of the reacting mixture and of the samples is given in Table 1.

The magnetic properties of the samples were studied by the crossed alternating and direct fields method [7]. The direct field value could be changed from 0 up to 3 kOe. The alternating field amplitude was less than 1 Oe, and its frequency was 10^3 Hz. At such a frequency the skin effect may be neglected altogether, and the susceptibility is determined only by the superconducting phase presence (Meissner effect). The susceptibility value was normalized by an etalone so, that the real part of the susceptibility of an ideal diamagnetic was equal to $-1/4\pi$. The sample was at Dewar vessel at the temperature of liquid nitrogen boiling point, and all was placed in the magnetic field. For the investigation of current characteristics the samples in the microbridge form with the crossection less than 1 mm^2 were studied.

On the samples the silver contacts were deposited by the annealing process. The bias on the contacts were measured by the microvoltmeter. The sample was placed into the liquid nitrogen, and in the magnetic field of an electromagnet. The results of the investigation are given in Fig. 1-4.

In the first turn it must be noted that the samples show rather sharp transition during the cooling, and the half of the transition width is nearly 2K for the sample N9' (n = 3), and near 3.5K for the sample N5 (n = 4).

The temperature of transition is 105K for the sample N9' and 103K for the N5 (Fig.1).

As it may be seen from Figs.1, 3, the two-stage thermoprocessing of the powder of the Bi-system superconductors during the synthesis has a strong influence on the magnetic properties of the pressed samples of both compositions (n = 3 or n = 4). For example, during the processing the samples at the same conditions (840^0C, 4 hours), the samples N9 (Table 1, n = 3) and N5 (Table1, n = 4), which were additionally annealed at 840^0C during 20 hours (the second stage of synthesis) show rather significant improvement of the diamagnetic

$Bi_{1.7}(Pb_{0.3})Ca_2Sr_2Cu_nO_x$

Fig.1.

$Bi_{1.7}(Pb_{0.3})Ca_2Sr_2Cu_3O_x$
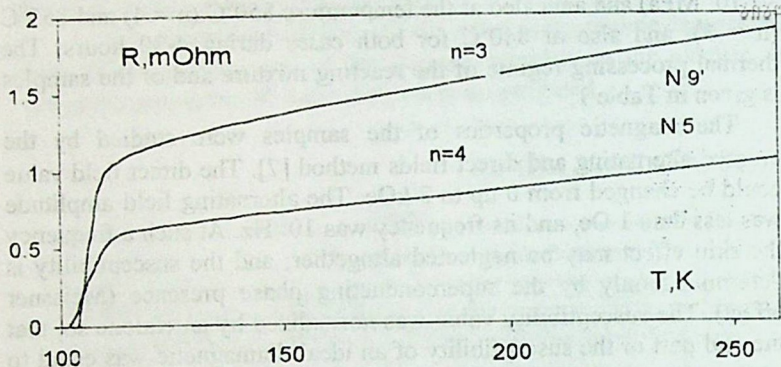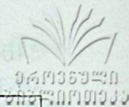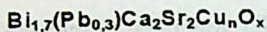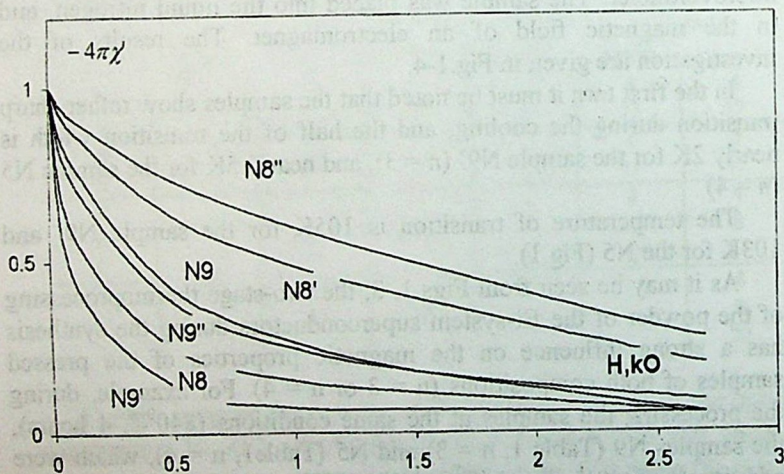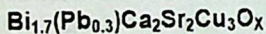
Fig.2.
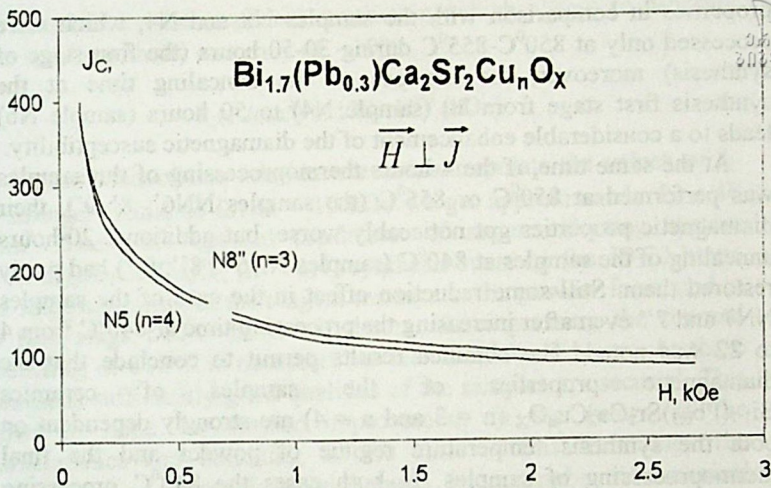
Fig.3.
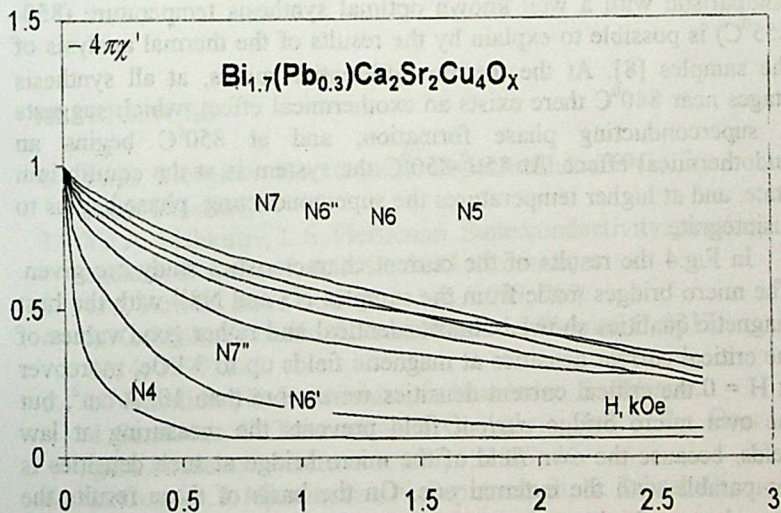
Fig.4.

properties in comparison with the samples N8 and N4, which were processed only at $850^{0}C$-$855^{0}C$ during 30-50 hours (the first stage of synthesis) moreover, the increase of the annealing time at the synthesis first stage from 30 (sample N4) to 50 hours (sample N6) leads to a considerable enhancement of the diamagnetic susceptibility.

At the same time, if the 4-hours thermoprocessing of the samples was performed at $850^{0}C$ or $855^{0}C$ (the samples NN6', 8' 9'), their diamagnetic properties got noticeably worse, but additional 20-hours annealing of the samples at $840^{0}C$ (samples NN6'', 8'', 9'') had partly restored them. Still some reduction effect in the case of the samples NN7 and 7'' even after increasing the processing time at $840^{0}C$ from 4 to 22 was noted. The obtained results permit to conclude that the diamagnetic properties of the samples of ceramics $Bi_{1.7}(Pb_{0.3})Sr_2Ca_2Cu_nO_x$ ($n = 3$ and $n = 4$) are strongly dependent on both the synthesis temperature regime of powder and the final thermoprocessing of samples. In both cases the $840^{0}C$ processing leads to a considerable enhancement of the diamagnetic properties of the samples. The diamagnetism reduction effect of the Bi-system ceramics after the processing at some lowered temperature ($840^{0}C$) in comparison with a well known optimal synthesis temperature (850-$855^{0}C$) is possible to explain by the results of the thermal analysis of the samples [8]. At the thermo differential curves, at all synthesis stages near $840^{0}C$ there exists an exothermical effect, which suggests a superconducting phase formation, and at $850^{0}C$ begins an endothermical effect. At 850^{0}-$850^{0}C$ the system is at the equilibrium state, and at higher temperatures the superconducting phase begins to disintegrate.

In Fig.4 the results of the current characteristics study are given. The micro bridges made from the samples N5 and N8'' with the best magnetic qualities showed almost identical and rather good values of the critical current densities at magnetic fields up to 3 kOe, moreover at H = 0 the critical current densities were more than 10^{3} A/cm^{2}, but the own micro bridge current field prevents the measuring at law fields, because the own field of the micro bridge at such densities is comparable with the external one. On the basis of these results the dependence of critical current density for the both samples can be

approximated by the empirical expression, which allows to describe these results with the accuracy of ~10%:

$$J_C(A/cm^2) \cong 130 \cdot H^{0.5} (kOe)$$

On the basis of this relation one can extrapolate the values of J_C for stronger fields, so for $H = 10$ kOe we get approximately $J_C \sim 40$ A/cm^2. Thus, the optimal conditions of superconducting system $Bi_{1.7}(Pb_{0.3})Sr_2Ca_2Cu_nO_X$ ($n = 3,4$) synthesis must be the 50-70 hours two-stage annealing of the reagent mixture in the powder form, and at the first stage 840^0C for 30-50 hours. After pressing the thermal processing at 840^0C is necessary no less than for 4 hours. At these conditions sufficiently good qualities of the samples are secured. This allows to hope for further improvement in the future of the characteristics and obtaining on the basis of this technology the superconducting materials good enough for a number of technical applications.

REFERENCES

1. Yu.D. Tretiakov, E.A. Gudilin. Uspekhi Chem. **69**(1), 3, 2000. (Russian).
2. Yu.A. Bishkirov, L.S. Fleishman. Superconductivity: physics, chemie, technics. **4**, **8**, 1992, 1351, (Russian).
3. I.M. Rowell. Solid St.Comm. **102**, 1997, 269.
4. A. Goldish, Y. Beilin, E. Yashchin. et al Physica C, 2213, 2214, 1997, 282.
5. N. Kekelidze, R. Kokhreidze, G.Mumladze, S. Odenov, J. Sanikidze, G. Tsintsadze, M. Chubabria. Bull. of the Geor gian Academy of Sciences. **156**, 1, 1997, 46.
6. L. Gogava, I. Mjavanadze, N. Papunashvili, N. Sabashvili, M. Chubabria. Ceramics. 3, 2000, 18 (Georgian).

7. V.I. Chechernikov. The magnetic measurements MGU, Moscow, 1989, (Russian).

8. D. Adamia, I. Mjavanadze, N. Papunashvili, N. Sabashvili, G. Tsintsadze, M.Chubabria. Ceramics. 2, 22, 1999, (Georg.).

Georgian Academy of Sciences
Institute of Cybernetics

რ. კოხრეიძე, ა. მესტვირიშვილი, გ. მუხლაძე, ს. ოდენოვი, ნ. პაპუნაშვილი, ჯ. სანიკიძე, შ. ჭუბაბრია

სინთეზის ტექნოლოგიის გავლენა Bi(Pb)Sr-Ca-Cu-O ზეგამტარების ელექტრულ და მაგნიტურ თვისებებზე

დასკვნა

ამ სტატიაში გამოკვლეულია თერმული დამუშავების პირობების გავლენა Bi(Pb)Sr-Ca-Cu-O სისტემის ზეგამტარებზე. ზეგამტარების მაგნიტური თვისებების გამოკვლევა ხდება ჯვარედინა ველთა მეთოდით, რაც საშუალებას იძლევა, მივიღოთ საჭირო ინფორმაცია ზეგამტარის ხარისხის ცვლილების შესახებ თერმული დამუშავების პროცესში. ფხვნილის ორსაფეხურიანი თერმული დამუშავება სინთეზის დროს და შემდგომში გამოწვა სხვადასხვა. ტემპერატურისას საშუალებას გვაძლევს არსებითად გავაუმჯობესოთ ნიმუშთა თვისებები. შედეგების ანალიზი ხორციელდება თერმოდიფერენციალური მრუდების გათვალისწინებით. გამოკვლეულია აგრეთვე ნიმუშების კრიტიკული დენის დამოკიდებულება მაგნიტურ ველზე.

ON CONCENTRATION NONLINEARITY UNDER HOT ELECTRON CAPTURE BY REPULSIVE CENTERS

Z. Kachlishvili, N. Metreveli

ABSTRACT. The hot electron concentration as a function of applied field and the parameters characterizing the scattering mechanisms is calculated in the approximation of quasielastic scattering under conditions when their lifetime is controlled by capture on the negatively charged centers. It is taken into account that along with Zommerfeld multiplier the capture probability must be exponentially depended on the energy of tunneled through the barrier electron.

From the estimations it is clear that in strong electric field taking into consideration of the exponential multiplier is necessary, while in comparatively weak fields the Bonch-Bruevich approximation gives good results.

Account of additional multiplier in capture probability decreases the concentration minimum, which in its turn signifies that the disappearance of concentration nonlinearity becomes more rapid. The weak magnetic field does not change the situation, while the strong magnetic field increases the concentration minimum and thus the disappearance of concentration nonlinearity becomes slower.

The concentration nonlinearity due to hot electron capture by repulsive centers has been extensively studied both theoretically [1-5] and experimentally (see [6,7]). These studies reached their peak in the 1970 s. However, rapid advances in the theory provided the impetus for further consideration of this problem. Here the following is meant: in all earlier works the expression for the capture probability first derived by Bonch-Bruevich [1] was used to estimate the capture coefficient. However, in [8] it is shown that during the electron capture by a repulsive center the capture probability along with Zommerfeld

multiplier must depend exponentially on the energy of the electron having tunnelled through the barrier. In the same work, in the electron temperature approximation, and in [9,10], under transverse runaway and needle-like distribution conditions, the capture coefficient was calculated. It was shown that when electron temperature was much lower than the oscillation quantum energy far away from the runaway threshold and in the presence of a center with high capture multiplicity, the Bonch-Bruevich effective section was a good approximation, while under opposite conditions the above-mentioned exponential multiplier should be taken into account.

In the present work, using the capture probability from [8] a hot electron concentration has been calculated in the quasielastic scattering approximation and its explicit dependence on the applied fields and even on parameters characterizing the scattering mechanisms has been obtained. The latter allows one to predict the capture probability approximation according to the experimental conditions.

It is well-known that the solution of the recombination kinetics equation related to the hot electron concentration (n) has the form [11]:

$$n = N_0 \Delta^{-1}, \qquad (1)$$

where $N_0 \equiv \dfrac{N_I N_D}{N - N_D}$, $N_I = \dfrac{N - N_0^-}{N_0^-} n_0$, N and N^- are the concentrations of negatively charged centers "before capture" and "after capture", N_D is the concentration of shallow, entirely ionized donors, the index "0" points to the corresponding value in the thermal equilibrium, $\Delta \equiv \dfrac{C(E,H)}{C(O)}$ is the capture coefficient ratio in the electric and magnetic fields (C (E,H)) and in equilibrium conditions (C(0)).

With some lattice temperature (T ≤ 100K), trap depth (≤ 0.26 eV) restrictions and considering the multiplier with exponential energy dependence of the electron tunnelled through the barrier for Δ we have:

$$\Delta = \frac{\sqrt{\pi}}{2} \times \frac{\int\limits_0^\infty dx\, f_0(x)\left[\exp\!\left(\frac{\gamma}{\sqrt{x}}\right)-1\right]^{-1} \exp[-\gamma_0 x]}{\int\limits_0^\infty dx\,\exp(-x)\left[\exp\!\left(\frac{\gamma}{\sqrt{x}}\right)-1\right]^{-1} \exp(-\gamma_0 x)\int\limits_0^\infty x^{1/2} f_0(x)dx} \qquad (2)$$

Here $\gamma \equiv \dfrac{2\pi z e^2}{\varepsilon \hbar v_T}$, $\gamma_0 = \dfrac{2\tau_1}{\hbar} kT$, z is the repulsive center charge in electron charge units, ε is the permittivity, V_T is the thermal velocity, τ_1 is the tunnelling time, $x \equiv \dfrac{W}{kT}$, W is the electron energy; the rest symbols are universally accepted. $f_0(x)$ is the nonequilibrium distribution function, which in the quasielastic scattering approximation in the crossed fields under strong heating

$$\alpha \gg \alpha^{(0)} \equiv \xi^{\xi-1}\eta^\zeta\left(\Gamma\!\left(\frac{5}{2\xi}\right)\Big/\Gamma\!\left(\frac{3}{2\xi}\right)\right)^{\xi(\xi-1)} \quad \text{has the form [12]:}$$

$$f_0(x) = A\exp\left(-\frac{\eta^\zeta}{\alpha}\times\frac{x^\xi}{\xi}\right), \qquad \xi>0, \qquad (3)$$

where in the weak magnetic field $(\eta \ll 1)$: $\zeta = 0,$, $\xi = \xi_1 = 1 - \dfrac{t+s}{2}$,

and in the strong magnetic field $(\eta \gg 1)$: $\zeta = 1$, $\xi = \xi_2 = 1 + \dfrac{t-s}{2}$.

t and s are the indices of degree in the energy dependence of the momentum and energy mean free path, respectively:

$$l = l_0 x^{\frac{1+t}{2}}, \quad \tilde{l} = \tilde{l}_0 x^{\frac{1+S}{2}}, \quad \alpha \equiv \left(\frac{E}{E_0}\right)^2, \quad \eta \equiv \left(\frac{H}{H_0}\right)^2,$$

145

A is the normalization factor, $E_0 \equiv \sqrt{3}\,\dfrac{k_0 T}{e\left(\tilde{l}_0 \tilde{l}_0\right)^{1/2}}$, $H_0 \equiv \dfrac{\left(2mc^2 k_0 T\right)^{1/2}}{el_0}$

m is the effective electron mass, c is the light velocity.

Taking into account that under the required conditions $\gamma \gg 1$, discarding the unity in integral denominator (2) and calculating the integrals by the passover method, we obtain:

1. At

$$\alpha \gg \frac{\alpha^{(0)}}{\gamma_0^{\xi}} \qquad (4)$$

$$n/n_0 = \Delta_{0,1}^{-1}\left(\alpha/\eta^{\varsigma}\right)^{\frac{3}{2\xi}}\left[\frac{\eta^{\varsigma}}{\alpha}(\xi-1)\left(\frac{\gamma}{2\gamma_0}\right)^{2(\xi-1)/3}+3\gamma_0/2\right]^{1/2} exp\left[\frac{\eta^{\varsigma}}{\alpha\xi}\left(\frac{\gamma}{2\gamma_0}\right)^{2\xi/3}\right], \qquad (5)$$

where

$$\Delta_{0,1} \equiv \frac{\sqrt{3\pi}\;\xi^{\frac{2\xi-3}{2\xi}}\,(1+\gamma_0)^{5/6}}{2^{3/2}\,\Gamma\left(\dfrac{3}{2\xi}\right)(\gamma/2)^{2/3}\,\gamma_0^{1/3}}\;exp\left[3\,(\gamma/2)^{2/3}\left[(1+\gamma_0)^{1/3}-\gamma_0^{1/3}\right]\right]. \qquad (6)$$

2. At

$$\alpha \ll \frac{\alpha^{(0)}}{\gamma_0^{\xi}} \qquad (7)$$

$$n/n_0 = \Delta_{0,1}^{-1}\left(\frac{\alpha}{\eta^{\varsigma}}\right)^{\frac{\xi+3}{2\xi(2\xi+1)}} exp\left\{\frac{1}{\xi}\left(\frac{\gamma}{2}\right)^{\frac{2\xi}{2\xi+1}}\left(\frac{\eta^{\varsigma}}{\alpha}\right)^{\frac{1}{2\xi+1}}\left[1+2\xi\left(1+\frac{\gamma_0}{\gamma}\left(\frac{\alpha\gamma}{2\eta^{\varsigma}}\right)^{\frac{3}{2\xi+1}}\right)\right]\right\}, \qquad (8)$$

146

where

$$\Delta_{0,2} \equiv \frac{\sqrt{3\pi}\ (1+\gamma_0)^{5/6}}{2^{3/2}\ \Gamma\left(\dfrac{3}{2\xi}\right)\xi^{\frac{3-2\xi}{2\xi}}\left(\dfrac{\gamma}{2}\right)^{\frac{5(\xi-1)}{3(2\xi+1)}}(\xi+1/2)^{1/2}\exp\left[-3(\gamma/2)^{2/3}(1+\gamma_0)^{1/3}\right]}. \quad (9)$$

Now let us analyze the results obtained for particular scattering mechanisms and lattice temperature.

In usual experimental conditions the energy scattering by acoustic phonons (S = -1 in the low and high temperature approximation) and the momentum scattering by ions (t = +3) and acoustic phonons (t = -1) are the predominant scattering mechanisms.

Let us make estimations for Cu- or Au-doped n-Ge at T = 10K and T = 100K.

At T = 20K the scattering by impurity ions is the predominant momentum scattering mechanism. In the weak magnetic field $\xi = 0$, while in the strong magnetic field $\xi = 3$. Since in the first case condition (3) does not hold ($\xi > 0$), our results are not applicable. For $\xi = 3$ with allowance for $\gamma_0 \approx 0.02$ [10] and estimating $\alpha^{(0)}/\gamma_0^3$, as well as γ_0-containing multipliers in (5), (6), (8), (9), one can see that in this case inequalities (7) are fulfilled and we obtain for n/n_0:

$$n/n_0 = \Delta_{0,2}^{-1}\left(\frac{\alpha}{\eta}\right)^{1/7}\exp\left\{\frac{1}{3}\left(\frac{\gamma}{2}\right)^{6/7}\left(\frac{\eta}{\alpha}\right)^{1/7}\right\}, \quad (8.a)$$

where

$$\Delta_{0,2} = 1.5\sqrt{7}\ \frac{\exp\left[-3\left(\dfrac{\gamma}{2}\right)^{2/3}\right]}{\left(\dfrac{\gamma}{2}\right)^{10/21}}. \quad (9.a)$$

Expression (8.a) corresponds to Bonch-Bruevich approximation.

At $T = 100K$, $\gamma_0 \approx 0.1$, and the scattering by acoustic phonons is the predominant momentum scattering mechanism.

In the weak magnetic field $\xi = 2$. Then, according to our estimates, in the strong fields the exponential multiplier $\alpha \gg 2 \times 10^2 \left(\dfrac{\Gamma(5/4)}{\Gamma(3/4)} \right)^2$ is very important and we have for the concentration

$$n/n_0 = \Delta_{0,1}^{-1} \; \alpha^{3/4} \left[\frac{(5\gamma)^{2/3}}{\alpha} + \frac{3}{20} \right]^{1/2} exp\left[\frac{1}{2\alpha} (5\gamma)^{4/3} \right], \tag{5.a}$$

where

$$\Delta_{0,1}^{-1} = \frac{\sqrt{3\pi}}{2^{5/4}} \frac{1.1^{5/6}}{0.1^{1/3}} \; exp\left\{ \left(\frac{27}{10} \right)^{1/3} \left(\frac{\gamma}{2} \right)^{2/3} \left(11^{1/3} - 1 \right) \right\}. \tag{6.a}$$

In the electric field range $2 \left(\dfrac{\Gamma(5/4)}{\Gamma(3/4)} \right)^2 \ll \alpha \ll 2 \; 10^2 \left(\dfrac{\Gamma(5/4)}{\Gamma(3/4)} \right)^2$, our results agree with those obtained using Bonch-Bruevich approximation:

$$n/n_0 = \Delta_{0,2}^{-1} \; \alpha^{1/4} exp\left[\frac{5}{2\alpha^{1/5}} \left(\frac{\gamma}{2} \right)^{4/5} \right], \tag{8.b}$$

where

$$\Delta_{0,2}^{-1} \cong \frac{\sqrt{3\pi}}{2^{5/4} \, \Gamma(3/4)} \; \frac{exp\left[-3 \left(\frac{\gamma}{2} \right)^{2/3} \right]}{\left(\frac{\gamma}{2} \right)^{1/3} \left(\frac{5}{2} \right)^{1/2}}. \tag{9.b}$$

In the strong magnetic field $\xi = 1$ and at $\alpha \gg 10\eta$ the γ_0 - containing exponential multiplier should be taken into account. For n/n_0 we have:

$$n/n_0 = \Delta_{0,1}^{-1} \left(\frac{\alpha}{\eta}\right)^{3/2} \sqrt{\frac{3}{20}} \; exp\left(\frac{5\eta\gamma}{\alpha}\right)^{2/3}, \qquad (5.b)$$

where

$$\Delta_{0,1}^{-1} \equiv \frac{\sqrt{3\pi}}{2^{3/2}} \frac{10^{1/3}}{\Gamma(3/2)\,(\gamma/2)^{2/3}} \; exp\left[3(\gamma/2)^{2/3}\,0.1^{1/3}\left(11^{1/3}-1\right)\right], \qquad (6.b)$$

In the electric field range $1 \ll \dfrac{\alpha}{\eta} \ll 10$ we have:

$$n/n_0 = \Delta_{0,2}^{-1} \left(\frac{\alpha}{\eta}\right)^{2/3} \; exp\left\{3\frac{\eta}{\alpha}\left(\frac{\gamma}{2}\right)^{2/3}\right\}, \qquad (8.c)$$

where

$$\Delta_{0,2} = \frac{\sqrt{3\pi}}{2^{3/2}\,\Gamma(3/2)\,(3/2)^{1/2}} \; exp\left[-3(\gamma/2)^{2/3}\right], \qquad (9.c)$$

which corresponds to Bonch-Bruevich approximation.

The above estimations show that in strong electric field the exponential multiplier in the capture probability should be taken into account, while in relatively weak fields Bonch-Bruevich approximation gives better results.

Thus, according to the experimental conditions inequalities (4) and (7) are estimated and thereby it is established which approximation should be used for the scattering probability in theoretical estimations. Besides, calculating minimum concentration fields (5) and (8) one can

see that allowance for an additional multiplier in the capture probability strongly decreases the minimum concentration field. Taking into account the fact that the differential conductivity is reversed in the minimum concentration field, one can suggest that allowance for the additional multiplier in the scattering probability facilitates the removal of the concentration nonlinearity. In the weak magnetic field this situation remains unchanged, while in the strong magnetic field the minimun concentration field increases.

REFERENCES

1. V.L. Bonch-Bruevich. FTT. **6**, 1964, 2047.
2. V.L. Bonch-Bruevich, S.G. Kalashnikov. FTT. **7**, 1965, 750.
3. V.L. Bonch-Bruevich, Z.S. Kachlishvili. Vestnik MGU. Fizika, Astronomia. **5**, 1974, 580.
4. K.Kh. Asratyan, Z.S. Kachlishvili. FTT. **16**, 1974, 3497.
5. Kh. Z. Kachlishvili, A.G. Mironov. Bulletin of Tbilisi State University, **37**, 1989, 291.
6. N.G. Zhdanova, M.S. Kagan, S.G. Kalashnikov. FTT. **8**, 1966, 788.
7. M.S. Kagan, S.G. Kalashnikov, N.G. Zhdanova. Phys. Stat. Sol., **24**, 551.
8. V.N. Abakumov, V. Karpus, V.I. Perel, I.N. Assievich. FTP. **22**, 1988, 262.
9. Z.S. Kachlishvili, Kh.Z. Kachlishvili, F.G. Chumburidze. FTP. **31**, 1997, 204.
10. Kh.Z. Kachlishvili, Z.S. Kachlishvili, F.G. Chumburidze. FTP. **31**, 1997, 944.
11. V.L. Bonch-Bruevich, I.P. Zviagin, A.G. Mironov. Domain electric instability in semiconductors. M., 1972.
12. Z.S. Kachlishvili. Phys. Stat. Sol (a). **33**, 1976, 15.

Tbilisi State University

ზ. ქაჩლიშვილი, ნ. მეტრეველი

კონცენტრაციული არაპროფილობა ცხელი ელექტრონების განმზიდავ ცენტრებზე ჩაჭერისას

დასკვნა

ცხელი ელექტრონების უარყოფითად დამუხტულ ცენტრებზე ჩაჭერისას ჩაჭერის ალბათობა გამოითვლებოდა ბონჩ-ბრუევიჩის ცნობილი გამოსახულებით. მოგვიანებით ნაჩვენები იქნა, რომ ჩაჭერის ალბათობა ზომერფელდის მამრავლის გარდა ექსპონენციალურად უნდა იყოს დამოკიდებული ბარიერში გამავალი ელექტრონის ენერგიაზეც. ნაშრომში ამ ექსპონენციალური მამრავლის გათვალისწინებით, კვაზიდრეკადი გაბნევების მიახლოებაში გამოთვლილია ელექტრონების კონცენტრაციის დამოკიდებულება მოდებულ ელექტრულ და მაგნიტურ ველებზე.

ნაჩვენებია, რომ ძლიერ ელექტრულ ველში ჩაჭერის ალბათობაში ექსპონენციალური მამრავლის გათვალისწინება აუცილებელია, რადგან იძლევა მნიშვნელოვან შესწორებას, ხოლო შედარებით სუსტ ველებში ბონჩ-ბრუევიჩის აპროქსიმაცია კარგ შედეგებს იძლევა.

151

ANALYSIS OF THE CHARGED SECONDARY HADRONS IN THE COLLISIONS OF RELATIVISTIC NUCLEI IN THE FRAMEWORK OF THE CLUSTER -CASCADING AND PARTICLE -STIMULATING EMISSION MODELS

L. Akhobadze, S. Esakia, V. Garsevanishvili,
T. Jalagania, G. Kuratashvili, Yu. Tevzadze

ABSTRACT. Multiplicity of charged secondary hadrons produced in the relativistic (p, d, He,C)Ta collisions in energy range (2-10)Gev/nucleons are analysed on the basis of partial stimulating emmission and cluster cascading models. The experimental data are obtained by means of the 2 meter propane buble chamber (PBC-500) of JINR (Dubna). The results are compared with the corresponding data for pp, $\bar{p}p$, μp and $e^+ e^-$ - collisions at higher energies. It is shown that in spite of significantly low energies, the principal nature of charged secondary hadrons multiplicity distributions in nucleus-nucleus collisions is in general the same for pp, $\bar{p}p$, μp and $e^+ e^-$ - interactions.

In the present paper multiplicities of charged secondary hadrons in nucleus – nucleus collisions in the energy range (2 - !0) Gev / nucleon are analysed on the basis of the so-called negative binomial distribution

$$P_n(<n>,k) = \frac{(n+k-1)!}{(k-1)!\,n!}\left(\frac{<n>}{<n>+k}\right)^n\left(\frac{k}{<n>+k}\right)^k, \qquad (1)$$

where $<n>=<n\pm>$ is the total multiplicity of all charged secondaries. The parameter k determines the form of the distribution and is related to dispersion D by the formula

$$k = \frac{<n>^2}{D^2 - <n>}. \qquad (2)$$
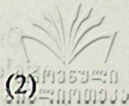
The recurrance relation between P_n and P_{n+1} is written in the form [1]

$$\frac{(n+1)P_{n+1}}{P_n} \equiv g(n) = \alpha + \beta n, \qquad (3)$$

where the parameters α and β are related to $<n>$ and k:

$$<n> = \frac{\alpha}{1 - \beta}, \qquad k = \frac{\alpha}{\beta} \qquad (4)$$

For comparison the data on $pp(\bar{p}p)$, μp and $e^+ e^-$ - collisions at present energies [2-6] are also given. The results obtained are analysed on the basis of two models: partial stimulating emission (PSE) and cluster cascading (CC). [1].

PSE admits the following interpretation of the distribution (1) and the relation (3).

The emitted particles are uniformly distributed among k cells. These cells do not correlate and there is no connection between the particles in different cells. The additional $(n+1)$ -th particle can be emitted in the initial act of the collision independently of the already existing n particles. This is reflected by the constant α in the function $g(n)$. But such an emission can be intensified as a result of quantum interference effects. The average effect of this intensification is expressed by adding the linear term βn in the formula (3). Taking into account the relations (4) the formula (3) takes the form

$$g(n) = \alpha \left(1 + \frac{n}{k} \right) \qquad (5)$$

One can conclude that k^1 is the relative average fraction of paricles among already existing n particles which promote the creation of a new $(n+1)$ -th particle.

In the CCM one assumes that after the collision of high energy particles some exited n - particle system is produced which is formed as N - cluster state. Each of these clusters is formed by the particles which are produced directly or indirectly from one particle produced in the initial act of the collision. These particles are called the "patriarchs" and consequently clusters are produced independently from each other. Therefore for the multiplicity of clusters the Poisson distribution holds

$$F(N) \sim \frac{1}{N!} <n>^N .\qquad (6)$$

The average number of clusters is given by the formula

$$<N> = \frac{<n>}{<n_c>}, \qquad (7)$$

where $<n_c>$ is the average number of hadrons in the cluster.

The characteristics of clusters $<n_c>$ and $<n_c^2>$ are expressed via the parameters α and β entering the recurrance relation (3).

$$<n_c^2> = \frac{<n_c>}{1-\beta}, \qquad <n_c> = -\frac{\beta}{(1-\beta)ln(1-\beta)}. \qquad (8)$$

By means of Eq (8) one can derive the dispersion of particles in the cluster.

The experimental data are obtained on the two–metre propane bubble chamber (PBC –500) of the laboratory of High Energies of JINR (Dubna) with tantal targets in it which were bombarded by p, d, He and C beams in the energy range (2-10) Gev/nucleon. Methodical problems of handling the data are described in [10].

Characteristics of the Multiplicity Distributions of Charged Hadrons in pp-collisions

	Energy in c.m.s. $\sqrt{s}$ GeV						
	5.97	6.85	7.42	8.33	9.78	30.4	62.2
$\langle n \rangle$	3.91±0.04	4.30±0.04	4.56±0.04	4.78±0.03	5.32±0.13	10.7	13.6
D	1.72±0.02	1.90±0.04	2.09±0.04	2.23±0.03	2.58±0.05	4.59	6.01
$\langle n \rangle / D^2$	1.32±0.02	1.19±0.03	1.04±0.02	0.96±0.04	0.80±0.03	0.51	0.38
K^{-1}	-0.062	-0.037	-0.009	0.008	0.05	0.09	0.12
β	-0.0321	-0.19	-0.044	0.039	0.20	0.49	0.62
$\langle n_c \rangle$	0.088	0.92	0.98	1.02	1.12	1.43	1.69
D_c	-	-	-	0.14	0.38	0.87	1.26
$\langle n_c \rangle / D_c^2$	-	-	-	51	7.76	1.88	1.06
$\langle n \rangle / K$	-0.24	-0.16	-0.04	0.04	0.25	0.97	1.66
$\langle N \rangle$	4.44	4.66	4.66	4.69	4.75	7.48	8.05
$\langle n_c^2 \rangle / \langle n_c \rangle^2$	-	-	-	1.02	1.12	1.37	1.56

Characteristics of the Multiplicity Distributions of Charged Hadrons in $\bar{p}p$-collisions

	Energy in c.m.s. $\sqrt{s}$ GeV		
	200	546	900
$\langle n \rangle$	21.3±0.8	29.1±0.9	34.6±1.2
D	10.9±0.4	16.3±0.4	20.7±0.6
$\langle n \rangle / D^2$	0.18±0.02	0.11±0.01	0.08±0.01
K^{-1}	0.22	0.27	0.31
β	0.82	0.88	0.92
$\langle n_c \rangle$	2.66	3.46	4.55
D_c	2.77	4.11	6.01
$\langle n_c \rangle / D_c^2$	0.34	0.20	0.12
$\langle n \rangle / K$	4.65	7.88	10.31
$\langle N \rangle$	8.07	8.41	7.60
$\langle n_c^2 \rangle / \langle n_c \rangle^2$	2.09	2.41	2.75

Table 2.

Characteristics of the Multiplicity Distributions of Charged Hadrons in pTa-collisions

	Energy per nucleon in the lab.system, Gev			
	2.48	4.30	5.48	9.94
$\langle n \rangle$	2.98±0.06	4.73±0.07	6.12±0.09	7.84±0.13
$\langle n \rangle / D^2$	1.38±0.05	0.74±0.05	0.53±0.05	0.30±0.03
K^{-1}	-0.08±0.01	0.07±0.01	0.15±0.01	0.31±0.02
β	-0.38	0.26	0.47	0.71
$\langle n_c \rangle$	0.86±0.04	1.18±0.05	1.41±0.09	1.97±0.12
$\langle n \rangle / K$	-0.27	0.34	0.91	2.40
D_c	-	0.45	0.82	1.71
$\langle n_c \rangle / D_c^2$	-	5.83	2.08	1.47
$\langle N \rangle$	3.47±0.18	4.01±0.21	4.34±0.22	4.22±0.23
$\langle n_c^2 \rangle / \langle n_c \rangle^2$	-	1.14	1.34	1.75

Table 3

Characteristics of the Multiplicity Distributions of Charged Hadrons in dTa-collisions

	Energy per nucleon in the lab.system, GeV		
	2.48	4.30	5.18
$\langle n \rangle$	4.46±0.07	7.15±0.10	7.68±0.21
$\langle n \rangle / D^2$	0.68±0.03	0.40±0.05	0.31±0.03
K^{-1}	0.09±0.01	0.22±0.01	0.29±0.03
β	0.29	0.61	0.69
$\langle n_c \rangle$	1.20±0.06	1.65±0.09	1.90±0.12
$\langle n \rangle / K$	0.40	1.57	2.23
D_c	0.50	1.23	1.59
$\langle n_c \rangle / D_c^2$	4.80	1.08	0.75
$\langle N \rangle$	3.73±0.20	4.22±0.23	4.04±0.25
$\langle n_c^2 \rangle / \langle n_c \rangle^2$	1.17	1.55	1.70

Table 4

Characteristics of the Multiplicity Distributions of Charged Hadrons in HeTa-collisions

	Energy per nucleon in the lab.system, GeV		
	2.48	4.30	5.18
$\langle n \rangle$	7.64±0.14	10.81±0.15	11.79±0.25
$\langle n \rangle / D^2$	0.42±0.03	0.21±0.02	0.16±0.02
K^{-1}	0.22±0.02	0.35±0.03	0.45±0.05
β	0.61	0.79	0.84
$\langle n_c \rangle$	1.67±0.08	2.41±0.10	2.88±0.16
$\langle n \rangle / K$	1.70	3.78	5.30
D_c	1.22	2.38	3.12
$\langle n_c \rangle / D_c^2$	0.89	0.42	0.29
$\langle N \rangle$	4.57±0.14	4.48±0.23	4.09±0.22
$\langle n_c^2 \rangle / \langle n_c \rangle^2$	1.53	1.97	2.17

Table 5

Characteristics of the Multiplicity Distributions of Charged Hadrons in CTa-collisions

	Energy per nucleon in the lab.system, GeV	
	2.48	4.30
$\langle n \rangle$	12.73±0.61	19.75±0.39
$\langle n \rangle / D^2$	0.18±0.02	0.08±0.01
K^{-1}	0.36±0.05	0.56±0.04
β	0.82	0.92
$\langle n_c \rangle$	2.66±0.10	4.55±0.12
$\langle n \rangle / K$	4.66	11.03
D_c	2.78	6
$\langle n_c \rangle / D_c^2$	0.35	0.12
$\langle N \rangle$	4.77±0.22	4.29±0.24
$\langle n_c^2 \rangle / \langle n_c \rangle^2$	2.09	2.74

Table 6

Characteristics of the Multiplicity Distributions of Charged Hadrons in e+e--collisions

	Energy in c.m.s. $\sqrt{s}$ GeV				
	14	22	34	91	130
$\langle n \rangle$	9.4±0.4	11.3±0.4	13.5±0.5	20.71±0.81	23.84±1.00
D	3.22	3.77	4.47	6.28	7.55
$\langle n \rangle / D^2$	0.86	0.77	0.68	0.52	0.42
K^{-1}	0.011	0.023	0.036	0.044	0.058
β	0.094	0.208	0.325	0.470	0.580
$\langle n_c \rangle$	1.12	1.14	1.22	1.41	1.59
D_c	-	0.37	0.56	0.82	1.10
$\langle n_c \rangle / D_c^2$	11.89	7.12	3.99	2.10	1.28
$\langle n \rangle / K$	0.10	0.27	0.48	0.90	1.40
$\langle N \rangle$	8.40	9.65	11.06	13.02	14.99
$\langle n_c^2 \rangle / \langle n_c \rangle^2$	-	1.10	1.21	1.34	1.49
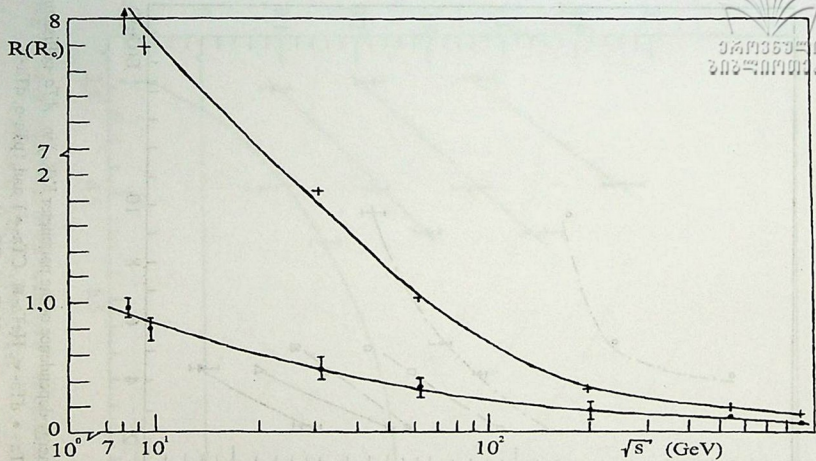
Fig. 1. Energy dependence of $R(R_c)$ in pp and $\bar{p}p$ -collisions:

$(\bullet) - R = <n>/D^2$ $(+) - R_c = <n_c>/D_c^2$.
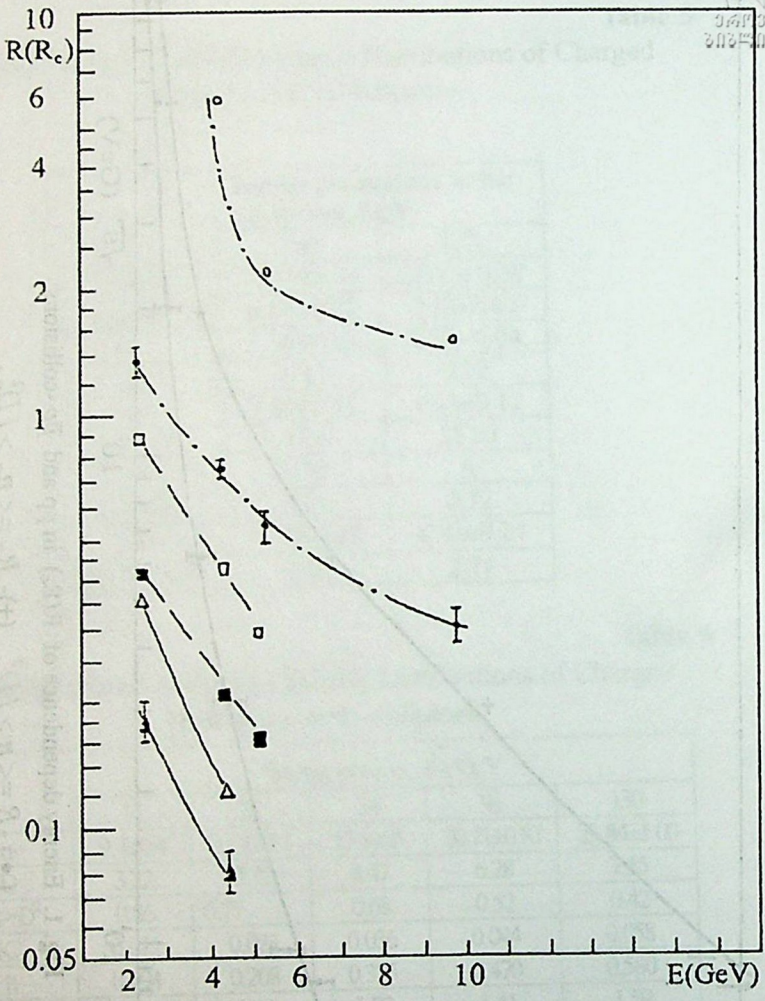
Fig. 2. Energy dependence of the parameter $K(K_c)$ in $A_i Ta$-collisions (pTa - •, dTa-▼, HeTa-■, CTa-▲) and (pTa-o, dTa-∇, HeTa-□, CTa-Δ).
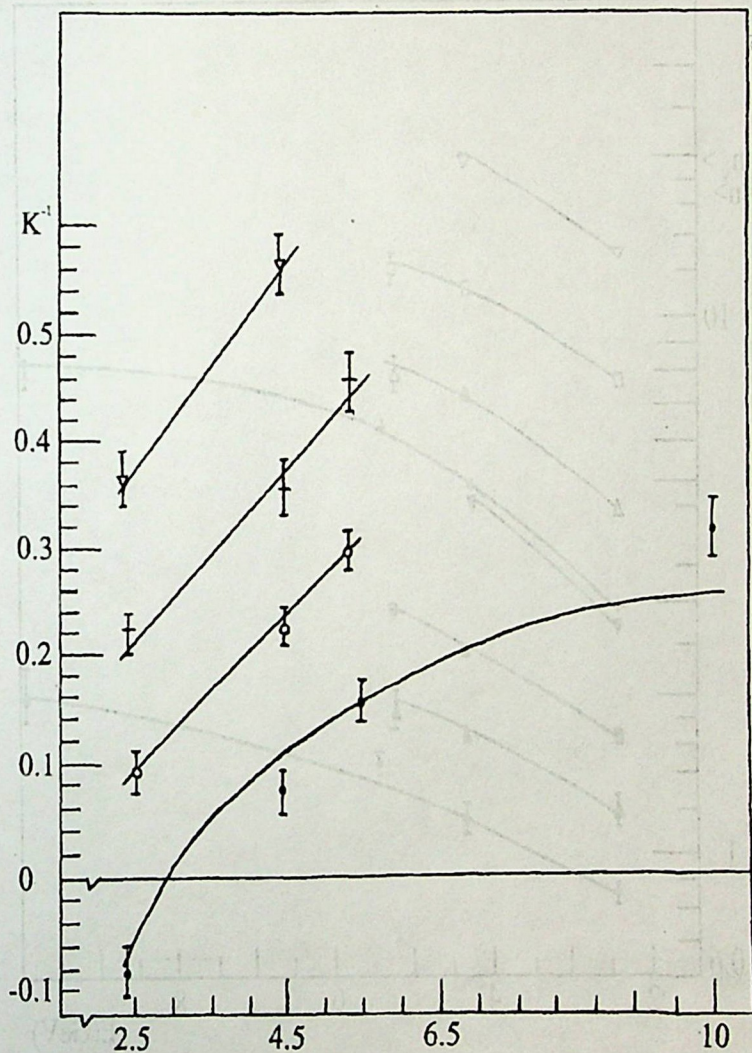
Fig. 3. Energy dependence of the parameter k^{-1} in A_iTa-collisions:
pTa - •, dTA-o, HeTa-+, CTa-Δ .
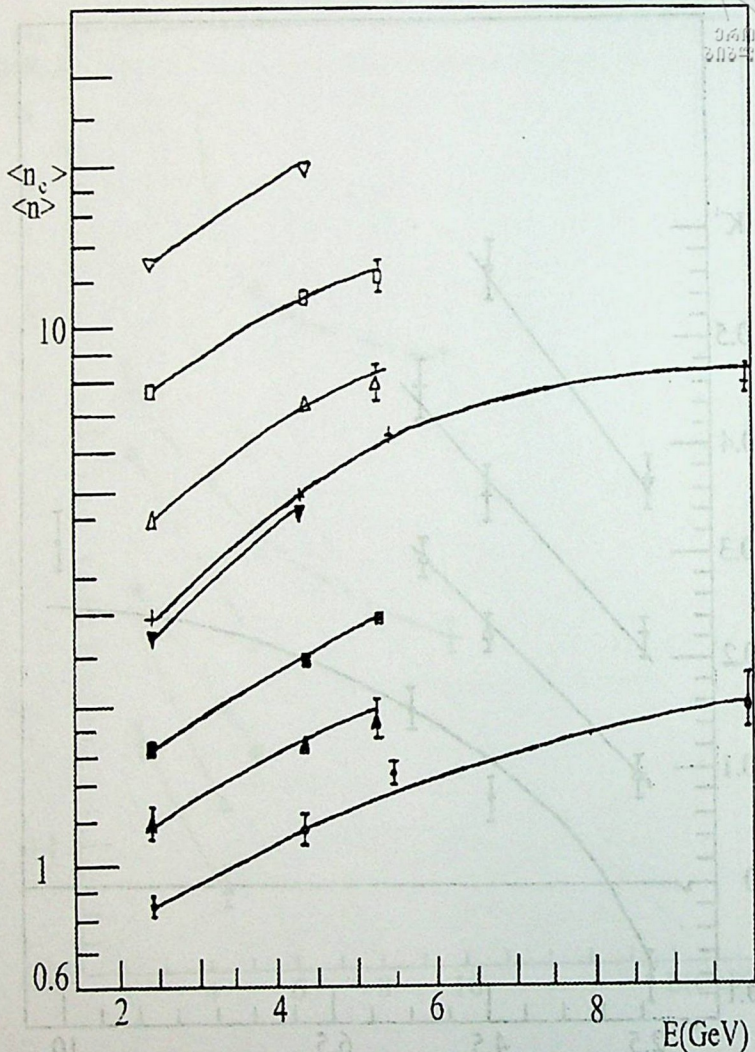
Fig. 4. Energy Dependence of $\langle n_c \rangle$ in A_iTa -collisions (pTa- •, dTa- ▲, HeTa- ■, CTa- ▼) and Energy Dependence of $\langle n \rangle$ in A_iTa -collisions ([(pTa-+ , dTa-△, HeTa-□ , CTa-▽).
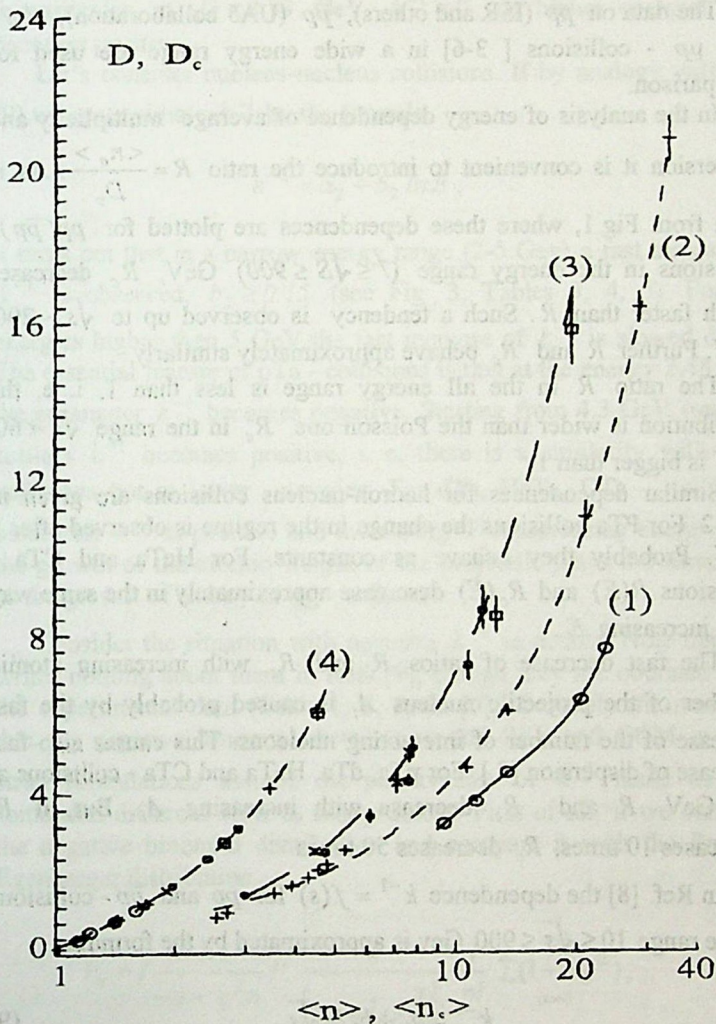
Fig. 5. Dependence $D_c(\langle n_c \rangle)$, $D(\langle n \rangle)$ in e^+e^-, pp, $\bar{p}p$ and A_iTa-

collisions ($e^+e^- - \circ$, pp, $\bar{p}p - +^\wedge$ pTa- •, dTa- ×, HeTa- ■,

CTa- □). Dependence $D(\langle n \rangle)$ – curve 1,2,3, $D_c(\langle n_c \rangle)$- curve 4.

The data on pp (ISR and others), $\bar{p}p$ (UA5 collaboration), e^+e^- and μp - collisions [3-6] in a wide energy range are used for comparison.

In the analysis of energy dependence of average multiplicity and dispersion it is convenient to introduce the ratio $R = \dfrac{<n_c>}{D_c}$. As is seen from Fig.1, where these dependences are plotted for $pp(\bar{p}p)$, collisions in the energy range $(7 \leq \sqrt{S} \leq 900)$ GeV, R_c decrcases much faster than R. Such a tendency is observed up to $\sqrt{s} \sim 200$ GeV. Further R and R_c behave approximately similarly.

The ratio R in the all energy range is less than 1, i. e. the distribution is wider than the Poisson one. R_c in the range $\sqrt{s} < 60$ GeV is bigger than 1.

Similar dependences for hadron-nucleus collisions are given in Fig. 2. For PTa-collisions the change in the regime is observed after 5 GeV. Probably they behave as constants. For HeTa and CTa - collisions $R(E)$ and $R_c(E)$ descrease approximately in the same way with increasing E.

The fast decrease of ratios. R and R_c with increasing atomic number of the projectile nucleus A_i is caused probably by the fast increase of the number of interacting nucleons. This causes also fast increase of dispersion [7]. For pTa, dTa, HeTa and CTa - collisions at 4,3 GeV. R and R_c decrease with increasing A_i. But, if R decreases 10 times, R_c decreascs 50 times.

In Ref. [8] the dependence $k^{-1} = f(s)$ for pp and $\bar{p}p$ - collisions in the range $10 \leq \sqrt{s} \leq 900$ Gev is approximated by the formula

$$k^{-1} = a_1 + b_1 \, ln\sqrt{s} \qquad (9)$$

$k^{-1} > 0$ and increases rather slowly with increasing energy $(b_1 \approx 0.06)$. It has been shown by our analysis that at lower energies,

164
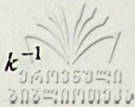
in particular, at $\sqrt{s} < 8.33$ GeV, $k^{-1} < 0$. At higher energies k^{-1} becomes positive.

Let's consider nucleus-nucleus collisions. If by analogy with Eq. (9) we approximate k^{-1} by the formula

$$k^{-1} = a_2 + b_2 \ln E, \qquad (10)$$

it turns out that in a narrow energy range (2-5 Gev) a fast increase of k^{-1} is observed, $b_2 \geq 0.15$ (see Fig. 3, Tables 3, 4, 5). For the energies higher than 5 GeV the fast increase of k^{-1} is slowed down. The essential feature of pTa - collisions is that at the energy 2.48 GeV the parameter k^{-1} becomes negative. Starting from 4.3 GeV (may be earlier) k^{-1} becomes positive, i. e. there is a similarity with pp - collisions but at lower energies. For dTa, HeTa, CTa – collisions parameter k^{-1} is positive and increasing with increasing energy, i. e. the growth of the atomic weight of the projectile plays the same role as the growth of energy in pp - collisions.

Consider the situation with negative k^{-1} in details. Note that one writes nothing about them in Refs.[9], though they are obtained from the experimental data (Table 1, 2, Refs. [9]). Probably the reason is that the negative binomial distribution and PSE and CCM in their strict formulations assume the positiveness of k^{-1} made us take somewhat different view to this problem. First of all, if we consider the negative binomial distribution and compare it with the Polya - Egenberger distribution

$$P_n = [\frac{<n>}{-1+g^2 n}]^2 \frac{1}{\left[1+g^2(n)\right]^{\frac{1}{g^2}}} \frac{1}{n!} \sum_{\alpha=0}^{n-1}(1+\alpha g^2), \qquad (11)$$

where

$$g^2 = \frac{D^2 - <n>}{<n>^2} \qquad (12)$$

it is evident that these two distributions coincide, if we take $k^{-1} = g^2$. But the sign of the parameter g^2 in Eq.(11) is not fixed. In particular, if $g^2 = 0$, we get the Poisson distribution, if $g^2 > 0$, this distribution is broader than the Poisson one, if $g^2 < 0$, it is narrower than the Poisson one. So the parameter g^2 can be thought as a measure of deviation of the distribution from the Poisson one and if we perform the analysis of the experimental data in terms of the Polya-Egenberger distribution, the parameter $k^{-1} = g^2$ can take positive and negative values as well. Further, there are some grounds to think that the negative values of k^{-1} are compatible with the assumptions of PSE and CCM. In fact, the second term in Eq. (3) corresponds to quantum – mechanical interference effects. If these effects stimulate the creation of $(n+1)$-th particle, then $\beta > 0$ and hence $k^{-1} = \frac{\beta}{\alpha} > 0$, since $\alpha > 0$. But it is natural to suppose that these effects can make the emission (capture of particle) weaker. In this case $\beta < 0$ and hence $k^{-1} < 0$. So one can conclude that $k^{-1} < 0$ corresponds to the capture of secondary particles (see also [7-10]).

Proceed now to consider the energy dependence of the total average multiplicity of particles $<n>$ and the average multiplicity of particles in the clusters $<n_c>$ in A_iTa – collisions and compare these data with corresponding results on pp and $\bar{p}p$ - collisions.

In the energy range 6 - 200 GeV in pp and $\bar{p}p$ - collisions $<n>$ and $<n_c>$ increase rather fast, but $<n>$ increases faster than $<n_c>$. In the range 200 – 900 GeV the increase of these quantities is slower and both of them increase approximately 1.6 times (Table1).

In pTa - collisions the energy range can also be divided into two parts. The first interval 2 - 5 GeV and the second one 5 - 9 GeV. In the

first interval we observe a more rapid increase of the average multiplicities $<n>$ and $<n_c>$ than in second one (Fig. 4. Tables 2, 3, 4). So we have qualitatively the same situation as in pp and $\bar{p}p$ - collisions, but the energy range is more narrow and low.

It is interesting to trace the dependence of $<n>$ and $<n_c>$ on the atomic weight, A_i of the incoming nucleus at fixed energy. It is seen from Tables 2 – 5 that at 2.5 GeV $<n>$ and $<n_c>$ increase 3 times. Similar behavior is observed at 4.3 GeV (Tables 2 - 5). So the increase of the atomic weight of the incoming nucleus in $A_i A_t$ - collisions plays a similar role as the increase of energy. As a result in $A_i A_t$ -collisions the same effect is observed as in hadron-hadron collisions, but at much lower energies.

Consider now the data on e^+e^- - annihilation and $\mu p \rightarrow$ hadrons [1,11,12], and compare them with the data on hadron – hadron and nucleus–nucleus collisions. As seen from Table 6 in e^+e^- - collisions up to $\sqrt{s} = 34$ GeV $\frac{<n>}{k} \ll 1$. From the CCM point of view this means that the average number of particles in the cluster is close to its minimum $<n_c>_{min} = 1$. This tells about a very weak cascading of particles in the clusters.

At much higher energies $\sqrt{s} = 91$ GeV, $\sqrt{s} = 130$ GeV the condition $<n> < k$, is violated and we have $<n> > k$. The quantities $<n>$, $\frac{<n>}{k}$, $<n_c>$ increase slowly. The number of clusters $<N>$ continues also to increase. Negative values of k^{-1} are observed in μp - collisions in the range $\sqrt{s} < 12$ GeV.

Comparing the situation in e^+e^- - collisions with the results on $pp(\bar{p}p)$ and $A_i A_t$ -collisions the following difference between these three cases arises.

In $A_i A_t$ -collisions charged secondary particles are distributed among the clusters in such a way, that the average number of clusters $<N>$ is relatively small and does not almost change with increasing

167

energy or atomic weight. ($<N> \sim 4$, see Tables 2 – 5).In the same conditions the average number of particles in the clusters $<n_c>$ is changed significantly. This means the significant role of cascading in the clusters. Thus the situation is opposite than in e^+e^- - collisions.

In $pp(\bar{p}p)$ - collisions $<N>$ increases and after that (after $\sqrt{s} > 60$ GeV) behaves as a constant $<N> \sim 8$ (see Table 1). $<n_c>$ increases slowly. So $pp(\bar{p}p)$ - collisions from the CCM point of view are in some intermediate position between e^+e^- and A_iA_t - collisions.

In order to understand this differences the following arguments are in order. The second term βn in Eq (3) corresponds to the growth of the emission in the cell or growth of cascading in the cluster due to quantum–mechanical Bose–Einstein interference effects. Such effects are more significant for higher densities of states in the phase space. It is evident that the density of states is maximal in A_iA_t - system in a more "macroscopic" system as compared to $pp(\bar{p}p)$ system. From this point of view it is minimal for e^+e^- - system.
Thus the cascading of secondaries in the clusters or average multiplicity of particles in the clusters $<n_c>$ will be maximal and at the same time $<N>$ will be minimal for A_iA_t - collisions and vice versa $<n_c>$ will be minimal and $<N>$ will be maximal for $pp(\bar{p}p)$ - collisions.

It is interesting to study the dependences of the dispersions on $<n>$ and $<n_c>$

$$D = f(<n>) \tag{13}$$

$$D_c = f(<n_c>) \tag{14}$$

It is seen from Fig. 5 that the data on the dependence (13) in e^+e^-, hadron–hadron and nucleus–nucleus collisions lie on three different curves (curves 1, 2,3), but the data on the dependence (14) lie on the same curve (curve 4).

Note that if we plot these dependences in the usual scale we get the well known Malhotra – Wroblewski straight lines [12-13].

Thus on the basis of Fig. 5 one can conclude that intercluster dynamics in $A_i A_t$, $pp(\bar{p}p)$ and e^+e^- - collisions has the universal nature and is caused by the Bose – Einstein type interference effects.

Such a consideration is not valid for the formation of the centres of clusterization. This clusterisation proceeds at the initial stage of interaction and depends significantly on the type of interacting particles.

It becomes clearer when comparing the data on $A_i A_t$ and e^+e^- - collisions.

It is necessary to pay attention also to the differences in $A_i A_t$ and hadron--hadron collisions $(<N>_{A_i A_t} \sim 4, <N>_{hh} \sim 8)$. These differences might be caused by the pure nuclear collective effects in the process of formation of centres of clusterization at the initial stage of interaction. For more clear understanding of this problem it is necessary to study nucleus–nucleus interactions at ultra high energies.

The above mentioned picture does not contradict the models of production and hadronisation of partons.

According to these models the multiple production can be considered as a two stage process. The first stage (production of partons) depends on the type of interaction. The second stage (hadronisation of partons) is of the more universal nature, which depends on the DSD vacuum properties.

REFERENCES

1. A. Giovannini, L.Van Hove. Z. Phys. C. Particles and Fields. **30**, 1986, 391.
2. E.O. Abdrakhmanov et al. JINR. E1-11517, DUBNA 1978.
   N. Angelov et. al. JINR. **1**-12424, DUBNA 1979.
3. A. Breakstone et al. Phyz. Rev. **D30**, 1984,528.
4. G.J. Alner et al. Phyz. Lett. B. **138**, 1984, 304.
   R.Ansorge et al. CERN-EP/88-172, 1988, Charge particle

multiplicity distributions at 200 and 900 GeV C.M.energy (UA5 Collaboration); CERN-EP88-72.

5. M. Althoff et al. (TASSO Collaboration) Z. Phys. C 22, 1984, 307.
6. G.J. Alner et al. (UA5 Collaboration), Phys. Lett. B, (1986), v. 167, 476.
7. V. Garsevanishvili et.al. Sov. J. Nucl. Phys. E. 61, 1988, 668..
8. V. Grishin. Kvarki i adroni vo vzaimodeistviakh chastits visokikh energii. Moscow. 1988, (Russian).
   -G.J. Alner et al., CERN-EP/85-197, 1985, Phys > Lett. B167 1986, 176.
9. C. Vokal, M. Shumbera. JINR. 1-82-3886, 1982.
   -N. Kutsidi, Yu. Tevzadze Sov. J. Nucl. Phys. 41, 1985, 236.
10. N. Grigalashvili et al. Sov. J. Nucl. Phys. 48,1988, 476.
11. P. A. Abreu et al. (DELPHI collaboration). Z. Phyz. C. 50, 1991, 185.
12. P.K. Malhotra. Nucl. Phys. 46, 1963, 559.
13. A .Wroblevski. Proceeding of the III international Colloquim on Multiparticle Reactions, Zakopane, 1972, 140.

Tbilisi State University

ლ. ახობაძე, შ. ესაკია, ვ. გარსევანიშვილი, თ. ჯალაღანია, გ. კურატაშვილი, ი. თევზაძე

რელატივისტური ბირთვების დაჯახებებში დაბადებული დამუხტული ადრონების მრავლობითობის ანალიზი კლასტერულ-კასკადურ და პარციალურ-სტიმულირებულ ემისიის მოდელში

დასკვნა

შესწავლილია რელატივისტური ბირთვების დაჯახებებში ენერგიის ინტერვალში (2-10) ევ/ნუკლონზე დაბადებული ამუხტული ადრონების მრავლობითობა კლასტერულ-კასკადურ და პარციალურ-სტიმულირებულ ემისიის მოდელების ფარგლებში. ექსპერიმენტული მასალა მიღებულია დუბნის ბირთვული კვლევების გაერთიანებული ინსტიტუ-

ტის 2 მეტრიანი პროპანის ბუშტოვანი კამერის საშუალე-
ბით. შედეგები შედარებულია შესაბამის მონაცემებთან pp,
$\bar{p}p$, μp, $e^+ e^-$ – ურთიერთქმედებების მონაცემებთან მაღალ
ენერგიებზე. ნაჩვენებია, რომ რელატიური იონების
ურთიერთქმედებებისას შედარებით დაბალ ენერგიებზე
მასების ეფექტის გამო დამუხტული მეორადი ადრონების
მრავლობითობის ყოფაქცევა ქართადად მსგავსია მათი
ყოფაქცევისა pp, $\bar{p}p$, $p \, e^+ e^-$ – ურთიერთქმედებებში
ზემაღალ ენერგიებზე. ნაჩვენებია, რომ კლასტერების
ცენტრების ფორმირების პროცესი დამოკიდებულია
ურთიერთქმედ ნაწილაკების ტიპებზე, ხოლო კლასტერე-
ბის შემდგომი ევოლუციის პროცესი უნივერსალურია.
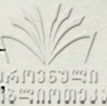
171

POLARIZATION EFFECTS IN PP-ELASTIC SCATTERING IN THE NON-ASSOCIATIVE THEORY

D.F. Kurdgelaidze, G. A. Begeluri, D. D. Kurdgelaidze

ABSTRACT. Experimental curve of ratio of differential cross-sections of elastic pp scattering at parallel and antiparallel spins and at high energies (1 GeV-13 GeV in laboratory system) is analytically written as a curve of second order, which contains necessarily falling proton pulse in the first degree that contradicts representation of contemporary physics. Authors assume that the new quantum number of proton-associator appears in the given process. Associator is a vector, and its introduction in the theory removes the above-mentioned contradiction.

According to the well known representation, the role of polarization effects must be decreased at high energies particles collision. Given experiments have shown the opposite picture. At high energies the contribution of polarization effects increases [1-5].

In this paper the possibility of solution of the above mentioned problem is researched on the basis of some theoretical speculations in the frame of the non-associative field theory [6]. In this theory, fermions besides the pseudo -vector of a spin - $\bar{\sigma}$ contain, the vector of an associator - $\bar{\xi}$.

Mathematical description of octonions spinors field requires to introduce non-commutative and non-associative algebras. Octonions can be represented as a $Q = K + A$, where $K = a_o e_o + a_n e_n$ - quaternions ($n = 1,2,3$), $A = a_\mu e_\mu$ - associatorm ($\mu = 4,5,6,7$) which contents non-associative properties. In the non-associative octonions the spinors field theory is developed in works [6], the Lorentz group of motion in the 4-dimensional Minkovskian space, remains invariable. Only spins generators

$$I_{\mu\nu} = (e_\mu e_\nu - e_\nu e_\mu)/4. \tag{1}$$

and spinors

$$\varphi = (\varphi_0 e_0 + \varphi_1 e_4 + \varphi_2 e_5 + \varphi_3 e_4 e_5)D_{45}D_{07} \tag{2}$$

have been determined through the octonions. Here $D_{\mu\nu} = (1 + i\varepsilon e_\mu e_\nu)/2$ projection operators, $\varepsilon = \pm 1$. Besides K- is a Lorentz scalar and A-is a Lorentz vector.

Non-associative octonions are characterized by the associator

$$\Delta(e_\mu e_\nu e_\lambda) = (1/2)\{(e_\mu e_\nu)e_\lambda - e_\mu(e_\nu e_\lambda)\}. \tag{3}$$

which permits to introduce a new quantum number – the associator.

Generators of a spin and an associator have a form:

$$\sigma_\rho = i\varepsilon_{\rho\mu\nu}I_{\mu\nu}., \qquad \xi_\rho = iI_{\rho7}. \tag{4}$$

For spins and associators we have obtained:

$$S_\rho = -\varepsilon_{\rho\mu\nu\lambda}(\overline{\psi}e_\mu e_\nu e_\lambda\psi)/3!2 = (\psi^+\sigma_\rho\psi)/2, \tag{5}$$

$$A_\rho = -(\overline{\psi}\Delta(e_\mu e_\nu e_\lambda)\psi)/3!2 = (\psi^+\xi_\rho\psi)/2, \tag{6}$$

$\overline{\sigma}$ and $\overline{\xi}$ are connected with magnetic and electric-dipole moment of particles

$$\overline{\mu} = (e\hbar/2mc)\overline{\sigma}, \qquad \overline{d} = (i\hbar/2mc)\overline{\xi}, \tag{7}$$

where

$$\sigma_4 = ie_5 e_6/2, \qquad \sigma_5 = ie_6 e_4/2, \qquad \sigma_6 = ie_4 e_5/2.$$

173

$$\xi_4 = ie_7e_4/2, \quad \xi_5 = ie_7e_5/2, \quad \xi_6 = ie_7e_6/2,$$

$$\sigma_4\xi_4 = \sigma_5\xi_5 = \sigma_6\xi_6 = e_8, \tag{8}$$

$$e_8 = e_4e_5e_6e_7e_8.$$

According to discrete transformations a spin and associator have different properties:

$$P\bar{A} = -\bar{A}, \quad T\bar{A} = \bar{A}, \quad P\bar{\sigma} = \bar{\sigma}, \quad T\bar{\sigma} = -\bar{\sigma}, \tag{9}$$

and have a connection $\bar{\xi} = -e_8\bar{\sigma}$.

Let's consider curves of spin-dependent differential cross-sections of PP – elastic scattering as function of $p_\perp^2$ or p_L at high energies with fixed scattering angle ($Q_{cm} = 90^o$ in the system of masses). Where $p_\perp^2$ is a square of orthogonal transmissing momentum in the range of $1 < p_\perp^2 < 6$ (Gev/c)^2 and p_L is an incident proton's laboratory momentum in the range of $0 < p_L < 13$ Gev/c. (See Fig. 1 in the appendix). On the curve a) and b) correspondingly, there are plotted $d\sigma(\uparrow\uparrow)/d\Omega$ -spin-parallel differential cross-section and $d\sigma(\uparrow\downarrow)/d\Omega$ - spin-antiparallel differential cross-section against $p_\perp^2$ or p_L for the $Q_{cm} = 90^o$. It is very apparent that the large - $p_\perp^2$ hard-scattering events rarely occur unless the spins are parallel.

In Fig. 2 it is plotted the spin-parallel to spin-antiparallel ratio against $p_\perp^2$ for both the fixed-energy 11.75 Gev/c data and fixed-angle $Q_{cm} = 90^o$ data (See Fig. 2 in appendix).

The spin-parallel and the spin-antiparallel differential cross-sections we have considered as function [7]

$$d\sigma(\uparrow\uparrow)/d\Omega = f(p)W_I^2(p,\sigma),$$

174

$$d\sigma(\uparrow\downarrow)/d\Omega = f(p)W_2^2(p,\sigma), \qquad (10)$$

where $f(p)$ is a spin-independent function, then all the spin-dependence of $d\sigma/d\Omega$ contents in functions $W_1^2(p,\sigma)$ and $W_2^2(p,\sigma)$ and for their ratio we have:

$$\frac{d\sigma(\uparrow\uparrow)}{d\sigma(\uparrow\downarrow)} = \frac{W_1^2(p,\uparrow\uparrow)}{W_2^2(p,\uparrow\downarrow)} = 1 + \varphi^2(p), \qquad (11)$$

$$\varphi(p) = W_3(p)/W_2(p) \qquad (12)$$

where

$$W_3^2(p) = W_1^2(p,\uparrow\uparrow) - W_2^2(p,\uparrow\downarrow) \qquad (13)$$

From Fig. 2 one can see that the function $\varphi^2(p)$ in the given range of moment has three extreme points: P_1 and P_2 are the points of minimums, P_0 is a point of maximum.

As $W_2(p) \neq 0$, then from the equation $\varphi(p) = 0$ we have got, that $W_3(p) = 0$ and points P_1 and P_2 are also solutions of $W_3(p) = 0$ quation.

In the phenomenological approach $\varphi(p)$ must be built up of invariant of the 0(3) group with variables : $\vec{P}, \vec{\sigma}_a$ and $\vec{\sigma}_b$, where $\vec{\sigma}_a$ and $\vec{\sigma}_b$ are the spins of the incident proton and the target proton (in the lab system). Analyzing the concrete experiments we convince that to get the square polynomial functions for W_1, W_2 is W_3 are impossible.

In the non-associative theory in a phenomenological approach of 0(3) group one can build invariant with variables: $\vec{P}, \vec{\sigma}_a, \vec{\zeta}_a; \vec{\sigma}_b, \vec{\zeta}_b$, where $\vec{\zeta}_a$ and $\vec{\zeta}_b$ are associators of the incident proton and the target proton. In the frame of exact 0(3) symmetry a spin and an associator

175

are undistinguished. Therefore, one can see, if a spin and an associator are parallel then in the phenomenological approach for PP elastic scattering we have no new results.

If we suppose, there is no strong correlation between a spin and an associator of particles, then between the vectors $\vec{p}$, $\vec{\sigma}$, $\vec{\zeta}$ occur angles and only in this case W_1, W_2, W_3 functions are square polynomial.

Consequently, we can present the function $W_3(p)$ as a polynomial

$$W_3(p) = A_3 + B_2 P + D_3 P^2 = const(p - p_1)(p - p_2), \qquad (14)$$

where A_3, B_3, D_3 are constant parameters.

From the formulas (12) and (14) we can assume that $W_1(P)$ and $W_2(P)$ also have forms:

$$W_1(p) = (\alpha_1 + \alpha_2) + (\beta_1 + \beta_2)p + (\delta_1 + \delta_2)p^2, \qquad (15)$$

$$W_2(p) = (\alpha_1 - \alpha_2) + (\beta_1 - \beta_2)p + (\delta_1 - \delta_2)p^2. \qquad (16)$$

Here $\alpha_i, \beta_i, \delta_i$ $(i = 1, 2)$ are constants.

The equation $W_3^2(p) = W_1^2(p) - W_2^2(p)$ on parameters $\alpha_i, \beta_i, \delta_i$ $(i = 1, 2)$ lays out five conditions, from which we define

$$A_3 = 2\varepsilon_A \sqrt{\alpha_1 \alpha_2}, \qquad D_3 = 2\varepsilon_D \sqrt{\delta_1 \delta_2},$$

$$B_3 = (\alpha_1 \beta_2 + \alpha_2 \beta_1) / \varepsilon_A \sqrt{\alpha_1 \alpha_2}, \qquad (17)$$

$$\beta_1 = \pm \sqrt{\alpha_1 \delta_1}, \quad \beta_2 = \pm \sqrt{\alpha_2 \delta_2}. \qquad (18)$$

From the equations (14), (17) and (18) we have excluded five parameters. Then for $W_1(p)$, $W_2(p)$ and $W_3(p)$ we have following functions:

$$W_1 = \frac{-(\beta_1 p_2 + \beta_2 p_1)}{2 p_1 p_2} \left\{ p^2 - 2 p_1 p_2 \frac{\beta_1 + \beta_2}{\beta_1 p_2 + \beta_2 p_1} p + \right.$$

$$\left. + p_1 p_2 \frac{\beta_1 p_1 + \beta_2 p_2}{\beta_1 p_2 + \beta_2 p_1} \right\},$$

$$W_2 = \frac{-(\beta_1 p_2 - \beta_2 p_1)}{2 p_1 p_2} \left(p^2 - 2 p_1 p_2 \frac{\beta_1 - \beta_2}{\beta_1 p_2 - \beta_2 p_1} p + \right.$$

$$\left. + p_1 p_2 \frac{\beta_1 p_1 - \beta_2 p_2}{\beta_1 p_2 - \beta_2 p_1} \right\}, \tag{19}$$

$$W_3 = \sqrt{\beta_1 \beta_2 / p_1 p_2} \left\{ p^2 - (p_1 + p_2) p + p_1 p_2 \right. .$$

Let's consider the amplitude of PP - elastic scattering as a structure of $O(3)$ – invariant in the non-associative field theory. From vectors $\vec{p}, \vec{\sigma}_a, \vec{\sigma}_b$ we have built up an invariant for the following forms:

$$I(\vec{p}, \vec{\sigma}_a \uparrow, \vec{\sigma}_b \uparrow) = A_1 + B_1 P + D_1 P^2 , \tag{20}$$

and we identify it to the amplitude $W_1(p, \uparrow\uparrow)$.

Accomplishing the spin reflections $\vec{\sigma}_a \to -\vec{\sigma}_a, \ \vec{\sigma}_b \to \vec{\sigma}_b$ or $\vec{\sigma}_a \to \vec{\sigma}_a, \ \vec{\sigma}_b \to -\vec{\sigma}_b$, we have got two new invariants $I^a(\vec{p}, \vec{\sigma}_a \downarrow, \vec{\sigma}_b \uparrow)$ and $I^b(\vec{p}, \vec{\sigma}_a \uparrow, \vec{\sigma}_b \downarrow)$.

According to the experiments we have

$$I^a = I^b = W_2(p, \uparrow\downarrow) \tag{21}$$

177

These equations lay out limits on the invariant $I(\vec{p},\vec{\sigma}_a\uparrow,\vec{\sigma}_b\uparrow)$ and gives opportunity to define parameters $\alpha_1,\alpha_2,\beta_1,\beta_2,\delta_1,\delta_2$ through the constants of an invariant $I(\vec{p},\vec{\sigma}_a\uparrow,\vec{\sigma}_b\uparrow)$ and from components of the spin and the associator.

Let's consider a very important case, when $\beta_1=\beta_2$. In this way the linear terms in the $W_2(p)$ became zero, as experiment demands. But $\varphi(p)$ function has poles in the points $p=\sqrt{p_1 p_2}$, which contradict experimental data.

For avoiding the pole in the equation $\varphi(p)=0$, we have introduced a new parameter α. Hence, we changed functions

$$\tilde{W}_1(p)=W_1(p)+F(p,\alpha), \quad \tilde{W}_2(p)=W_2(p)+F(p,\alpha), \quad (22)$$

and demand to fulfill the condition $\tilde{W}_3(p)=W_3(p)$.

The function $F(p,a)$ has the form:

$$F(p,\alpha)=\beta_1^2\left\{\frac{(p_2-p_1)^2}{2p_1 p_2}\right\}\alpha\left(p^2+\frac{\alpha-2}{2}p_1 p_2\right). \quad (23)$$

By variation of α for $\alpha=2$ we had good results for functions $\tilde{W}_1(p)$, $\tilde{W}_2(p)$, $\tilde{W}_3(p)$,

$$\tilde{W}_1^2/\beta_1^2=\left\{\frac{p_1+p_2}{2p_1 p_2}\right\}^2\left(p^2-\frac{4p_1 p_2}{p_1+p_2}p+p_1 p_2\right)^2+\frac{(p_1-p_2)^2}{p_1 p_2}p^2,$$

$$\tilde{W}_2^2/\beta_1^2=\left\{\frac{p_1-p_2}{2p_1 p_2}\right\}^2(p^2+p_1 p_2)^2, \quad (24)$$

$$\tilde{W}_3^2/\beta_1^2=1/p_1 p_2\left\{(p-p_1)(p-p_2)\right\}^2$$

178

$$\frac{d\sigma(\uparrow\uparrow)}{d\Omega} \Big/ \frac{d\sigma(\uparrow\downarrow)}{d\Omega} = 1 + \varphi^2(p) =$$

$$= 1 + \frac{4p_1 p_2}{(p_2 - p_1)^2} \left\{ \frac{(p - p_1)(p - p_2)}{p^2 + p_1 p_2} \right\}^2 \qquad (25)$$

(See Fig. 3 in the appendix).

From the formula (24) we can see, that with two experimental points P_1 and P_2 it's possible to build up all the curves in the given range of moments.

Taking into consideration (for another experimental data) poles of the $\varphi(p)$ function we can plot also the spin-parallel and spin antiparallel differential cross-sections for the fixed $\theta_{cm} = 49^0$ scattering angle against P_L (See Fig. 4 in the appendix).

We ought to underline, that terms in odd degrees in formula (24) are parity violation terms in habitual theory. But in the non-associative field theory O(3)- invariant amplitudes of PP-elastic scattering contain the term $(\vec{p}.\vec{\zeta})$ instead of $(\vec{p}.\vec{\sigma})$ which gives odd degrees of moment without parity violation.

$W_2(p,\uparrow\uparrow)$ - invariant amplitude corresponds to the proton-proton collision state, when effective full spins and associators of the system are equal to one. Therefore, we suppose that maximum of contribution in polarization effects gives exactly $W_2(p,\uparrow\uparrow)$ - amplitude which has been confirmed experimentally.
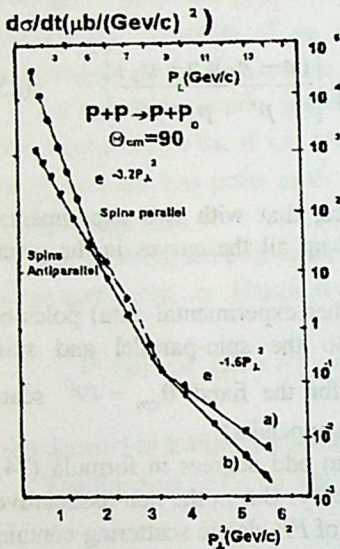
Fig.1. 90°_{cm} Spin cross-sections
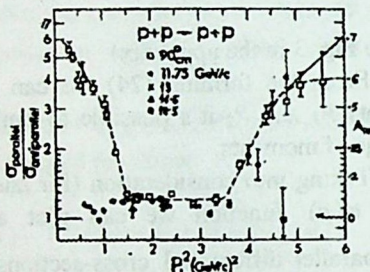
Fig.2. $d\sigma/dt(\uparrow\uparrow):d\sigma/dt(\uparrow\downarrow)$ plotted against $P_\perp$
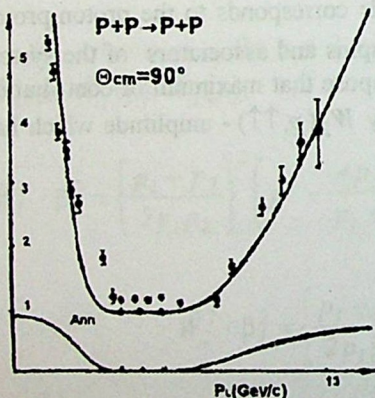
Fig.3. Theoretical curves of the ratio and Ann for 90°_{cm} against $P_\perp$
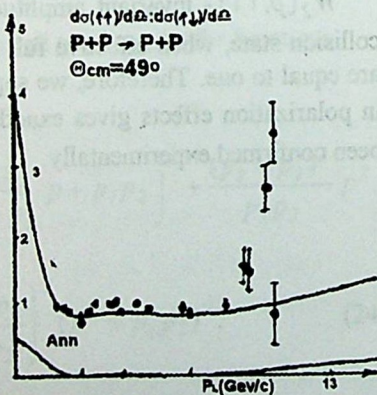
Fig.4. Theoretical curves of the ratio and Ann for 49°_{cm} against $P_\perp$

180

REFERENCES

1. A.D. Krisch. High $p_\perp^2$ spin experiments with polarized Protons
    Second International Workshop on high energy spin physics.
    Protvino, 8-10 October, 1984, 27.
2. S.J. Brodsky et al. Phys. Rev. **D20**, 1979, 2278.
3. A.W. Hendry. Phys. Rev. **D23**, 1982, 2075.
4. D.G. Crabb. Measurment of Ann in PP elastic scattering between
    13 and 18.5 Gev/c. VII International Symposium on high energy
    spin physics. Protvino 22-27 September, **2**. 1986, 74.
5. D.G. Crabb, I. Gialas, A.D. Krish, at al. Phys. Rev. Letters, **60**,
    23, 1988, 2351.
    D.G. Crabb, W.A. Kakfman, A.D. Krish, at al. Phys. Rev. Letters,
    68, 26, 1990, 3241.
6. D.F. Kurdgelaidze. Acta Physica Hungarica., **57**, 1985, 79.
    Izvestia Vuzov, Physica, 11, 1986, 22; 12, 1986, 58.
5. D.F. Kurdgelaidze, G.A. Begeluri, D.D. Kurdgelaidze.
    Polarization effects of *PP* and *PP* elastic scattering in the non-
    asociative field theory. V-International Work-shop at high energy
    spin physics, Protvino, September. 5-8, 1993.

Tbilisi State University

დ.ფ. კურდღელაიძე, გ. ბეგელური, დ.დ. კურდღელაიძე

პოლარიზაციული ეფექტები დრეკადი **PP**-გაბნევისას არა-
ასოციატიურ თეორიაში

დასკვნა

თანამედროვე ფიზიკის წარმოდგენების თანახმად სპინუ-
რი ურთიერთქმედების როლი, ნაწილაკების დაჯახების
პროცესში მაღალ ენერგიებზე, უნდა უმნიშვნელო იყოს და
მცირდებოდეს ენერგიის ზრდის შესაბამისად.

მაგრამ, დრეკადი გაბნევის ექსპერიმენტმა აჩვენა, რომ დაჯახების ენერგიის ზრდისას ერთი გევიდან ზუდა ადგილი აქვს სპინური ურთიერთქმედების როლის ზრდას და გარკვეულ პირობებში დიფერენციალური კვეთების შეფარდება პარალელური და ანტიპარალელური სპინების შემთხვევაში აღწევს 4.

როდესაც იზომება ლაბორატორიულ სისტემაში მოცემული კუთხით PP დრეკადი დაჯახების შედეგად გაბნეული პროტონების რიცხვი, პროცესის დიფერენციალური კვეთა შეიძლება დამოკიდებული იყოს მხოლოდ პროტონების სპინებზე - σ_1, σ_2 და დაცემული პროტონის იმპულსზე P_1.

ზემოთ აღნიშნული დიფერენციალური კვეთების შეფარდების P_1 - ზე დამოკიდებულების ექსპერიმენტულ მრუდს რთული ხასიათი აქვს და მოცემულ ნაშრომში კერძოდ ნაჩვენებია, რომ როდესაც P_1 იცვლება (1 გევ/ც - 13 გევ/ც) შუალედში ეს მრუდი მეორე რიგის მრუდია და თანაც ისე, რომ ის აუცილებლად შეიცავს P_1-ს პირველ ხარისხში. ეს პრინციპული მომენტია, რადგან დიფერენციალური კვეთა ინვარიანტია როგორც O_3 ჯგუფის, ისე დისკრეტული გარდაქმნების მიმართ, ამავე დროს, P_1-ისა და σ_1, σ_2 სპინებისაგან ასეთი ინვარიანტის აგება შეუძლებელია. ეს გარემოება მიაჩნია ავტორებს როგორც გამოვლინება იმისა, რომ მაღალ ენერგიებზე უკვე თავს იჩენს პროტონების ახალი კვანტური რიცხვი -ასოციატორი ξ.

ასოციატორი-ξ ვექტორია და P_1, σ_1, ξ_1, σ_2, ξ_2 ცვლადებისაგან შეიძლება აგებული იქნეს საჭირო ინვარიანტი.

შრომაში გამოყვანილია პარალელური და ანტიპარალელური სპინებით დრეკადი PP გაბნევის დიფერენციალური კვეთების შეფარდების ანალიზური გამოსახულება როგორც მეორე რიგის პოლინომი P_1-ს მიმართ. ის შეიცავს ორ თავისუფალ პარამეტრს და ორი ექსპერიმენტული წერტილის მოცემით შესაძლებელია შესაბამისი მრუდის აგება განხილული ენერგიის მთელ ინტერვალში.

CONTENTS

183

შინაარსი

თბილისის უნივერსიტეტის გამომცემლობა,
380028, თბილისი, ი. ჭავჭავაძის გამზ. 14.
თბილისის უნივერსიტეტის
სარედაქციო-სადუბლიკაციო
კომპიუტერული სამსახური,
თბილისი, ი.ჭავჭავაძის გამზ., 1.